`

`

SEISMIC ANALYSIS OF THE ONSHORE MOZAMBIQUE BASIN RESERVOIRS, INHASSORO AREA

A dissertation submitted in partial fulfilment of the requirements for the degree of Master of Science

By

Bonginkosi Mbatha

School of Geosciences

University of the Witwatersrand

Johannesburg,

January 2025

`

DECLARATION

I declare that this thesis is my own, unaided work. It is being submitted for the Degree of Master of Science at the University of the Witwatersrand, Johannesburg. It has not been submitted before for any degree or examination in any other University.

Bonginkosi Mbatha

Student Number: 1547949

`

ABSTRACT

The Mozambique Basin has proven to be rich in hydrocarbon resources, with gas production since 2004. Exploration in this basin has, in the past, focused mainly onshore and centred around the Pande, Temane, and Inhassoro gas and oil fields. The use of amplitude characterization has assisted explorers in identifying gas accumulations, especially the stratigraphically trapped gas in Pande and Temane. The hydrocarbon-rich reservoirs in this basin are those mainly of the Lower Grudja Formation. These are Maastrichtian to Campanian aged reservoirs in the Late Cretaceous period. Seismic attributes can be used to understand these formations and their fluid content. Amplitude-based attributes have been studied successfully in the central part of the basin where the Lower Grudja Formation is relatively thick and, in some parts, saturated with hydrocarbon pore fluids. The study makes use of recently acquired high-resolution three-dimensional (3D) surface seismic data and well data information to characterize Mozambique Basin Lower Grudja reservoirs.

Before the acquisition of the 3D seismic data, interpreters mainly relied on qualitative interpretation of 2D seismic surveys following anomalous amplitude events across seismic sections. The 2D seismic data had many limitations, including wide (2-4 km) line spacing, relying on projections from gridding algorithms. Attributes from seismic amplitudes extracted from stacked data can lead to misinterpretation, often referred to as false positives, and the drilling of dry holes. The study looks at the fundamental causes of these anomalous amplitude events. This implies that direct hydrocarbon indicators (DHI) require further analysis before being confirmed as representing hydrocarbon fluid-filled porous reservoirs. This is achieved through analysis of stacked seismic data (full and variable angle data), post-stack migrated data, pre-stack seismic gather data, and well information. Three main questions are investigated to quantitatively describe Mozambique Basin reservoirs: Rock Physics Modelling - is there a unique response due to changes in fluid composition in the subsurface that can be characterized using seismic data? Amplitude Variation with Offset (AVO) analysis – are these changes uniquely related to changes in fluid composition, or are they coupled with other reservoir and bounding rock properties? Seismic inversion – can we quantitatively predict the distribution of hydrocarbons across the Inhassoro block using both seismic attributes and quantitative interpretation methods?

`

Pande seismic analysis and inversion of lower Grudja facies demonstrate that existing seismic gathers could be conditioned and made AVO compliant. This enables the determination of the AVO behaviour of Lower Grudja reservoirs, in this case, Pande G6 and G10. These reservoirs, owing to their high porosity gas sands capped by a relatively stiff rock, exhibit a class IV AVO response. True AVO class of Lower Grudja reservoirs is revealed when extracted from conditioned seismic gathers. This is complemented by intercept and gradient crossplots. AVO synthetics from wells with reliable well log data help model the expected AVO behaviour of Lower Grudja reservoirs. Quantitative analysis was also conducted in Temane and Inhassoro and included AVO modelling based on fluid and saturation scenarios. Crossplotting of elastic properties with petrophysical parameters concluded that bulk density is a proxy for relative porosity and relative fluid saturation, and shear modulus is a proxy for relative shale volume.

`

ACKNOWLEDGEMENTS

This dissertation is a culmination of the work and support I have received throughout the MSc journey. I am highly indebted to my supervisor Prof. Musa Manzi. Thank you for your guidance, patience, and your willingness to freely share your insights and expertise.

I also received great support from co-supervisors who are industry experts in geophysics, Dr. Vincent Mashaba and Chris Wells. I particularly worked closely with Chris, and I acquired substantial knowledge about Rock Physics and Quantitative Seismic Interpretation. I have also benefitted from many work-related discussions with my colleagues at the office.

Special thanks to Sasol for allowing me to use the company data and enable me to access the relevant software packages required for seismic data analysis and interpretation.

Lasty, thanks to God almighty for endowing me with the brain that enables me to take on demanding challenges. My family (Phumzile and our two kids, daughter Nala and son Nyezi) has been supporting me throughout this journey, despite some of the time I have taken away from them.

`

Table of Contents

`

`

List of Figures

`

`

`

`

`

`

`

1 Introduction

1.1 Background

High-resolution 3D surface seismic data were acquired onshore in Mozambique (Figure 2-1), and several oil and gas wells have been drilled based on the interpretation of this dataset. The main purpose of this seismic survey and associated wells is to assist in the development of the Pande and Inhassoro fields. The Pande field contains gas at the G6 reservoir level from the Upper Cretaceous Maastrichtian Grudja formation, whereas the Inhassoro field has oil with a gas cap at G6, and oil at G10 reservoir levels. The new seismic and well data acquired include Vertical Seismic Profiles (VSP), which provide enhanced subsurface imaging compared to conventional surface seismic surveys. The new information obtained from the VSP data provides insight into reservoir rock properties, petrophysical, and production data, as well as the extent of producible reservoirs.

Prior to the 3D seismic acquisition, seismic interpreters relied on qualitative interpretation of 2D seismic surveys following anomalous seismic amplitude events across seismic sections. This approach proved adequate for oil and gas exploration and, to some extent, the appraisal of these fields. This research looks at the fundamental causes of anomalous amplitude events in the seismic data and highlights certain limitations of the amplitude attributes that may lead to potential misinterpretation of reservoir rocks' properties. This study further applies techniques such as 'Amplitude Variation with Offset (AVO)' to the seismic data to improve the quality of the 3D seismic interpretation in the Mozambique Basin.

High-porosity gas sandstones capped by relatively stiff clay-rich rocks generally result in Class IV AVO responses and are often accompanied by a clear seismic amplitude response on full-stack seismic data. To assess quantitative properties from reservoir rocks across the Mozambique Basin, pre-stack seismic data are analysed and pre-conditioned using advanced data processing techniques to ensure that these data are AVO and QI (Quantitative Interpretation) compliant. VSP and well-log data are used to validate synthetic seismic models and assess the quality, resolution, and subsurface correlation of the newly acquired surface 3D reflection seismic data. Well synthetic seismograms are also generated using both acoustic and elastic impedance logs to validate seismic data quality in the offset domain. Seismic attributes are computed from the seismic data to enhance the detection of potential direct hydrocarbon indicators (DHI) as a function of elastic property proxies. Finally, seismic data are converted

`

into geologic and physical properties through an elastic seismic inversion process. Both coloured and model-based inversions are investigated, and the most accurate model is utilized.

1.2 Thesis structure

This thesis has ten chapters. Chapter 1 introduces the study and offers the background to the study area. This chapter also presents the research objectives and highlights key questions that are investigated in the study. Chapter 2 gives the geologic background of the study area, the Mozambique Basin. Chapter 3 introduces quantitative seismic studies. These include elastic impedance, effects on reservoir pore fluids on seismic data, amplitude variation with offset (AVO), and seismic attributes. In chapter 4, seismic acquisition, processing and interpretation in general is discussed and then specifically for the Inhassoro area in the Mozambican Basin. In chapter 5, quantitative analysis of Mozambique Basin reservoirs work is presented. The approach used incorporates both seismic data and well log information. Chapter 6 discusses the results; chapter 7 summarises the main conclusions from the study and discusses the recommendations that can be drawn from this study.

1.3 Research objectives

The main objective of the study is to characterise the Maastrichtian age reservoirs across Pande, Temane, and Inhassoro fields to reveal the distribution of rock and fluid properties from the elastic properties of these reservoirs. The study uses modern seismic and well log data to better describe reservoir characteristics from these oil and gas fields located in the southern Mozambique Basin. The study is designed to assist in delineating “sweet spots” that may drive the optimal placement of future exploration, development, and production wells. The study also seeks to demonstrate the role that quantitative seismic interpretation can play in improving the quality of the seismic interpretation, which in turn may benefit further exploration and production in similar geological environments.

1.4 Key questions

The key questions to be investigated in this study relate to the understanding of quantitative properties of Mozambique Basin reservoirs.

- **Rock physics modelling**: Is there a unique response due to changes in fluid composition in the subsurface that can be characterized using seismic data?

`

- **AVO analysis**: Are these changes uniquely related to changes in fluid composition, or are they coupled with other reservoir and bounding rock properties (i.e., reservoir pores, reservoir minerals, reservoir architecture, or reservoir thickness)?
- **Seismic inversion:** Can we quantitatively predict the distribution of hydrocarbons across the Inhassoro block using both seismic attributes and quantitative interpretation methods?

This research will be limited to the understanding of the relationships between the elastic properties and the petrophysical properties of reservoir and bounding rocks. The main elastic properties to be studied are seismic velocity, bulk density, bulk modulus, and shear modulus. The main petrophysical properties to be derived are total porosity, total fluid saturation, and volume of sand. Attributes derived from these properties will be generated and their accuracy in describing in-situ conditions reservoir rocks will be investigated.

2 Geologic background

The study area is located within the Mozambique Basin (Figure 2-1). This basin covers an area of about 275,000 km^2 onshore (Matthews et al., 2001) and about 105,000 km^2 offshore (Coster et al., 1989). The Mozambique Basin has an asymmetric depression, which is bound in the southwest by the Lebombo monocline and in the northwest by the Nuanetsi-Sabi monocline. Karoo basalts dip eastwards below the cretaceous sedimentary rocks of the basin (Mashaba & Alterman, 2015). Igneous rocks of the Karoo Supergroup outcrop on the west (Gwavava & Swain, 1992).

`

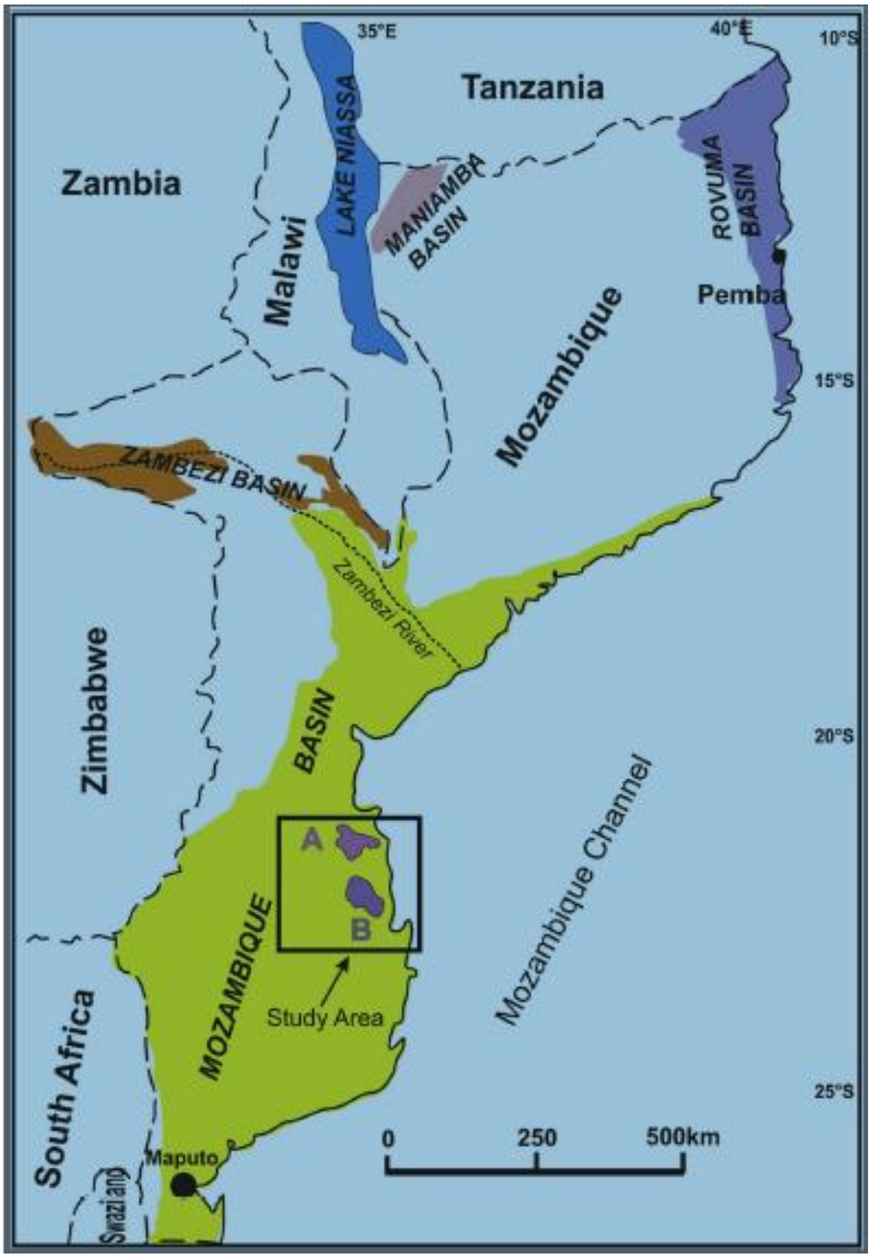

Figure 2-1 Map of Mozambique showing the study area in the Mozambique Basin (Mashaba & Alterman, 2015). The map shows the major onshore sedimentary basins of Mozambique. The highlighted study area shows existing fields, A and B, which cover the area around which this study is based.

`

The basement of the Mozambique Basin is formed by Precambrian crystalline and metamorphic rocks. The basement is overlain by Early Jurassic Karoo volcanic and sedimentary rocks, followed by the Late Jurassic continental red-beds of the Lupata Formation (Salman & Abdula, 1995). Marine deposition began in the Early Cretaceous with the Maputo Formation (Figure 2-2), followed by the Domo Formation, initially as a Lower Domo Shale in the Early Cretaceous and later as an Upper Domo Shale/Domo Sandstone in the Late Cretaceous (Coster et al., 1989).The Domo Sandstone has been a subject of hydrocarbon exploration, albeit with marginal success. The marine Lower Grudja Formation was deposited in the Late Cretaceous.

This study focuses on hydrocarbon-rich reservoirs of the Lower Grudja Formation. This formation is mainly composed of shallow shelf facies and clayey sand deposits interbedded with siltstones, and in certain places it contains glauconite. The Lower Grudja Formation is a thick interval (~1200 m) in the central part of the basin, and it pinches out towards the basin margins (Lächelt, 2004). These rocks were transported to the Mozambique Basin through eastward-draining river systems of the paleo-Zambezi River (Wellington, 1955). The Upper Grudja Formation was deposited during the Palaeocene and is overlain by carbonates and deltaic facies of the Cheringoma Formation of the Eocene age. An unconformity exists between the Cheringoma Formation and the overlying shallow marine deposits from the Miocene and Pliocene age – the Dunes formation (Mashaba & Alterman, 2015).

`

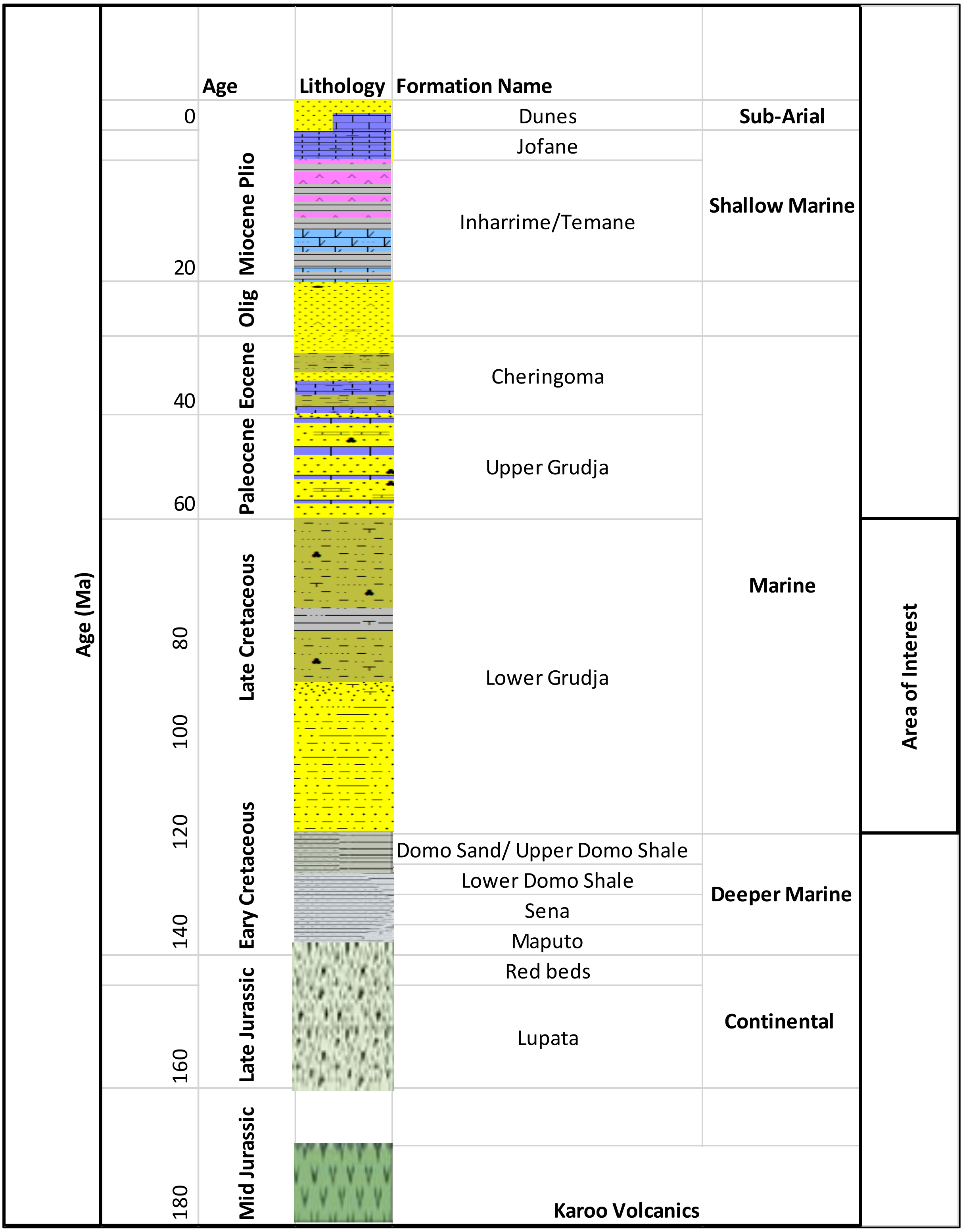

Figure 2-2. Stratigraphic column of the Mozambique Basin, adapted from (Walford et al., 2005). The area of interest for this study is Lower Grudja reservoirs, these are of Late Cretaceous age and are known to contain hydrocarbons in some parts of the basin. The reservoir units within Lower Grudja are composed mainly of clastic sedimentary rocks. Deeper reservoirs in the Mozambique Basin are the Domo and Sena formations.

`

3 Quantitative seismic studies

3.1 Elastic impedance

With the advent of 3D reflection seismic surveys, many quantitative methods have been developed to help identify exploration targets and reduce drilling risk. These methods relate to the acquisition, processing, and interpretation of seismic data. Seismic acquisition planning and design ensure that parameters used are adequate to image target reservoirs (Schulte & Manthei, 2014) and it requires that seismic data of sufficient imaging quality are available to properly characterize the zone of interest in the subsurface. Careful consideration must be taken when processing seismic data to ensure that they remain AVO and QI compliant. It is a standard practice during data processing to produce pre-stack gathers and angle stacks (from partial offset volumes) for reservoir characterization purposes. When seismic data are processed, they are gathered in offset bins by sorting source-receiver distances (or offsets) used during data acquisition. Changes in processed seismic amplitude information from zero-offset (that is, assuming only vertical seismic wave propagation) are related to the acoustic impedance of the rocks. Using well synthetic seismograms and post-stack inversion algorithms, zero-offset seismic data can be converted to seismic acoustic impedance (AI) data. Acoustic impedance is a product of density of rocks and seismic velocity (Becquey et al., 1979).

Extending the same concept to all remaining offsets in the seismic data, elastic impedance (EI) is estimated based on a pseudo-linear approximation by (Connolly, 1999) as a generalization of acoustic impedance (AI) for variable angles of incidence. This approximation was derived from plane-wave, far-field propagation equations, commonly known as Zoeppritz equations. The linearized Zoeppritz equation, for angles less than a critical angle, is defined as:

$$R(\emptyset) = A + BSin^2\theta + CSin^2\theta Tan^2\theta \qquad 1$$

where,

$$A = \frac{1}{2}(\frac{\Delta Vp}{\tilde{V}p} + \frac{\Delta\rho}{\acute{\rho}})$$

$$B = \frac{\Delta Vp}{\tilde{V}p} - \frac{4Vs^2}{Vp^2}\frac{\Delta Vs}{\tilde{V}s} - 2\frac{Vs^2}{Vp^2}\frac{\Delta\rho}{\acute{\rho}}$$

$$C = \frac{1}{2}\frac{\Delta Vp}{\tilde{V}p}$$

`

Where,

$$\tilde{V}p = (Vp(ti) + Vp(ti-1))/2$$

$$\Delta Vp = Vp(ti) - Vp(i-1)$$

$$\frac{Vs^2}{Vp^2} = (\frac{Vs^2(ti)}{Vp^2(ti)} + \frac{Vs^2(ti-1)}{Vp^2(ti-1)})$$

Vp is the compressional wave, Vs is the shear wave. ΔVp is the change in compressional velocity. ΔVs is the change in shear velocity. Particle motion of the P-wave is in the direction of propagation and S-wave particle motion is perpendicular to the direction of propagation. $\tilde{V}p$ is the average compressional velocity. ρ is the density, ρ́ is the average density, ti is time the wave travels at incident angle.

From the linearized Zoeppritz equation above, (Connolly, 1999) derived the elastic impedance (EI) equation:

$$EI = Vp^{(1+tan^2\theta)}Vs^{(-8Ksin^2\theta)}\rho^{(1-4Ksin^2\theta)} \quad 2$$

An alternative form of equation 2 is given by:

$$EI = Vp(Vp^{(tan^2\theta)}Vs^{(-8Ksin^2\theta)}\rho^{(1-4Ksin^2\theta)}) \quad 3$$

Where K = $\frac{Vs^2}{Vp^2}$.

For example, when a reservoir interval has a lower acoustic impedance than its upper bounding rock (i.e., the cap rock or reservoir seal), the zero-offset contrast (or reflectivity) between these two impedances creates a negative value calculated as follows:

$$R_0 = \frac{AI_{res} - AI_{seal}}{AI_{res} + AI_{seal}} < 0 \quad 4$$

Where AI_{res} is the acoustic impedance of the reservoir rocks and AI_{seal} is the acoustic impedance of the rocks overlying the reservoir, the sealing rocks that ensure hydrocarbons do not escape. This reflectivity contrast is estimated assuming zero-offset (i.e., near vertical) propagations, and it is typically insufficient to assess whether the lower AI of the reservoir is due to higher porosity, higher hydrocarbon saturation, or thickness-related anomalies compared to its upper bounding rock. In this regard, the EI approximation is estimated to calculate changes in reflectivity at multiple offsets to identify which reservoir property is controlling

`

such impedance contrast based on associated changes in seismic amplitude at different offsets, commonly known as AVO effects. For instance, if the EI value of a reservoir interval decreases with offset more rapidly than the EI value of its upper bounding rock, their reflectivity contrast will also decrease with offset and will be lower than their zero-offset reflectivity.

To better understand the expected geological changes in reflectivity with offset for different combinations of reservoir and non-reservoir intervals, (Rutherford & Williams, 1989) introduced an AVO classification scheme to facilitate the interpretation of such AVO effects. As in many reservoir characterization studies, EI can also be used to identify correlations between elastic and petrophysical properties from the seismic inversion. For well planning purposes, an Elastic Impedance (EI) volume can be used in optimally designing trajectories of development wells (e.g., Figure 3-1). EI also leverages the relative increase in seismic image quality at higher incident angles compared to lower angles (Connolly, 1999) to provide more robust interpretation results in areas where acoustic impedance from zero-offset data is compromised by near-offset noise and limited imaging quality.

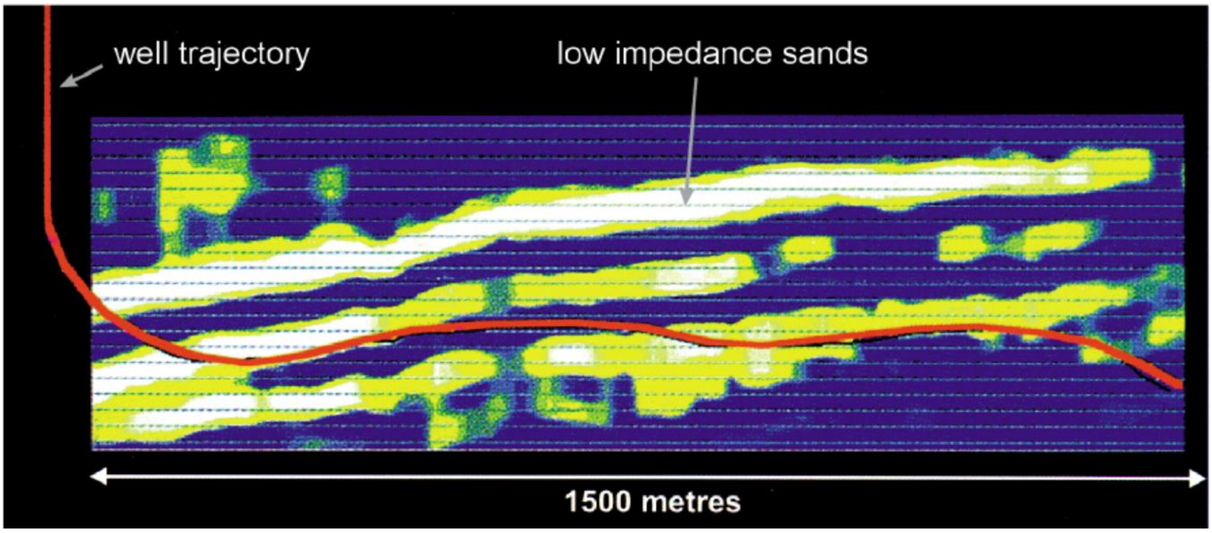

Figure 3-1. An example of the use of elastic impedance in designing a well drilling trajectory. Shown in this section, is a 30 degrees seismic inverted volume across oil-bearing reservoir sands with corresponding low elastic impedance (Connolly, 1999).

3.2 Reservoir pore fluids

This research aims to understand the seismic response associated with changes in reservoir properties in the study area caused by facies heterogeneity, that is, lateral or vertical changes in mineral composition, fluid composition, porosity, thickness, or potential combination of

`

such effects. In terms of fluid composition, there are three main pore fluids found in the Grudja reservoir rocks: water brines, hydrocarbon liquids, and hydrocarbon gases. (Batzle & Wang, 1992) concluded that seismic properties of fluids "vary substantially but systematically under subsurface pressure and temperature conditions". For instance, the Inhassoro field hosts both oil and gas deposits, and the primary reservoir is an oil rim with a gas cap. This presents a challenge in using seismic data and rock physics, especially in understanding which fluid the reservoir is saturated with, and the extent of the hydrocarbon deposit. For instance, when gas is present in substantial amounts and dissolved into light oils, it might have an effect of substantially decreasing the bulk modulus and viscosity of oil.

To model and quantify the effects of pore fluids on reservoir rocks, a multi-phase fluid substitution process is conducted. This involves the application of Gassmann's equations (Gassmann, 1951). The process outlined in Smith et al. (2003) is used in studying the behaviour of reservoir fluids in the Mozambique Basin reservoirs. An isotropic medium is assumed for simplicity and practicality of the fluid substitution process.

3.3 Amplitude variation with offset

One of the most familiar QI technologies is AVO (amplitude variation with offset) analysis. AVO is sometimes referred to as AVA (amplitude variation with angle) when considering incident angles rather than offsets. Ostrander (1984) defined the concept of AVO by stating that "the P-wave reflection coefficient at an interface separating two media varies with the angle of incident". He also showed that "the presence of gas in a sand capped by a shale would cause an amplitude variation with offset in pre-stack data". This change is sometimes related to the presence of gas in the reservoir. A linear approximation of the Zoeppritz equations (Shuey, 1985) made AVO technology to be easily applicable.

Given that the AVO analysis requires a thorough understanding of distinct changes in independent elastic properties (i.e., rock compressibility, rock rigidity, and rock bulk density) between two adjacent rock formations, there are at least 9 combinations of elastic properties that can create an AVO response. However, certain practices in the oil and gas industry have shown inconclusive AVO analysis mainly due to generalized or quick-look approaches (e.g., assuming constant bounding rock properties or using data with reduced offset ranges) that result in false-positive and misleading interpretations with significant economic implications.

`

In this regard, AVO analysis must be supported by rock physics analysis of reservoir and bounding rocks to thoroughly assess and characterize seismic responses related to the actual conditions of reservoirs and their bounding rocks (Wells, 2019). To execute a robust reservoir characterization workflow based on AVO analysis, offset gathers, AVO synthetics from well log data, and VSP stacks are integrated into the study.

AVO analysis aims to quantify changes in seismic signature caused by variations in the fluid and rock composition of a reservoir (Simm & Bacon, 2014). Key rock properties to be considered include porosity, mineralogy, and stiffness (often described in terms of bulk and shear modulus). It is also important to characterize non-reservoir sections because AVO contrasts depend highly on the cap rock response just above the reservoir. Key fluid properties to be considered are hydrocarbon and brine compressibility – related to bulk modulus since liquids are not susceptible to shearing – and density. Reservoir architecture is also an important consideration for an interpreter doing AVO analysis; this relates to morphology, layering, thickness, and lateral extent. The success of AVO analysis also depends on the usable seismic bandwidth (resolution) available and the quality of these data. There should be an adequate offset range to make AVO analysis meaningful, especially far-offset information. Therefore, it is critical to include longer offsets during the seismic survey design. Longer maximum offset also ensures that deeper targets are imaged with the maximum number of traces per common midpoint (CMP), commonly known as full-fold coverage (Cordsen et al., 2000).

Conditioned CMP gathers, with a reasonable mute function applied to remove residual events beyond critical refraction angles, clearly show offset seismic data at incident angles after a Normal Move Out (NMO) stretch is applied. These CMP gathers, commonly sorted by common offset values, are converted to angle gathers using an offset-to-incidence-angle relationship based on wave reflections in multi-layer media, a generalization of Snell's law for multiple layers:

$$sin^2\theta = \frac{x^2 V_i^2}{V_{rms}^2 (V_{rms}^2 t_0^2 + x^2)} \qquad 5$$

Where x is the offset, V_i is the velocity at the angle of incident, V_{rms} is the root mean square of the velocity, t_0 is the time at zero-offset. Using these CMP gathers, three main stacks are created based on associated offset ranges: angles from near offsets (also known as 'near angles'), angles from middle offsets (or 'middle angles'), and angles from far offsets (or 'far angles') (e.g., Figure 3-2). Sometimes an angle stack from ultra-far offsets (or 'ultra-far angles') is also

`

produced if the forward models support large angles (typically higher than 45°). Figure 3-2 is an example from (Simm & Bacon, 2014).

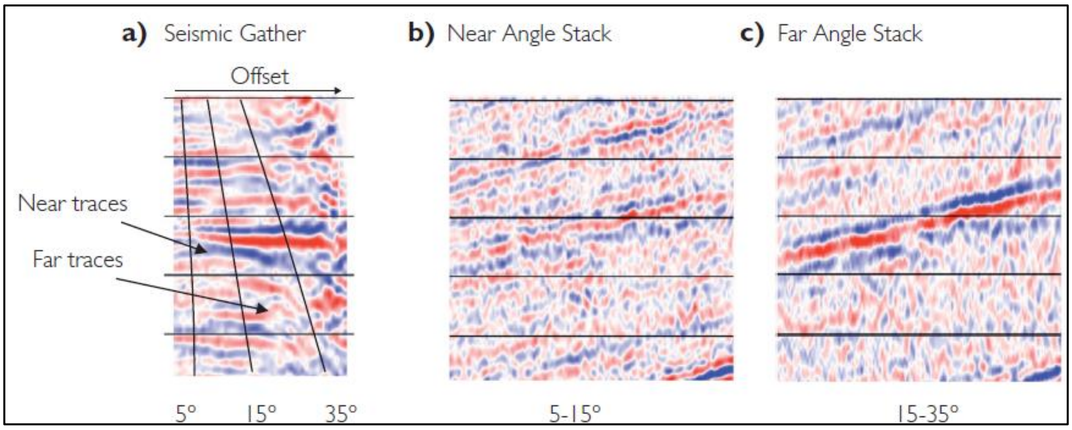

Figure 3-2. An example comparing traces from varying angle/offset ranges. a) Seismic Gather – this is a stacked gather consisting of all the angle ranges from low to high angles. b) Near Angle Stack – this is a stack of angle ranging from 5 to 15 degrees only. c) Far Angle Stack – this is a stack of angles from 15 to 35 degrees (Simm & Bacon, 2014) .

In Figure 3-2, a common-offset gather shows both near-offset and far-offset traces. Stacks for specific angle ranges (5°-15° and 15°-35°) are produced from this gather, and they show an apparent increase in the amplitude from the 'near angle' stack to the 'far angle' stack. This should be confirmed by other QI methods, such as AVO synthetics, to compare the expected changes in seismic amplitude with angle. Elastic impedance logs and inversion can also assist in confirming the AVO behaviour at different angles.

3.4 Seismic attributes

Quantitative measures of seismic attributes are used by geophysicists to understand geologic structures, stratigraphy, and rock/pore fluid properties (Chopra & Marfurt, 2005). One of the most popular attributes is seismic amplitude, which has a correlation with hydrocarbon pore fluids under certain reservoir and bounding rock conditions. "The goal of quantitative interpretation is to relate changes in amplitude to changes in rock properties" (Simm & Bacon, 2014). The seismic effects that show amplitude behaviour as a result of the change in rock and pore fluids are sometimes referred to as direct hydrocarbon indicators (DHI). Forward modelling of amplitude responses due to changes in reservoir properties, whether these are related to changes in mineral composition, fluid composition, pore distribution, or thickness, among others, is performed using borehole information and core-based rock physics models. Seismic data are also processed in a QI/AVO-compliant manner to ensure that data processing

`

steps do not reduce the character of the seismic data used for reservoir characterization purposes.

4 Seismic acquisition, processing, and interpretation

4.1 Seismic acquisition

The 3D seismic acquisition method was initially applied in offshore hydrocarbon exploration and experienced exponential growth from 1990 to 1996 (Chaouch & Mari, 2006). This growth contributed to improved subsurface imaging and reduced acquisition costs. Land 3D seismic acquisition has been developed ever since, thanks to improvements in field equipment, computer capabilities, positioning accuracy, data recording, and processing technologies. In the past, 3D seismic surveys were acquired mainly to support field development, and less frequently used as an exploration tool. Nowadays, the purpose of seismic acquisition is to acquire images from depth structures and stratigraphic sequences to better understand and characterize the subsurface geology to support exploration, development, production, and enhanced recovery processes.

Proper planning is important before embarking on a seismic acquisition campaign. This phase includes the design and testing of both geophysical and non-geophysical parameters, including a risk assessment of environmental, health, safety, and community conditions expected during the acquisition program (Chaouch & Mari, 2006). For instance, during the seismic acquisition campaign led by Sasol in Mozambique in 2016, a community liaison officer (CLO) was appointed to engage with local communities potentially impacted in advance, as well as to communicate and educate on the social and economic benefits expected from seismic acquisition programs. Enumerators or blue-carding staff were also tasked with the evaluation of potential compensation or resettlement claims within the extent of the seismic survey as needed.

One of the key considerations of a fit-for-budget seismic design and parameter optimization is the cost-benefit balance. Highly dense parameters may potentially enhance subsurface imaging quality, but their related acquisition costs might be prohibitive, and their environmental impact and safety risks increase. Conversely, coarsely gridded surveys might be less expensive to acquire at the expense of compromised imaging quality and subsurface requirements. To reach a balance, a cost-benefit analysis is necessary to ensure a fit-for-budget survey is designed to

`

maximize quality output, minimize impacts, and remain within a pre-approved acquisition budget (Cordsen et al., 2000).

3D Seismic acquisition program in the Inhassoro Field

The Inhassoro field is located in the Mozambique Basin which occupies the broad coastal plain and continental shelf of Southern Mozambique, and its Grudja reservoirs contain both oil and gas accumulations (Sasol, 2015). Figure 4-1 shows the location map of the Inhassoro field of the Mozambique basin, the 3D seismic survey, and key wells used in this study. The mature dry gas in neighbouring Pande and Temane fields is postulated to be from a distant kitchen in the Zambezi depression. Conversely, basin maturity modelling suggests that liquid hydrocarbons from the Grudja G6 and G10 reservoirs in Inhassoro migrated from a nearby sub-basin or secondary kitchen composed of relatively less mature source rocks, and the G6 reservoir was filled with gas from both kitchens resulting in an oil rim with a gas cap (Sasol, 2015).

The Inhassoro 3D seismic survey acquired by Sasol onshore Mozambique in 2016 covers an area of approximately 125 sq.km (Figure 4-1). This survey was designed to characterize both G6 and G10 gas reservoirs from the Cretaceous Grudja formation by imaging faults, delineating reservoir extents, and mapping reservoir properties to support the next tranche of development wells (Wells, 2016). The seismic survey was designed as a fit-for-budget program using an orthogonal layout with a seismic source interval of 50 m, source line spacing of 300 m, seismic receiver interval of 25 m, and receiver line spacing of 200 m. All source points falling within 500 m from the coastline with the Indian Ocean were removed from the final survey outline to protect this environmental habitat. To maintain a safe acquisition operation, minimum setback distances were defined based on a seismic source risk assessment and benchmark study, whereby source points were positioned 50 to 100 m away from existing water bodies and settlement infrastructure (Wells, 2016). Bush clearing or debushing is also often required to enable seismic vibrators to drive through source lines in the field. To comply with minimum setback distances, the actual source line layout may not always conform to the original field layout, but forward modelling using seismic design software ensured that imaging objectives and data quality were not compromised. Likewise, environmental features such as sacred sites and critical habitat areas of protected and endangered species were identified in the Inhassoro area during the survey design phase, and due to their high sensitivity, a substitution

`

of seismic sources was necessary using accelerated weight drops (AWD), albeit lower in power and drive, to generate an acceptable seismic signal strength. The AWD has an assembly weight of 750.2 kg, a hammer weight of 207.9 kg, and a baseplate weight of 104 kg.

The Inhassoro Central 3D seismic design targeted depths of about 3000 m with a nominal image fold coverage of 54 to image the Grudja G10 reservoir extent and the Eastern G6 oil rim boundary. Existing 2D surveys in the area provided a good reference and insight into how seismic waves propagate through clastic sediments across the Inhassoro block. In areas with no seismic coverage, seismic forward modelling was necessary to understand and assess the expected subsurface imaging quality. To achieve the survey objectives of the Inhassoro Central 3D survey, source stations were located 50 m apart and receivers were spaced every 25 m. The survey's maximum offset coverage was 3150 m with an inline-to-crossline aspect ratio of 61% (Wells, 2016). With these parameters, this seismic survey guided and supported well placement decisions made as part of the Inhassoro field development plan. Table 1 summarises the acquisition parameters of the survey.

Onshore seismic acquisition projects often require line clearance or debushing depending on the surface conditions. In the Inhassoro Central 3D seismic survey, a 4 m source clearance was required using dozers to grant field access to Vibroseis trucks. 40% of all seismic sources were placed along existing roads that did not require line clearing, and 33% of source lines located across the Critical Habitat Area (CHA) were cleared using only a 2 m line clearance to grant access to Accelerated Weight Drops (AWD) with smaller dimensions than Vibroseis trucks (Barkwith & Wells, 2017). Nonetheless, this source arrangement compromised shallow seismic imaging in areas where vibroseis source points were removed to comply with environmental restrictions. Shallow seismic imaging is essential for accurate static signal corrections, shallow velocity analysis, and well-to-seismic ties during data processing and interpretation (Wells, 2016). Nonetheless, the acquisition parameters designed for this survey ensured that deep events were adequately imaged for structural interpretation, reservoir delineation, and reservoir characterization purposes (Wells, 2016). In summary, the data available for this study include:

- 125 km^2 of 3D seismic data and various 2D seismic data vintages from 1990 to 2019.

`

- Wells (I-1, I-2, I-3, I-4, I-5, I-6, I-7, I-8, I-9/9Z, I-10/Z, I-11, I-12, I-13, I-14, PSA-I-15, PSA-I-16, PSA- I-17, PSA-I-18/Z/Y, PSA-I-19, PSA-I-20, PSA-I-20/Z, PSA-I-21, Temane-14, Temane-18 and Temane-19A).
- PSA-T-27, and other wells in Pande and Temane that will benefit the study.

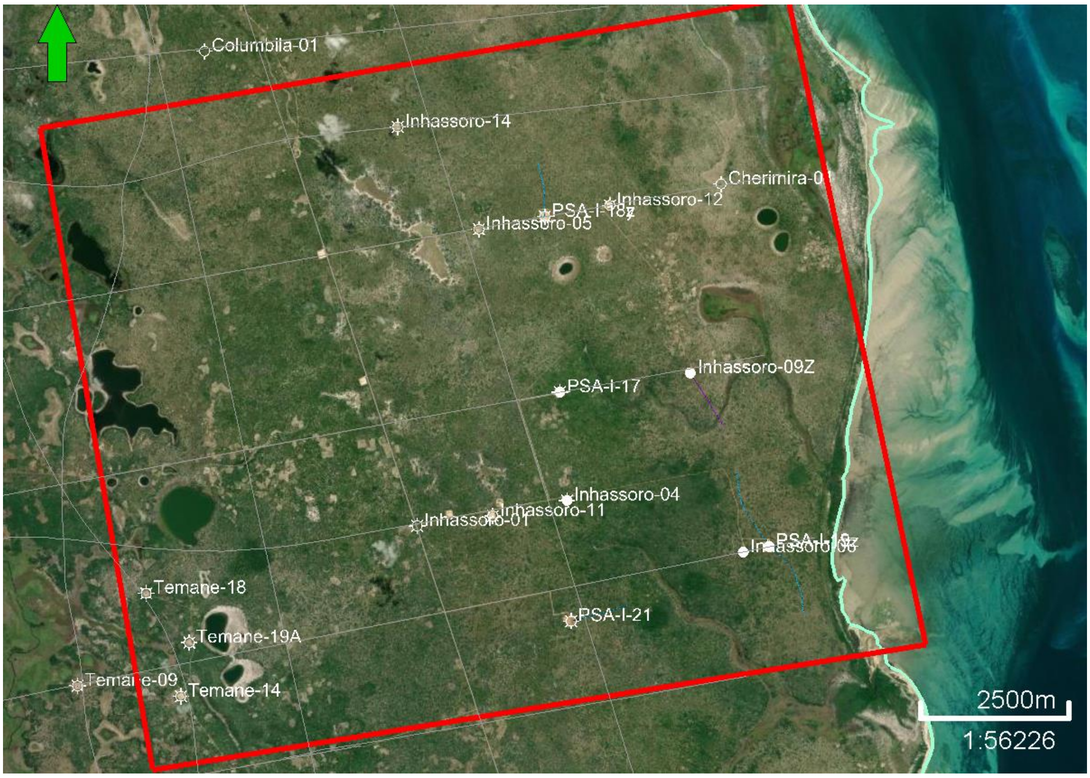

Figure 4-1. Map of the Inhassoro part of the Mozambique Basin showing the 3D seismic survey outline (red polygon). This seismic survey covered an area of approximately 130 km^2. The white starred dots represent boreholes drilled within and near the seismic survey.

Table 1. Inhassoro Central 3D seismic acquisition parameters (Wells, 2016).

Source Parameters		**Receiver Parameters**	
Station interval	50 m	Station interval	25 m
Line interval	300 m	Line interval	200 m
Max. length	10.6 km	Max. length	13.2 km
Max. width	12.6 km	Max. width	10.6 km
Source type	Vibroseis	Receiver type	Geophone (Circular array)
Unit/Station	2	Geophones/Station	6
Sweeps/Station	2 or 4	Swaths to roll	6
Sweep type	Linear	Active stations	216 nominal
Sweep bandwidth	6-112 Hz	Active lines	12 nominal
Sweep length	12 or 16 s	Max offset	3153.6 m

`

Record length	6 s	Patch aspect ratio	61.40%
Sample rate	2 ms	Total nominal fold	54
Total stations	8416 nominal	Total stations	25948 nominal
Total lines	43 nominal	Total lines	54 nominal
Total nominal length	420.6 km	Total nominal length	648.7 km
Total nominal area	126.24 sq.km	Total nominal area	129.74 sq.km

4.2 Seismic processing

4.2.1 Introduction

Three principal sequences in seismic data processing make up the foundation of subsurface imaging: deconvolution, stacking, and migration (Yilmaz, 1987). Deconvolution is conducted in the time domain to improve the temporal resolution of a signal by compressing a basic wavelet representative of the bandwidth of a seismic source signal to resemble a spike (Yilmaz, 1987). Stacking also compresses seismic data in the offset domain, therefore reducing data gathered from multiple offsets at each subsurface location to a single zero-offset stacked trace and increasing its signal-to-noise ratio (Yilmaz, 1987). The stacked seismic volume is then migrated to place all seismic energy across their true locations in the subsurface and enhance the lateral resolution of the final image. This is achieved by collapsing seismic diffractions and displacing dipping events (Yilmaz, 1987). Migration can be performed either pre-stack or post-stack, depending on whether spatial or vertical imaging enhancements are expected, respectively.

4.2.2 Seismic processing program in the Inhassoro Field

The Inhassoro Central 3D survey was processed between August and December 2016 by TEEC GmbH Isernhagen (TEEC), a service provider of Common Reflection Surface (CRS) true-amplitude seismic processing services. The processing workflow executed by TEEC during production is shown in Table 2. The seismic data were processed using CRS processing to go beyond the conventional common midpoint (CMP) processing approach and maximize the use of reflected and diffracted energy prestack to generate 3D seismic images from a coarsely gridded seismic layout over a refined, regularized 3D subsurface grid. This data processing approach helped to support the development of Inhassoro’ s G6 and G10 reservoirs. The resulting seismic volume was interpreted to provide a 3D structural framework, guide the placement of infill wells, and de-risk oil and gas extents across the field. The 3D survey was acquired along 9 swathes (Figure 4-2). Swaths 3 to 6 were acquired and processed in advance for quick-look interpretation. The final product included all swaths 1 to 9.

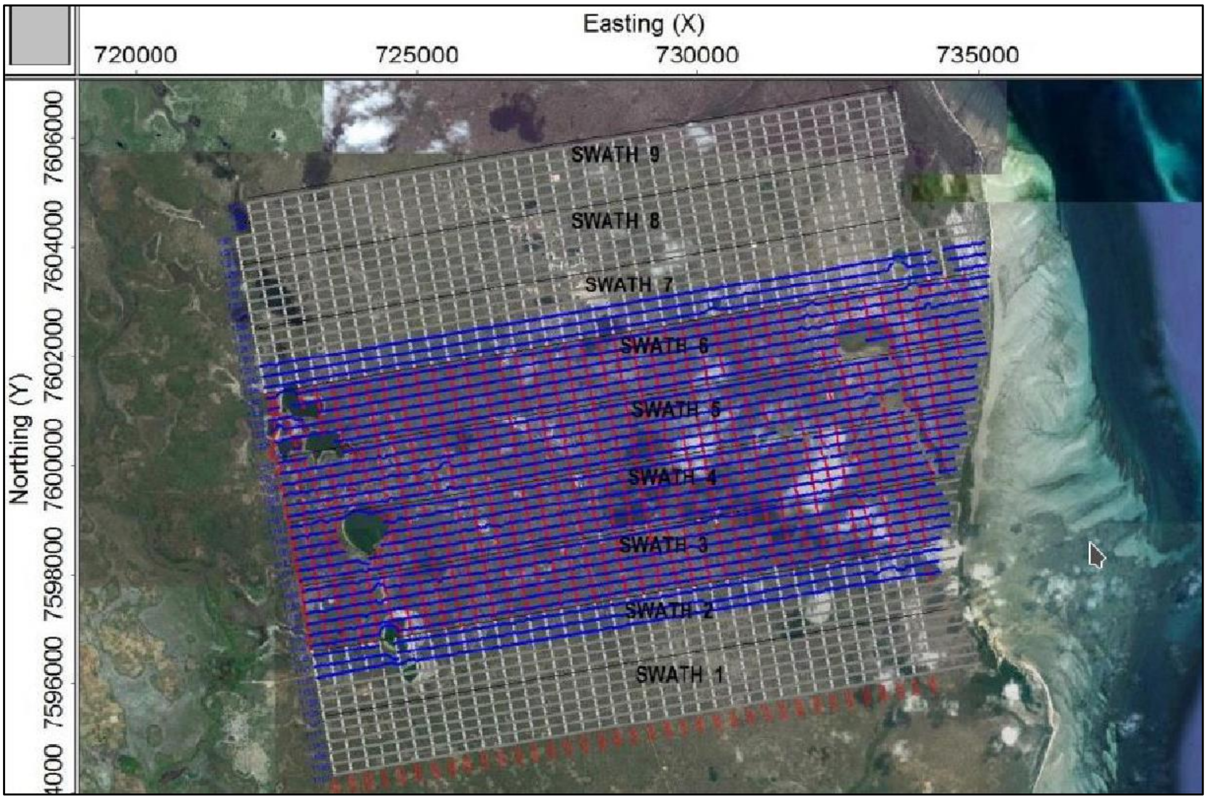

Figure 4-2. Inhassoro Central 3D seismic data. The seismic survey was acquired in 9 swaths. The gaps inside the survey area were due to obstacles like dams, or environmentally sensitive areas.

Table 2. Inhassoro Central 3D seismic data processing workflow applied by TEEC GmbH Isernhagen (TEEC) during the production of seismic data stacks.

Steps	Parameter
1	Data loading and geometry setup
2	Seismic and SPS (positioning) merge
3	Matching of vibroseis and AWD (accelerated weight drop) source wavelets
4	Time resample to 4 ms
5	Spherical divergence correction
6	Automatic suppression of noisy traces
7	Linear noise attenuation
8	Residual noise attenuation

`

9	Surface Consistent Amplitude Correction
10	Surface Consistent Predictive Deconvolution
11	First break picking and refraction statics calculation.
12	Refraction statics (single velocity layer refraction statics) application to floating datum
13	Stacking velocity analysis and residual statics calculation (2 passes)
14	Phase-only inverse Q (attenuation) compensation
15	CRS processing and CRS gather output
16	Velocity analysis
17	3D Curved Ray Kirchhoff Prestack time migration and shift to final datum 0 m, 100 ms bulk shift prior to PreSTM
18	Residual Moveout Correction
19	Radon demultiple
20	Automatic Gain Control (AGC)
21	Angle Mute (full, near, mid, and far) and stack
22	Amplitude-only inverse Q compensation
23	Scaling
24	FK (velocity-driven) filter
25	Bandpass filter
26	Application of Zero phase filter
27	SEGY output

Special attention was paid to short and long wavelength statics corrections, two of the most intricate processes usually required in the onshore seismic data processing. These corrections were necessary to “compensate for variations in elevation, near-surface low-velocity layer (weathering) thickness, weathering velocity and/or reference to the datum” (Sheriff, 2002). The parameters in Table 3 were used for computing the final 3D refraction statics solution.

`

Table 3. Parameters used for computing the final 3D refraction statics solution.

Offset range for first break picks	0-2000 m
Weathering layer (V0)	Variable V0, derived from production records
Replacement Velocity (Vr)	2800 m/s
Processing datum	0 ms

A unique feature of this processing sequence was the adoption and use of a common reflective surface (CRS) approach, which is a macro model-independent method performed in the time domain (Otto & Schueter, 2017). The CRS method was developed by Dr. Peter Hubrel and his research team at the University of Karlsruhe in Germany in the early 1990s. This processing method has advantages over CMP-based and Dip Move Out (DMO)-based methods in terms of better imaging of dipping reflectors and improved imaging in low-fold areas, a useful approach given the compromised fold coverage in some areas of the survey due to environmental restrictions. DMO process is a dip-dependent moveout correction that enables reflections from both horizontal and dipping reflectors to be stacked with the same NMO velocity (Hall, 1984). Figure 4-3 shows the graphical representation of differences between the CRS method and other conventional seismic data processing methods.

`

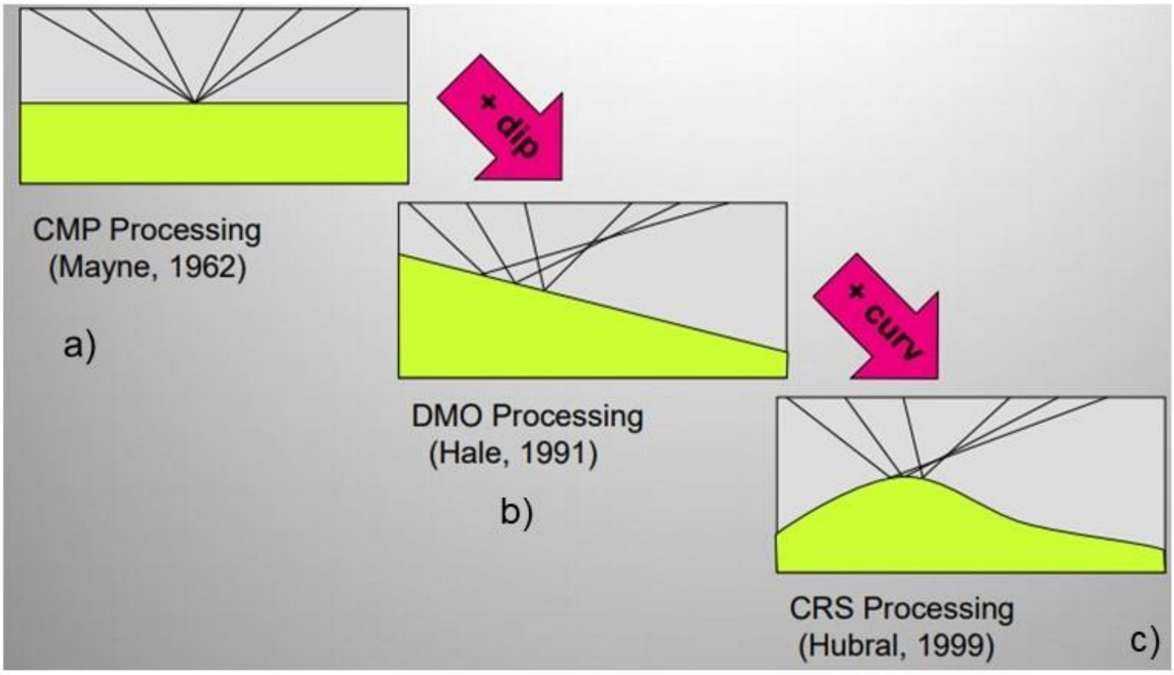

Figure 4-3. CRS method compared to other common processing methods. a) A schematic of seismic processing using the CMP method, b) a schematic of seismic processing using the DMO method, and c) a schematic of seismic processing using the CRS method (TEEC, n.d.).

The final seismic processing products included: full-stack data, partial angle stacks, migrated gathers, and stacking velocities. The partial angle stacks help in qualitatively analysing the effects of amplitudes concerning variations in incident angle. These stacks were defined using the following angle ranges:

- **Full offset:** 5-35 degrees
- **Low angle:** 5-15 degrees
- **Mid angle:** 15-25 degrees
- **High angle:** 25-35 degrees.

All the parameters used during the data processing sequence are summarized in a standard SEGY output format, and these can be accessed on its EBCDIC header. EBCDIC stands for Extended Binary Coded Decimal Interchange Code, introduced by IBM (Sheriff, 2002).

`

4.3 Seismic interpretation

Seismic data interpretation (Figure 4-4) was conducted using Schlumberger's Petrel software. Seismic and well data are hosted in an internal database called Petrel Studio. Seismic data consist of both full and angle stacks, as well as prestack seismic gathers and seismic velocity volume. Well data include well elastic logs and velocity information in the form of checkshots and Vertical Seismic Profiles (VSP) where available. The VSP measures vertical profiles of rock properties, mainly velocities, attenuation, and anisotropy, and it is also a vertical seismic imaging tool (Stewart, 2001). Recent well data acquired during the well drilling campaign in Inhassoro in 2016 contained VSP data useful to convert geologic depth tops on seismic data into two-way time stamps with high confidence. The well-to-seismic ties performed also ensured the correct depth positioning of all penetrated reservoirs. Lower Grudja horizons mapped included: G6, G7, G8, G9, G10, G11, G11A and G12. Some of the mapped horizons used to understand the structure and qualitative understanding of seismic amplitudes.

Time domain slices are useful seismic amplitude displays corresponding to a constant time stamp over a grid of data points. In other words, time slices are horizontal sections extracted from a 3D seismic volume (Sheriff, 2006). Time slices differ from horizon slices, sometimes referred to as geologic time slices, given that horizon slices are extracted along a horizon, that is, an interpreted surface following a geological marker with variable timestamps across the seismic 3D grid. Time slices are useful displays to understand geologic facies and stratigraphy, particularly to bring a qualitative understanding of amplitude behaviour around a reservoir. This interpretation is later confirmed through analysis of well information and quantitative interpretation of seismic data, which include analysis of angle stacks and gathers.

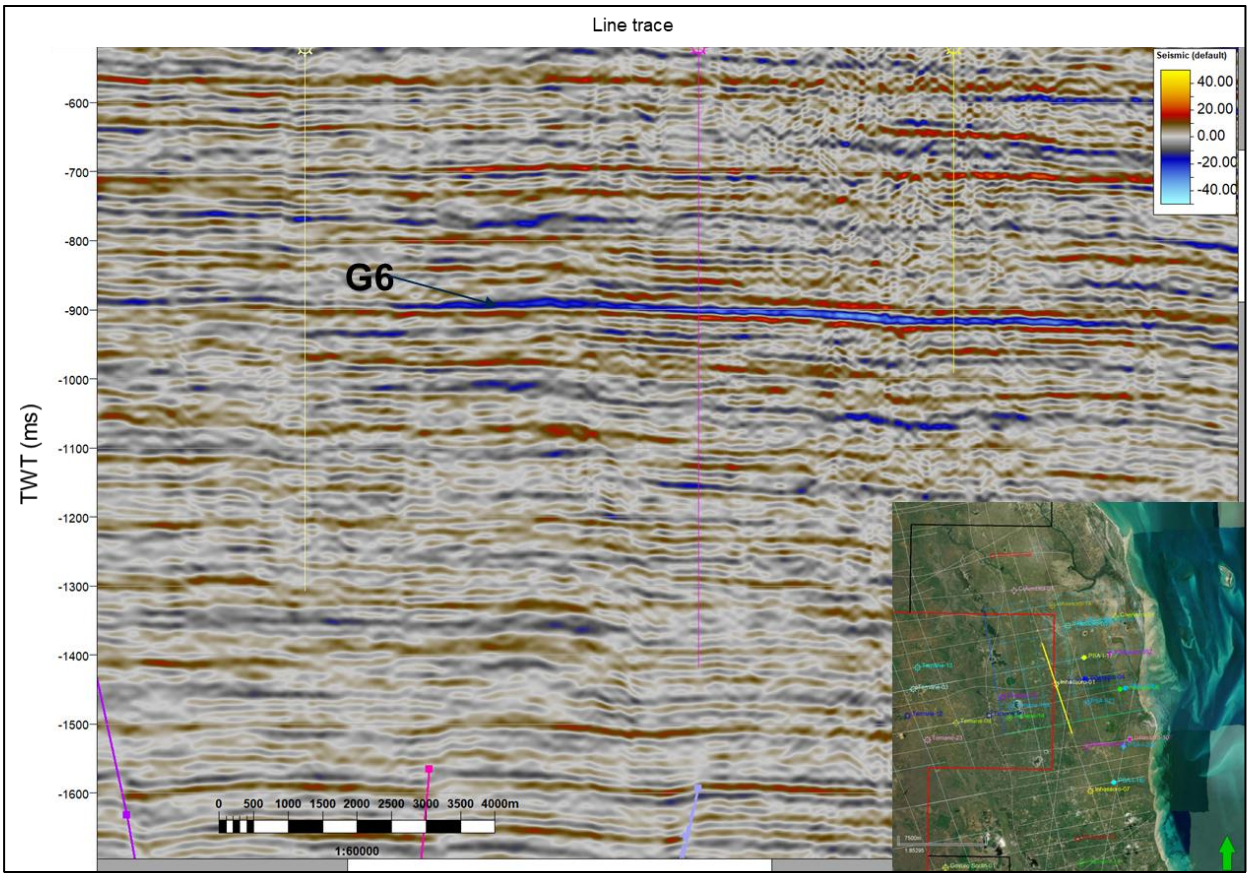

Figure 4-4. The seismic data line (AMT98-01) in the Inhassoro field. Lower Grudja reservoir levels can be observed around -900ms to about -1300ms. G6 reservoir is easy to identify on seismic data and has been confirmed through well to seismic tie. Vertical lines in yellow and purple show projections of where some of the wells have been drilled. The inserted base map shows the position of the seismic data line in the field.

4.3.1 Grudja G6

In the Inhassoro field, the top of Grudja G6 (Figure 4-5) is a reservoir marker relatively easy to identify on seismic data, unlike other reservoirs. Qualitative extraction of RMS (root mean square) amplitudes from angle stacks suggests an increase in amplitude with offset (AVO) characteristic of porous gas clastic sequences. Grudja G6 is a hydrocarbon-filled reservoir containing an oil rim with a gas cap. The G6 reservoir was mapped on full stack post-migrated seismic data following a trough, and amplitudes extracted from this horizon represent soft reservoir facies (Figure 4-6). Surface attributes were extracted from volumes of varying angle ranges (low to high angle) to understand the amplitude response of the G6 reservoir (Figure 4-7a-c). The 3D seismic volume enables visualisation of the data from different vantage points. This includes time slices above and below the reservoir of interest. Figure 4-8a, b shows amplitude distribution above the reservoir at -832 ms and -836 ms two-way time. The G6

`

reservoir distribution is delineated by anomalous amplitude as can be observed in Figure 4-9 a, b and Figure 4-10a, b.

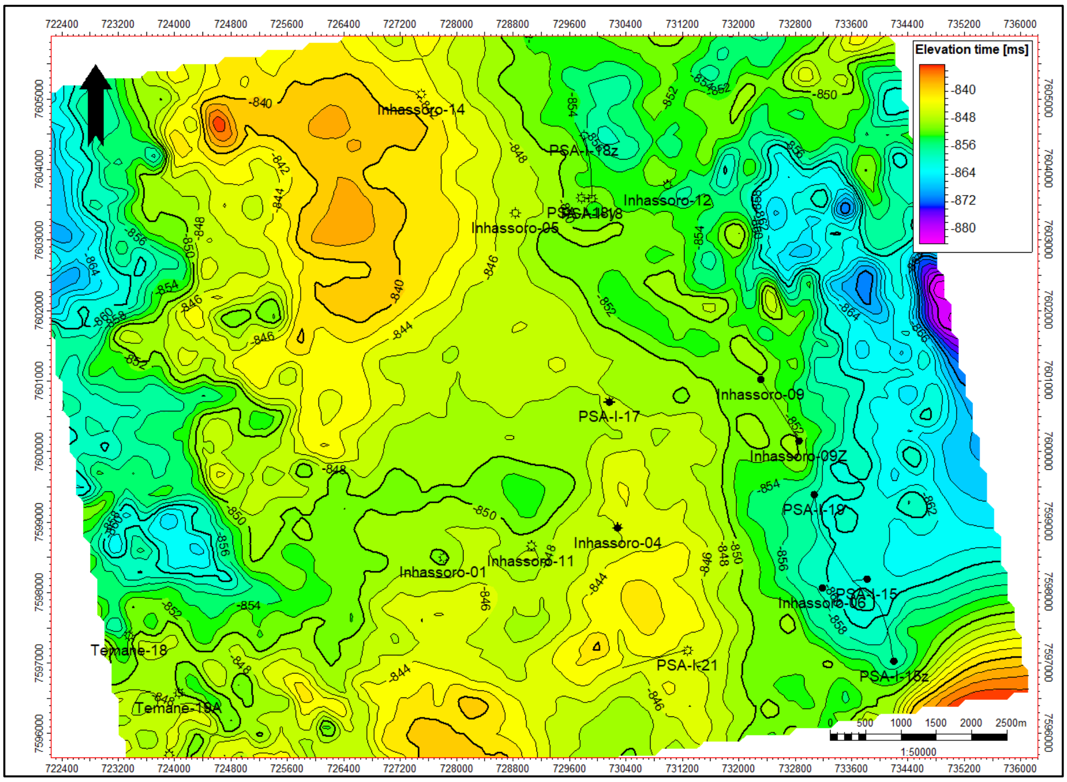

Figure 4-5. G6 two-way time structure map created by gridding the mapped G6 horizon on Inhassoro Central 3D seismic data through a convergent gridding algorithm. The generic structural trend of the G6 surface is a gentle dip towards the east. The G6 falls within -800 to -900 ms two-way time as indicated by the colour bar on the top right. Wellbores are annotated in white and represent all the wells that penetrated the G6 reservoir. The map has a contour interval of 2 ms. 2D lines are in grey and demonstrate the rationale for the position of well logs drilled before the 3D seismic survey.

`

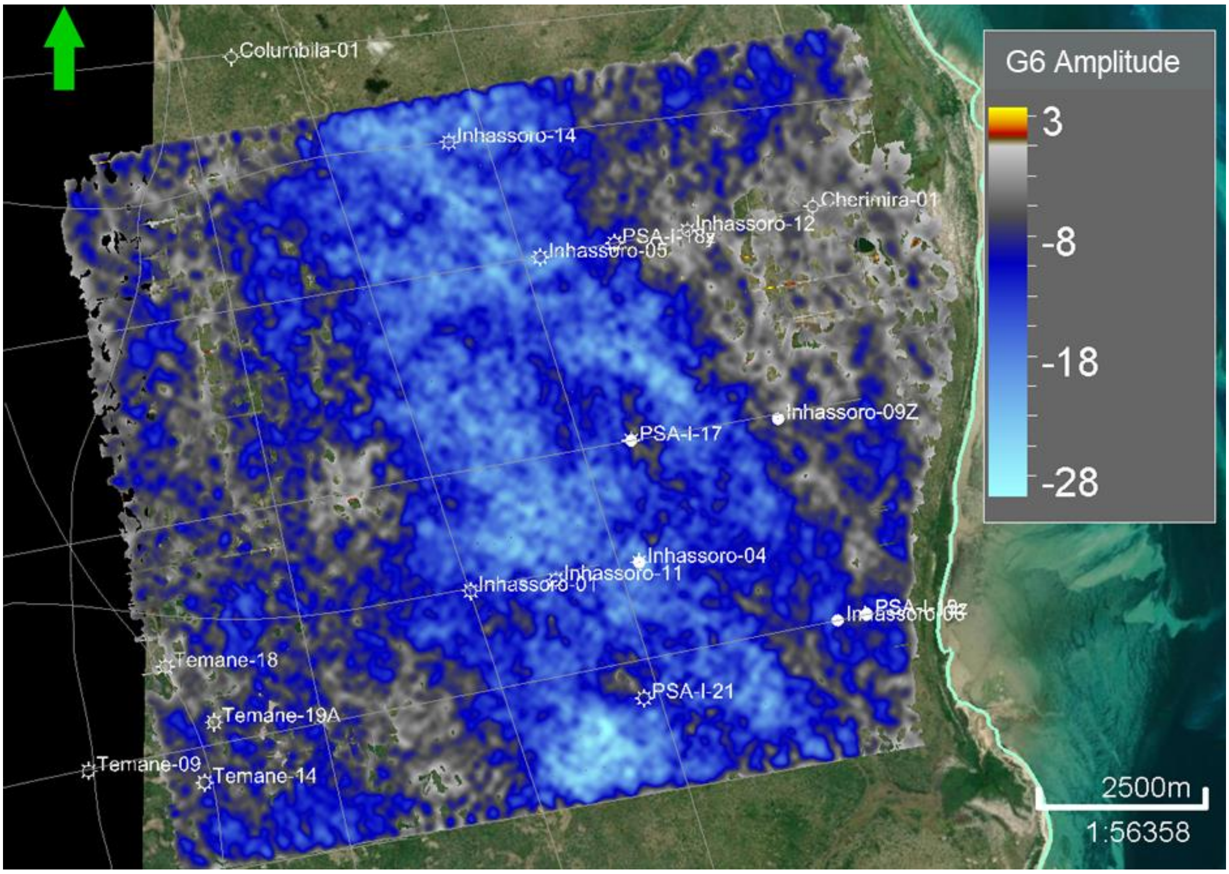

Figure 4-6. G6 amplitude auto-tracked on full-stack seismic data. The G6 horizon was mapped as a soft, on negative amplitude, thus mainly negative amplitude values on the auto-tracked map. 2D lines are in grey and demonstrate the rationale for the position of well logs drilled before the 3D seismic survey. Amplitude extracted only from the 3D seismic volume.

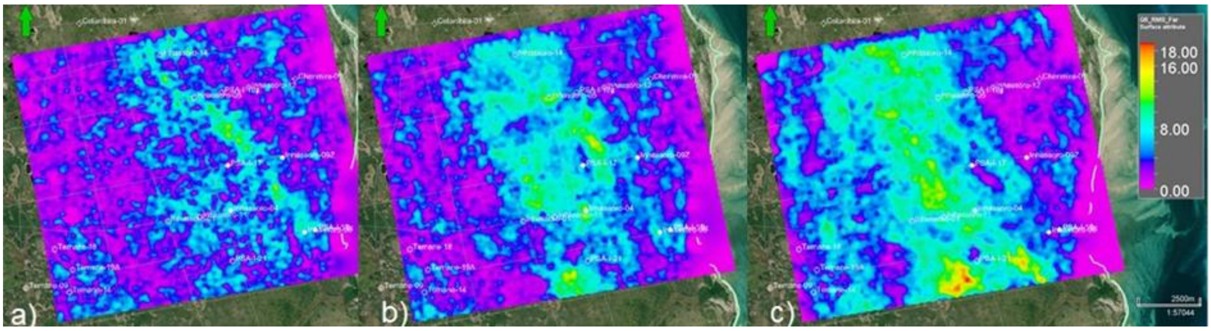

Figure 4-7. G6 surface attribute. a) Root Mean Square (RMS) amplitude information extracted from G6 horizon using seismic angles stack of (5 -15^{0}). b) Amplitude information extracted from the G6 horizon using seismic angles stack (15-25^{0}). c) Amplitude information extracted from G6 horizon using seismic angles stack of (25-35^{0}).

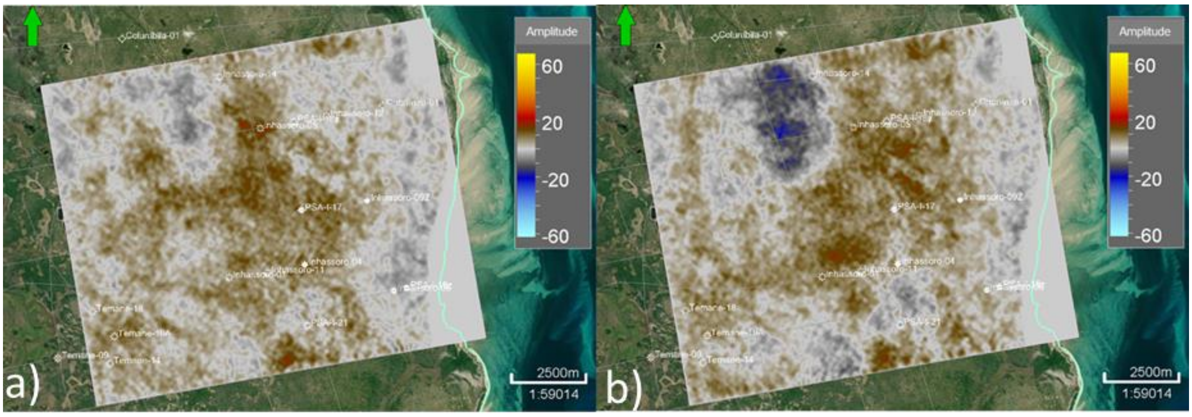

Figure 4-8. Time slices above the G6 reservoir show amplitude distribution. A time slice is a horizontal slice through a 3D seismic volume. It displays amplitude at the specified two-way time level. Time slices are useful displays to understand geologic facies, and stratigraphy and bring a qualitative understanding of amplitudes around a reservoir. Time slices enable a quick way to evaluate changes in amplitude seismic data. a) Time slice at -832 ms above the G6 reservoir. b) Time slice at -836 ms. Amplitude values range from -60 ms to 60 ms.

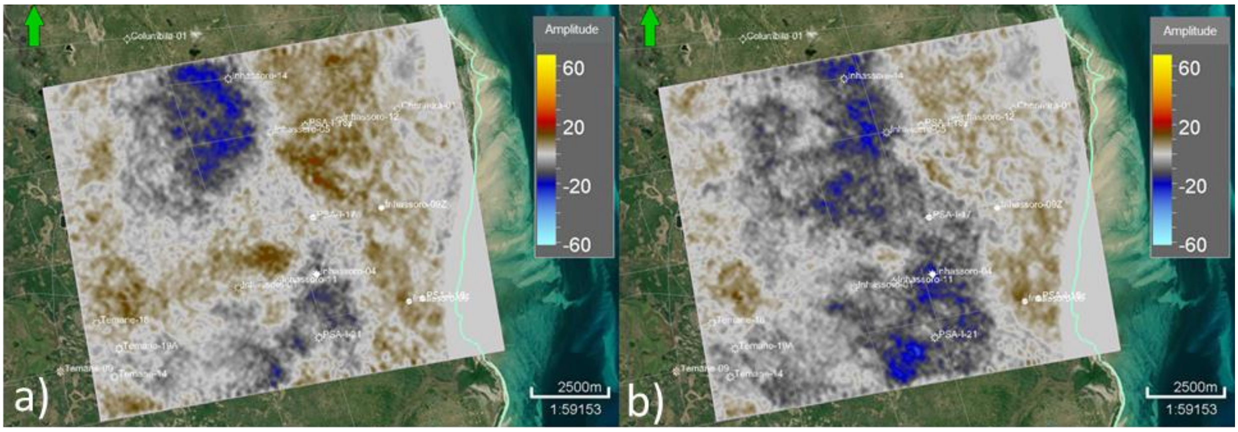

Figure 4-9. Time slices around the G6 reservoir show amplitude distribution. Time slices are useful displays to understand geologic facies and stratigraphy and bring a qualitative understanding of amplitudes around a reservoir. a) Time slice at -840 ms. b) Time slice at -844 ms.

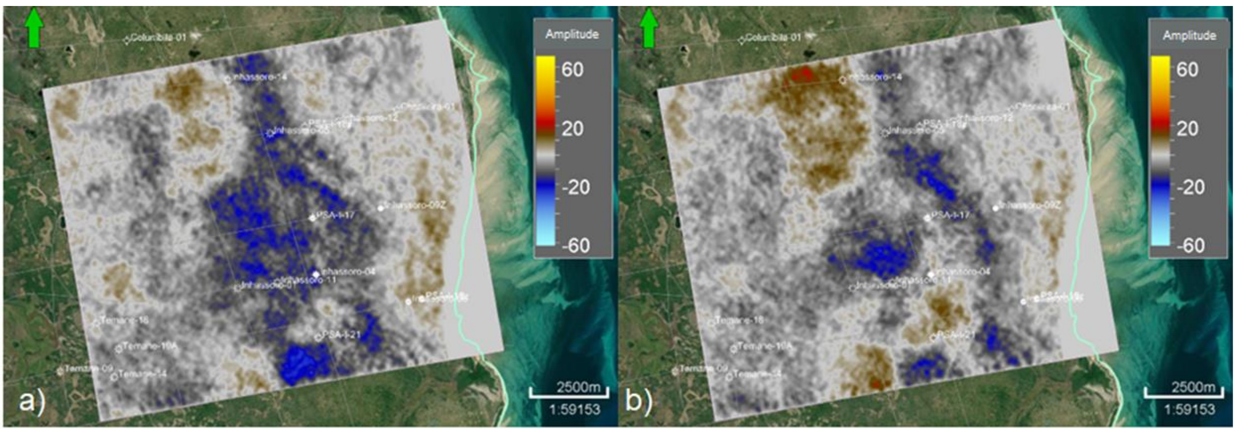

Figure 4-10. Time slices around the G6 reservoir show amplitude distribution. Time slices are useful displays to understand geologic facies and stratigraphy and bring a qualitative understanding of amplitudes around a reservoir. a) Time slice at -848 ms, and b) time slice at -852 ms.

4.3.2 Grudja G8

The Grudja 8 reservoir is not known to contain hydrocarbons in Inhassoro. However, there are amplitude-supported leads that can be investigated quantitatively. In the neighbouring field, Temane, Grudja 8 is a gas-filled reservoir, and its possible extension into Inhassoro remains to be investigated. Figure 4-11 is a G8 reservoir two-way time surface map created from 3D seismic data showing the G8 structure depth in time. Attributes were extracted at the G8 reservoir level based on the mapping from the full stack seismic data. These extractions include autotracked seismic amplitude, Figure 4-12, which shows the minimum amplitude information since the reservoir horizon was mapped on a trough which represents a soft seismic response, and RMS Amplitude extractions on angle stacks (Figure 4-13a-c). 3D seismic cube enabled the evaluation of data through a time slice (Figure 4-14). Time slice around G8 two-way time in Inhassoro doesn't reveal anomalous amplitudes to warrant further analysis.

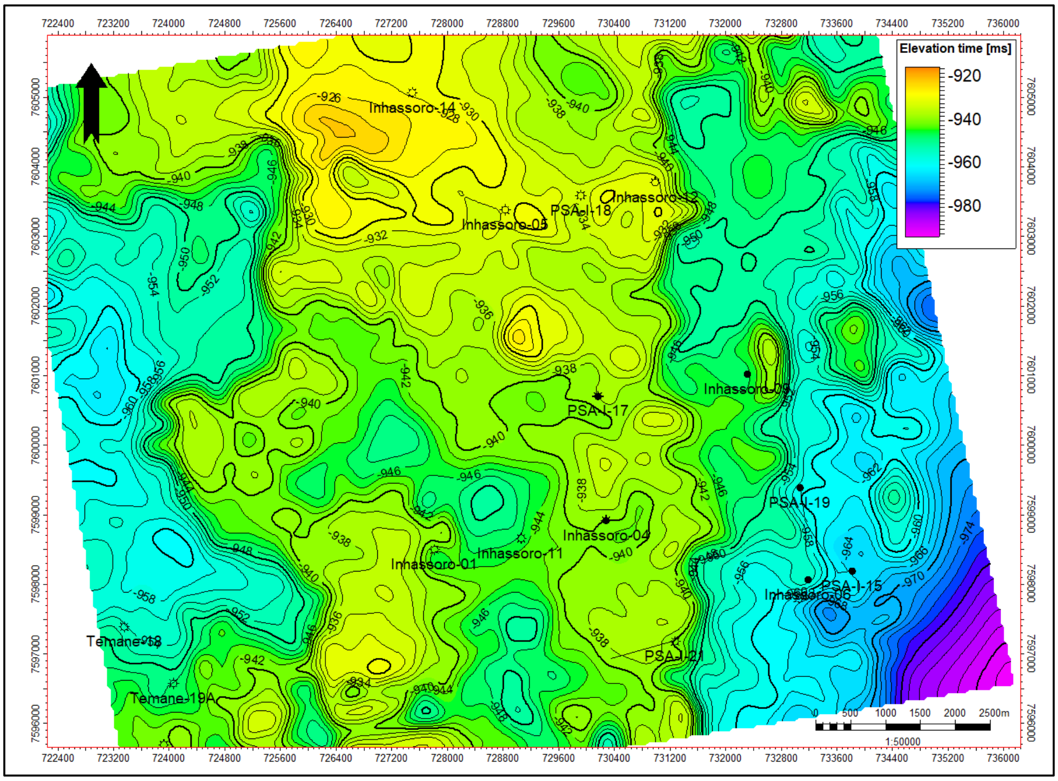

Figure 4-11. G8 two-way time structure map. This map was produced by gridding the G8 horizon that was mapped on a two-way time seismic section. The G8 structure is between -900 and -1000 ms two-way time. Boreholes are shown in white. The shoreline is shown in aqua colour.

`

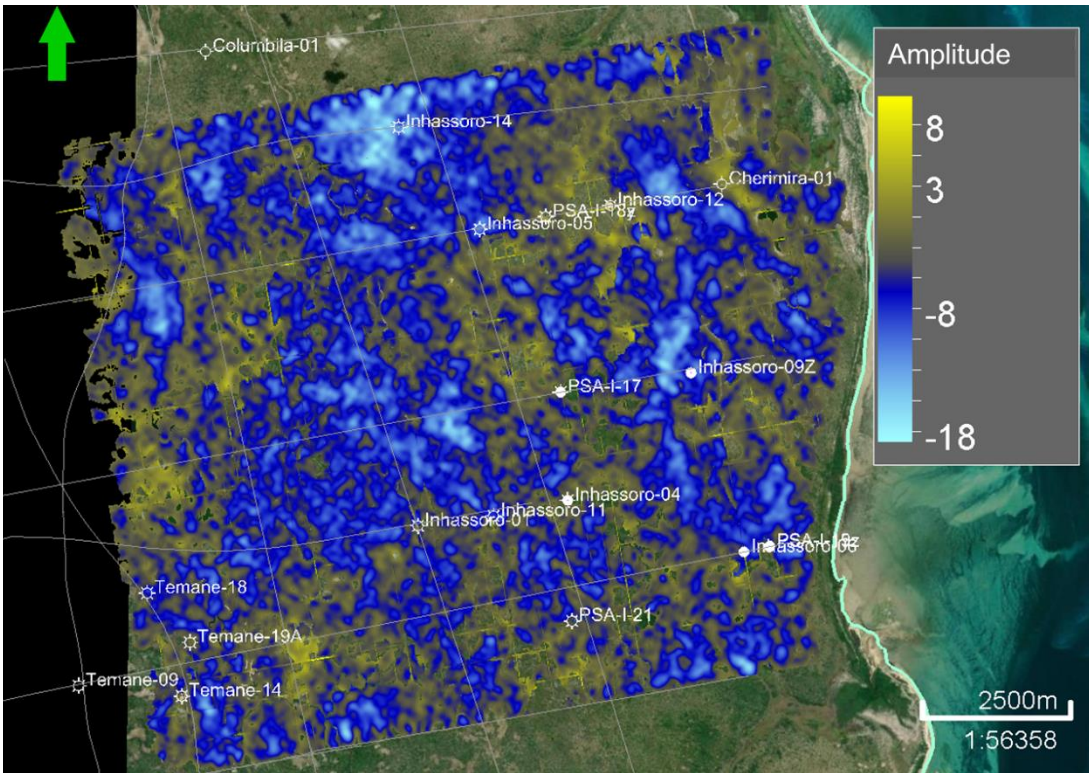

Figure 4-12. G8 auto-tracked amplitude on full-stack seismic data. Boreholes are shown in white and the shoreline on the right is shown in aqua colour. 2D lines are in grey and demonstrate the rationale for the position of well logs drilled before the 3D seismic survey. Amplitude extracted only from the 3D.

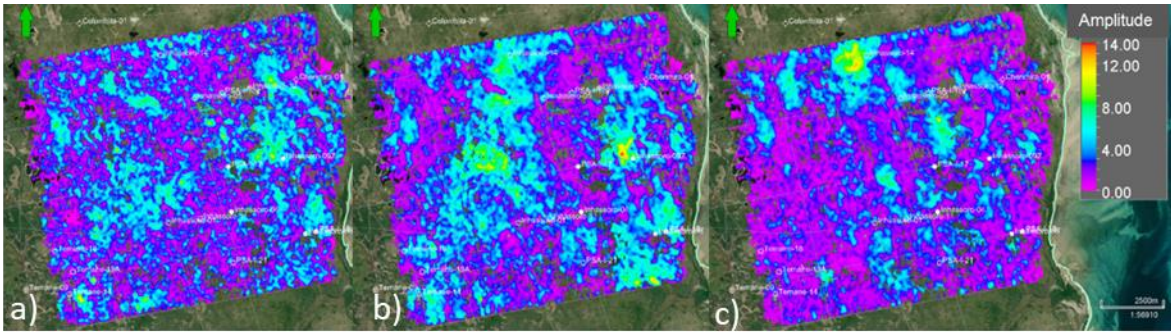

Figure 4-13. G8 surface attribute. a) Root Mean Square (RMS) amplitude information extracted from G8 horizon using seismic angles stack of (5 -15^0). b) Amplitude information extracted from G8 horizon using seismic angles stack (15-25^0). c) Amplitude information extracted from G8 horizon using seismic angles stack of (25-35^0).

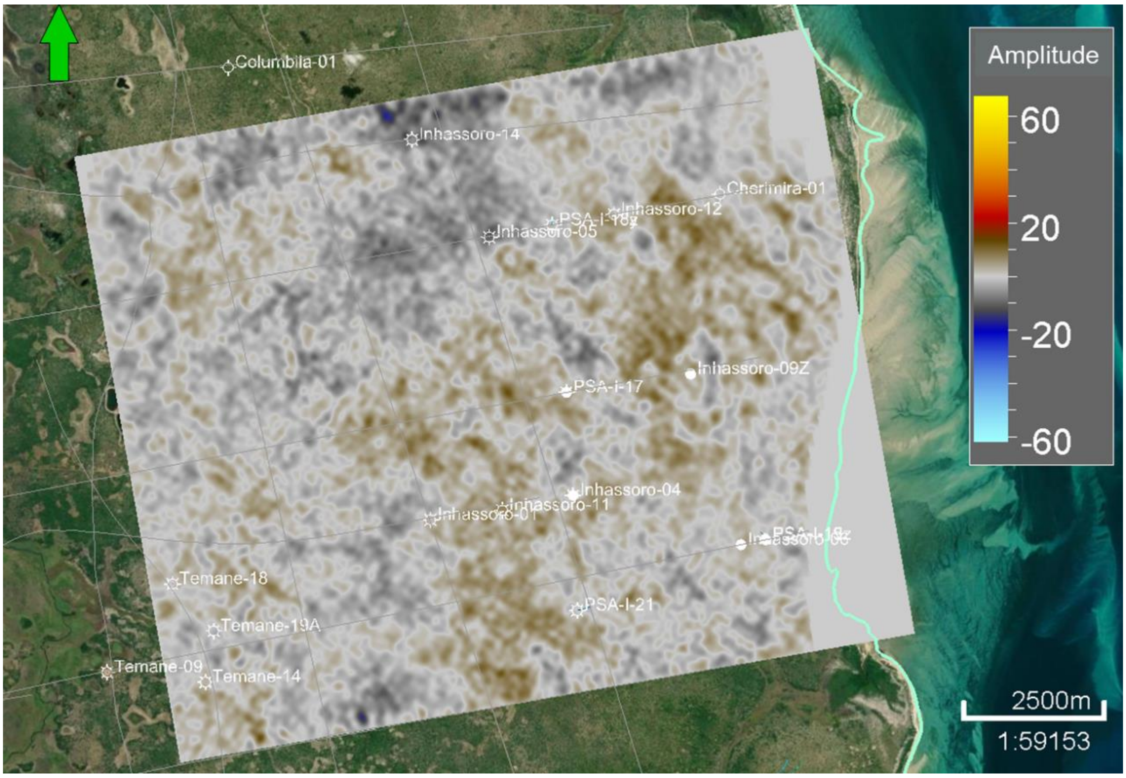

Figure 4-14. Time slice around the G8 reservoir. Time slices are useful displays to understand geologic facies and stratigraphy and bring a qualitative understanding of amplitudes around a reservoir. There is no visible anomalous amplitude at this level. The horizon slice did however show some amplitude anomalies, although it is not clear if they are lithology or fluid related at this reservoir level.

4.3.3 Grudja G9

The Grudja 9 (G9) is the main reservoir in Temane, which extends into Temane East. The Inhassoro 2016 3D seismic survey covers some parts of the Temane East block, and the Grudja 9 reservoir can be identified by its anomalous amplitude response. Standard maps to understand the reservoirs are shown in Figure 4-15 to Figure 4-18, including the two-way time map (Figure 4-15), amplitude extraction map from full stacks seismic data (Figure 4-16) and amplitude extraction derived from angle stacks (Figure 4-17a-c). These maps demonstrated that the G9 amplitude is mainly confined to the southwestern corner of the 3D cube, the Temane East area. The minimum amplitude from the full stack is not a good attribute for delineating this reservoir at the G9 level. RMS amplitude extraction, Figure 4-17, is a better Direct Hydrocarbon Indicator (DHI) since the results of wells in the area with anomalous amplitude are known. Time slices (Figure 4-18a, b) between -976 ms and – 984 ms capture the G9 reservoir.

`

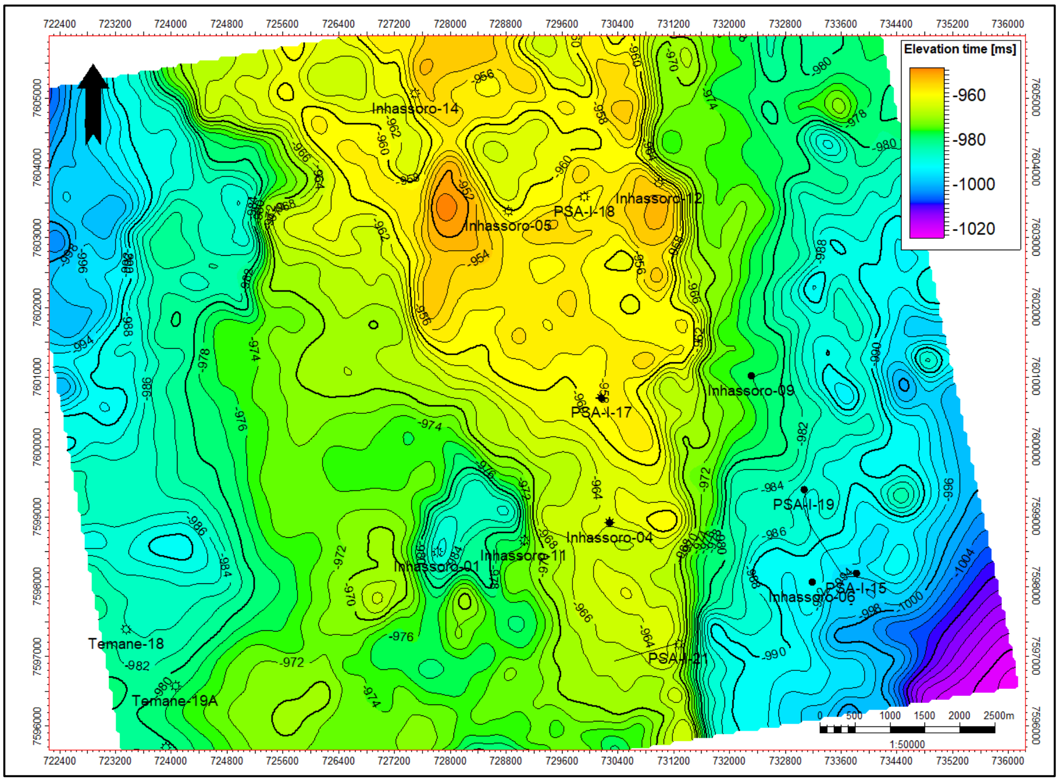

Figure 4-15. G9 two-way time structure map. This map was produced by gridding the G horizon that was mapped on a two-way time seismic section. The G9 structure is between -900 and -1050ms two-way time. Boreholes are shown in white. The shoreline is shown in aqua colour.

`

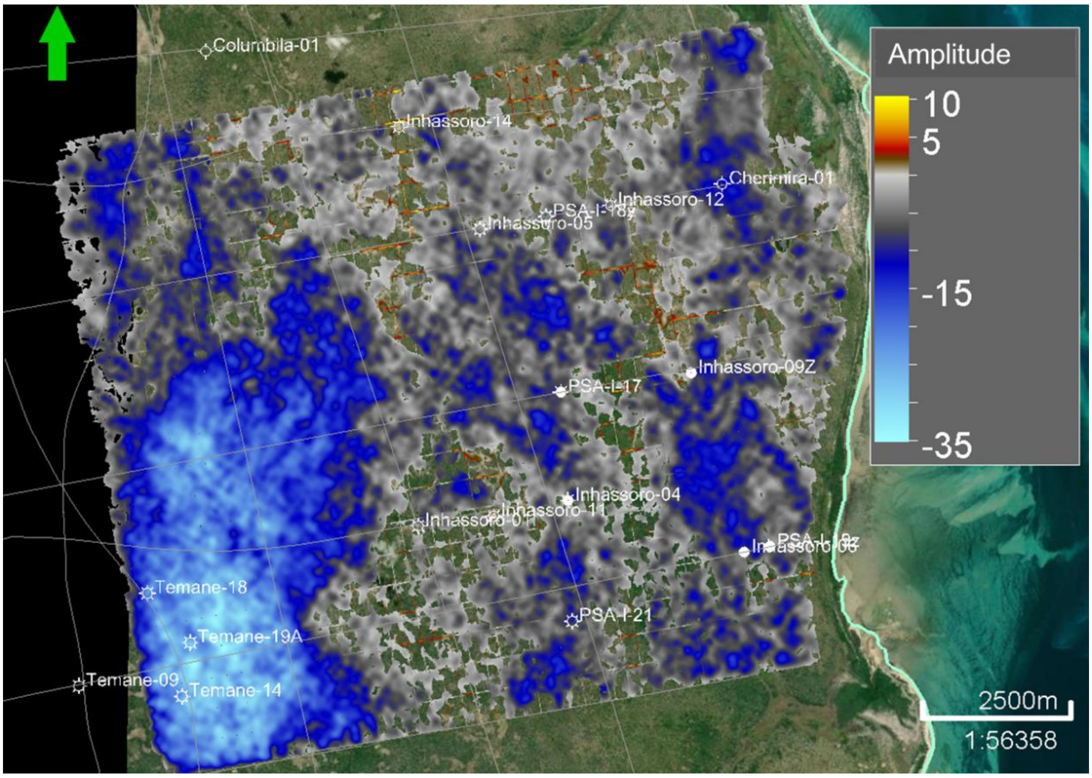

Figure 4-16. G9 auto tracked amplitude on full stack seismic data. Boreholes are shown in white and the shoreline on the right is shown in aqua colour. 2D lines are in grey and demonstrate the rationale for the position of well logs drilled before the 3D seismic survey. Amplitude extracted only from the 3D.

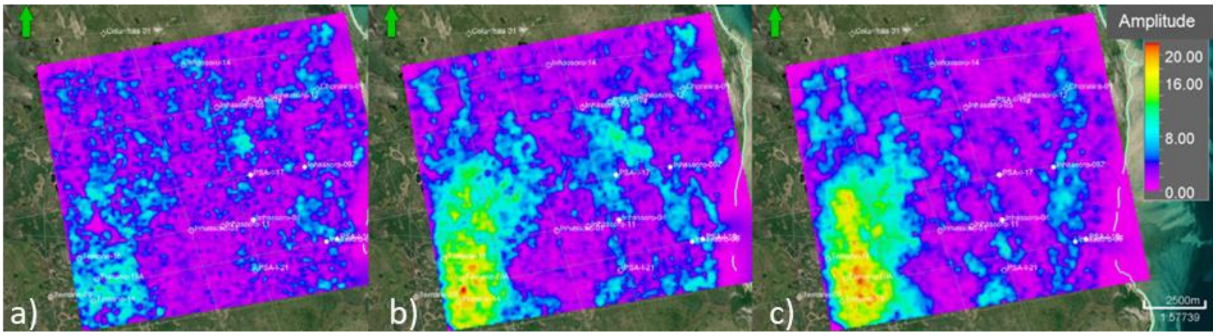

Figure 4-17. G9 surface attribute. a) Root Mean Square (RMS) amplitude information extracted from G9 horizon using seismic angles stack of (5 -15^0). b) Amplitude information extracted from G9 horizon using seismic angles stack (15-25^0). c) Amplitude information extracted from G9 horizon using angles stack (25-35^0).

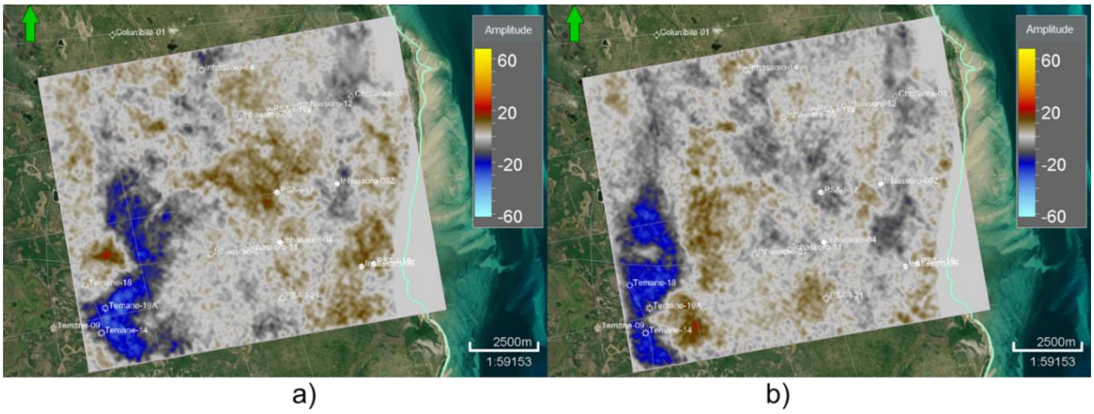

Figure 4-18. G9 Time slice. Time slices are useful displays to understand geologic facies and stratigraphy and bring a qualitative understanding of amplitudes around a reservoir a) Time slice at -976 ms and b) Time slice at - 984 ms. These time slices clearly show anomalous amplitudes at the G9 level at Temane East (lower left corner).

4.3.4 Grudja G10

The Inhassoro 4 well intersected gas at the G10 reservoir level. It was tested but suspended due to a hurricane. This reservoir was appraised in the 2016 drilling campaign by PSA-I-17 updip and PSA-I-21 downdip. All the wells targeting the G10 seat on a structural high on the two-way time map (Figure 4-19), do not exhibit an easily identifiable amplitude anomaly on an extraction map based on full stack data (Figure 4-20). This may be due to the reservoir being filled with oil, rather than gas and is also stratigraphically deeper. Analysis of angle stack amplitude at the G10 reservoir level from the 3D seismic cube, Figure 4-21a-c, reveals mainly amplitudes from the Temane East. A relative decrease in amplitudes around I-11 and I-4 can be observed on the time slice (Figure 4-22) but there is no appreciable difference from the background.

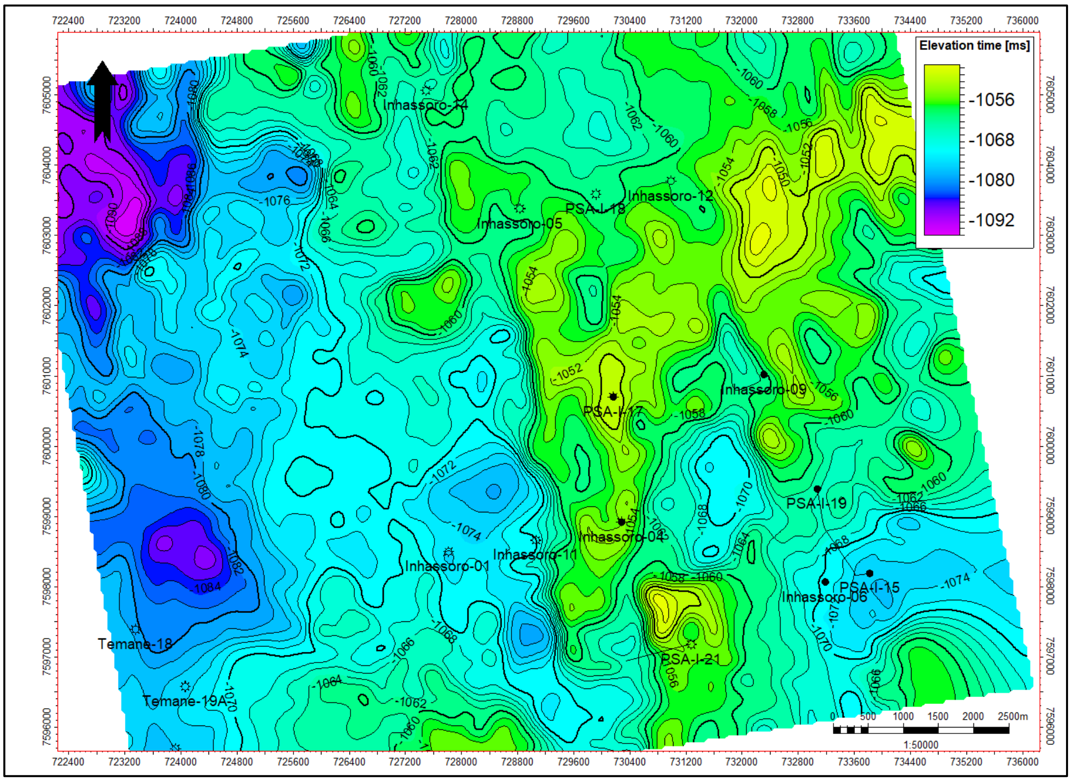

Figure 4-19. G10 two-way time structure map. This map is produced by convergent gridding of the G10 horizon that was mapped on a two-way time seismic section. The G10 structure is between -1000 and -1200 ms two-way time. Boreholes are shown in white. The shoreline is shown in aqua colour.

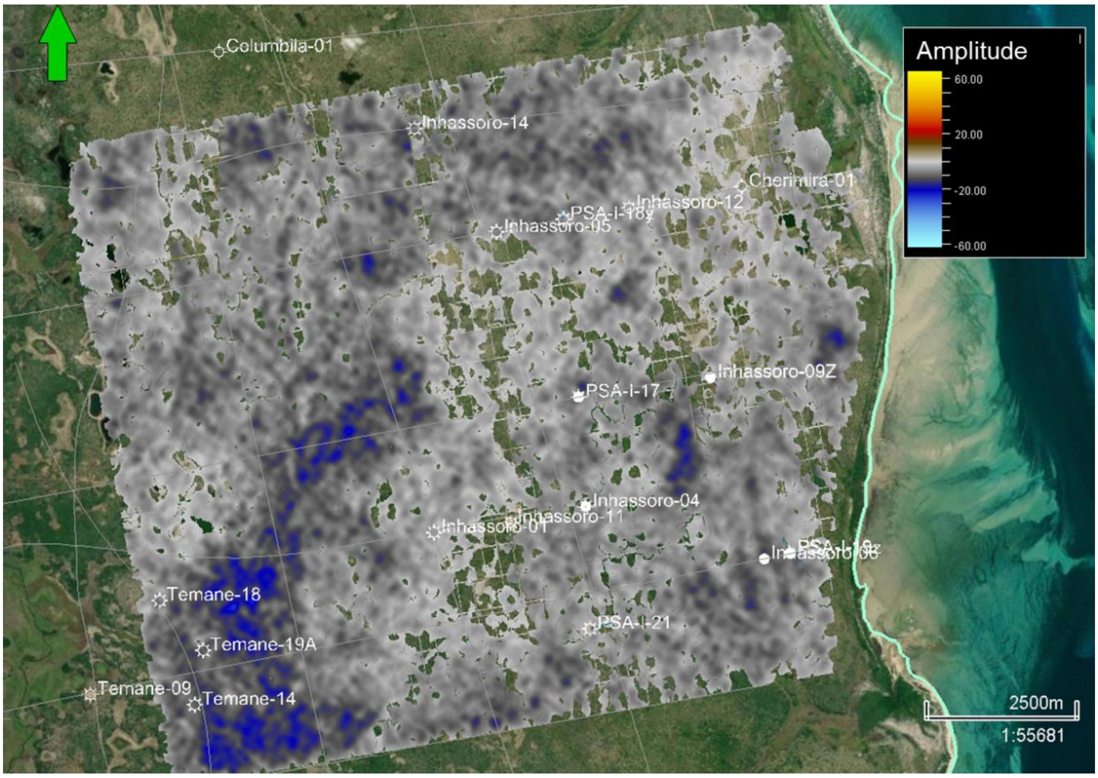

Figure 4-20. G10 auto tracked amplitude on full stack seismic data. Boreholes are shown in white and the shoreline on the right is shown in aqua colour.

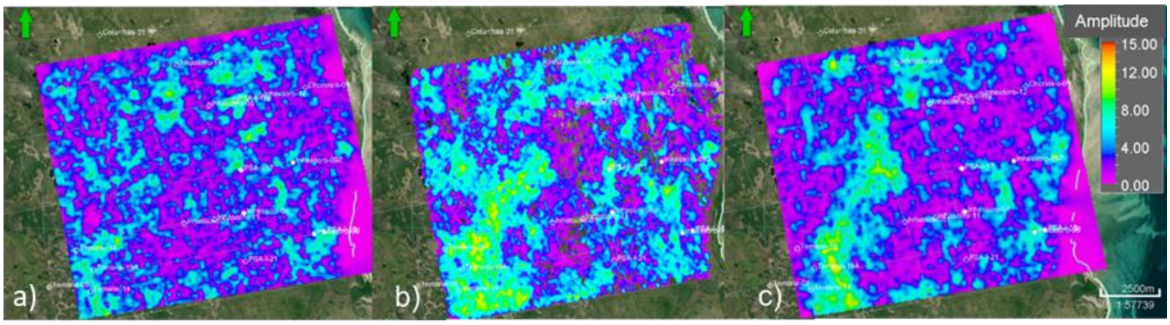

Figure 4-21. G10 surface attribute. a) Root Mean Square (RMS) amplitude information extracted from G10 horizon using seismic angles stack of (5 -15^{0}). b) Amplitude information extracted from the G10 horizon using seismic angles stack (15-25^{0}). c) Amplitude information extracted from G10 horizon using angles stack (25-35^{0}).

`

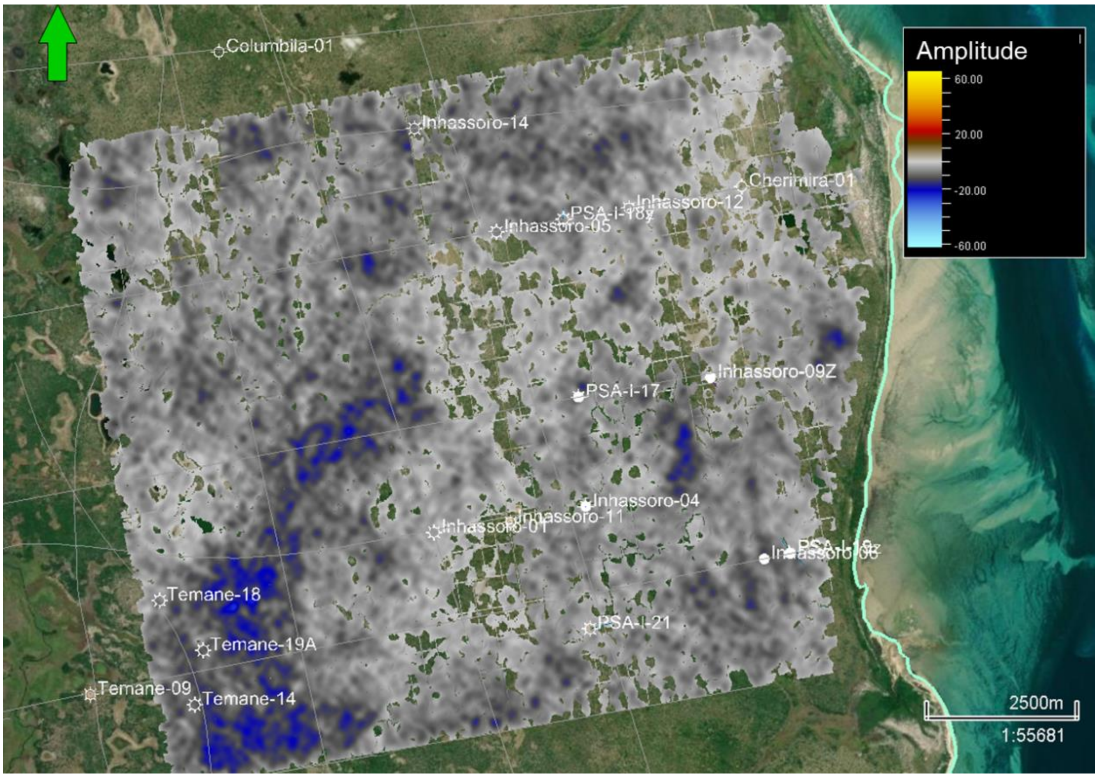

Figure 4-22. Time slice around G10 reservoir, at -1052 ms. Time slices are useful displays to understand geologic facies and stratigraphy and bring qualitative understanding of amplitudes around a reservoir Oil was tested at I-4 well; there is a decrease in amplitudes, but not as bright as it is the case of gas accumulations.

4.3.5 Grudja G11A

Structural trends observed on shallower Lower Grudja levels (G6-G11) are maintained at the G11A (Figure 4-23). No hydrocarbons have been discovered at G11A in Inhassoro. High amplitude areas, Figure 4-24 and Figure 4-25a-c, on the 3D seismic data might correspond to high rock compressibility (i.e., increases in porosity or soft mineral facies). In Figure 4-26, the G11A time slice shows the presence of soft mineral facies and their distribution around the G11A reservoir level in Inhassoro.

`

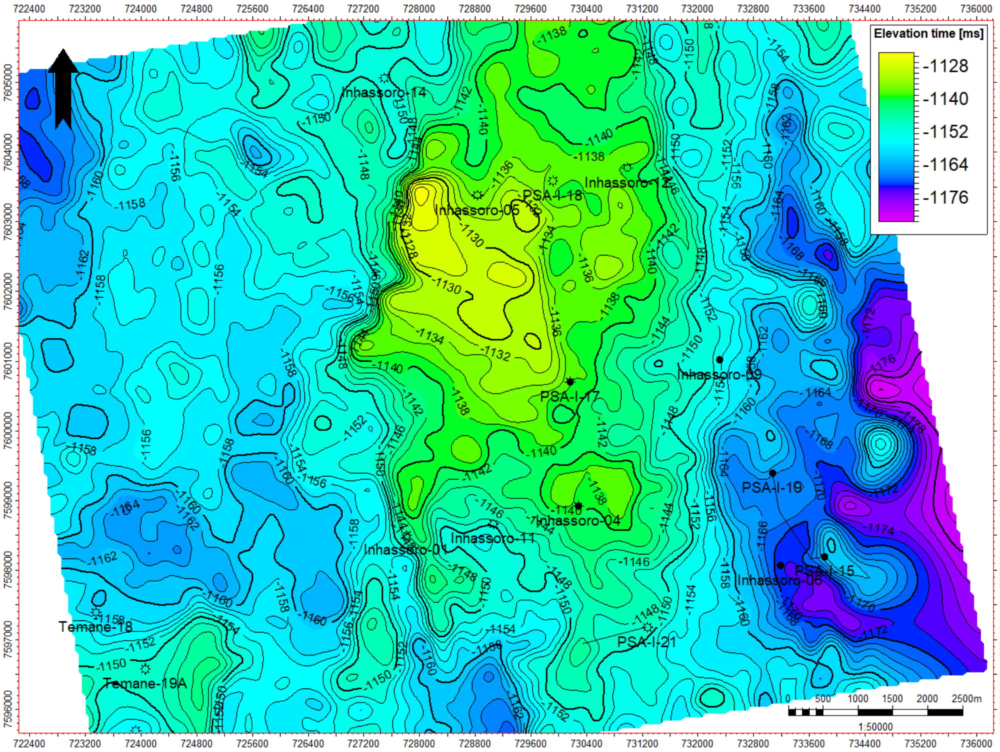

Figure 4-23. G11A two-way time structure map. This map was produced by convergent gridding of the G11A horizon that was mapped on a two-way time seismic section. The G11A structure is between -1100 and -1200 ms two-way time. Boreholes are shown in white. The shoreline is shown in aqua colour.

`

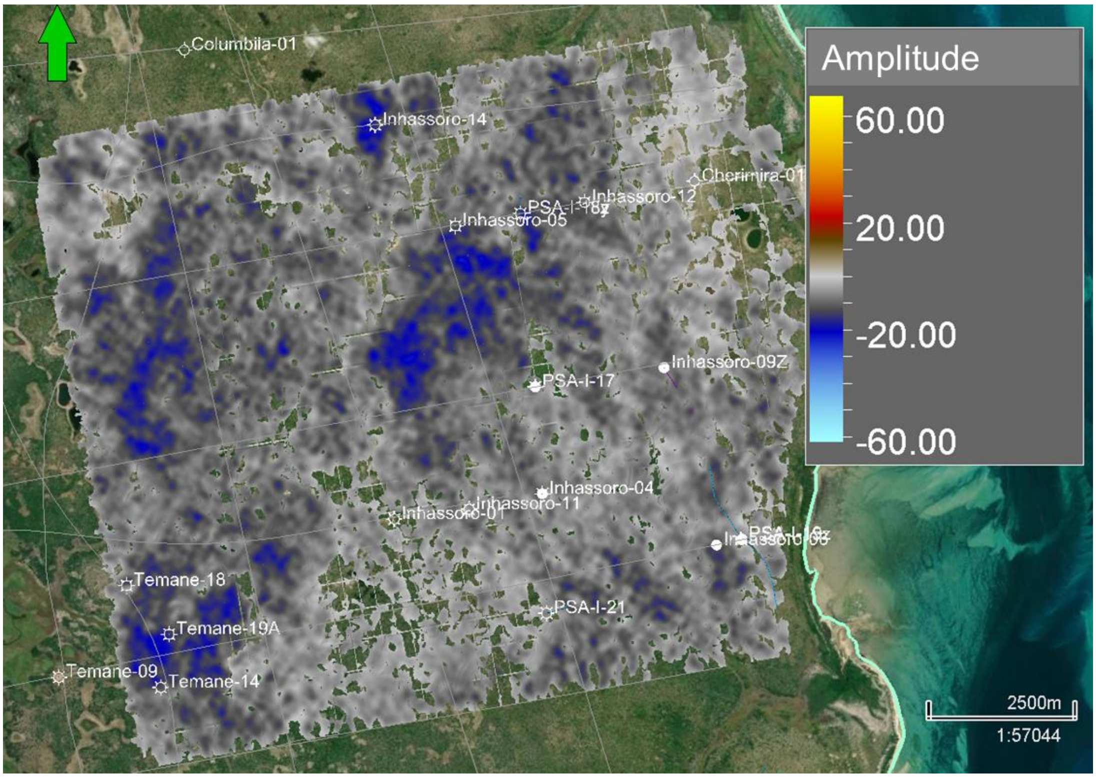

Figure 4-24. G11A auto tracked amplitude on full stack seismic data. Boreholes are shown in white and the shoreline on the right is shown in aqua colour. Soft reservoir facies, which are often related to good sands and in some cases hydrocarbon presence have lower amplitude values, a trough, and are negative on the amplitude colour bar.

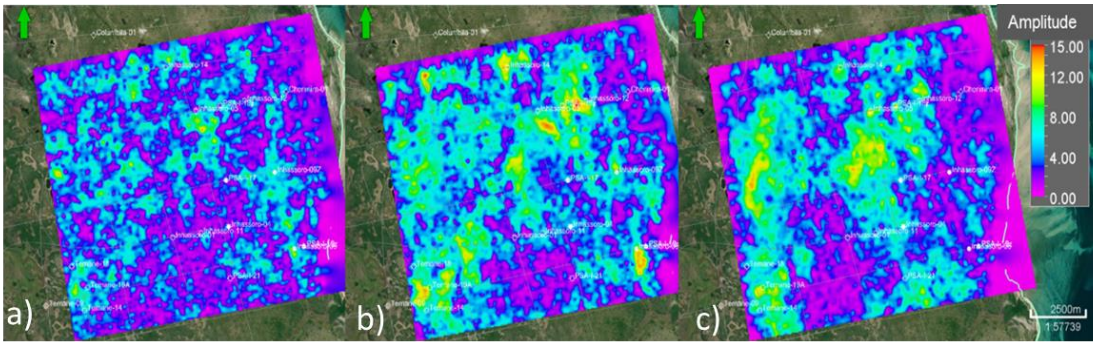

Figure 4-25. G11A surface attribute. a) Root Mean Square (RMS) amplitude information extracted from G11A horizon using seismic angles stack of (5 -15^0). b) Amplitude information extracted from G11A horizon using seismic angles stack (15-25^0). c) Amplitude information extracted from G11A horizon using angles stack (25-35^0).

`

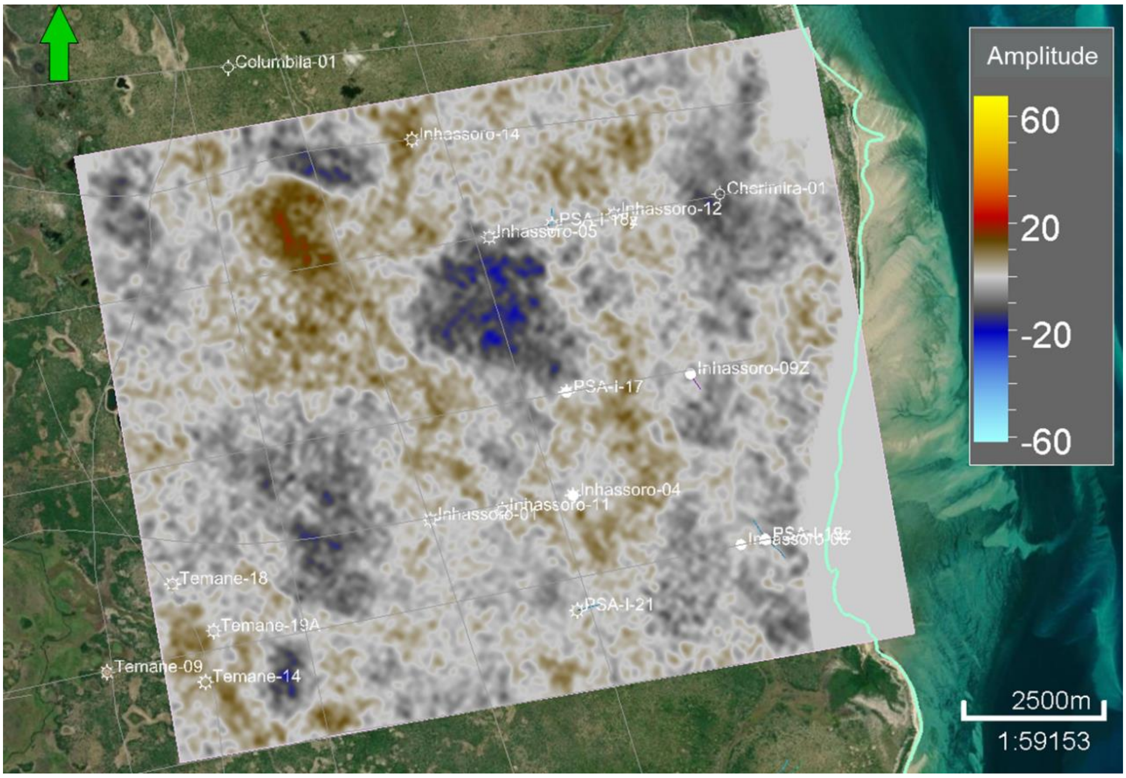

Figure 4-26. Time slice around the G11A reservoir, at -1128 ms. Time slices are useful displays to understand geologic facies and stratigraphy and bring a qualitative understanding of amplitudes around a reservoir. No hydrocarbons have been encountered at this level, but there are soft facies showing amplitude anomalies just south of the Inhassoro 5 reservoir. Boreholes are shown in white.

4.3.6 Grudja G12

The G12/12A is the deepest reservoir level in the Lower Grudja sequence, at about -1200+ ms (Figure 4-27). A surface seismic survey is designed to properly image this reservoir level as part of the primary targets. This was achieved through careful selection of acquisition parameters (shot spacing, receiver spacing, cable length, sweep, and record length). Few wells are deepened to the G12 level to enable proper rock physics/quantitative interpretation. Owing to the G12 reservoir being deeper, diagenetic processes impact on porosity and permeability capability of this reservoir and result in a dimmer amplitude response on extracted seismic facies (Figure 4-28, Figure 4-29a-c, and Figure 4-30a, b).

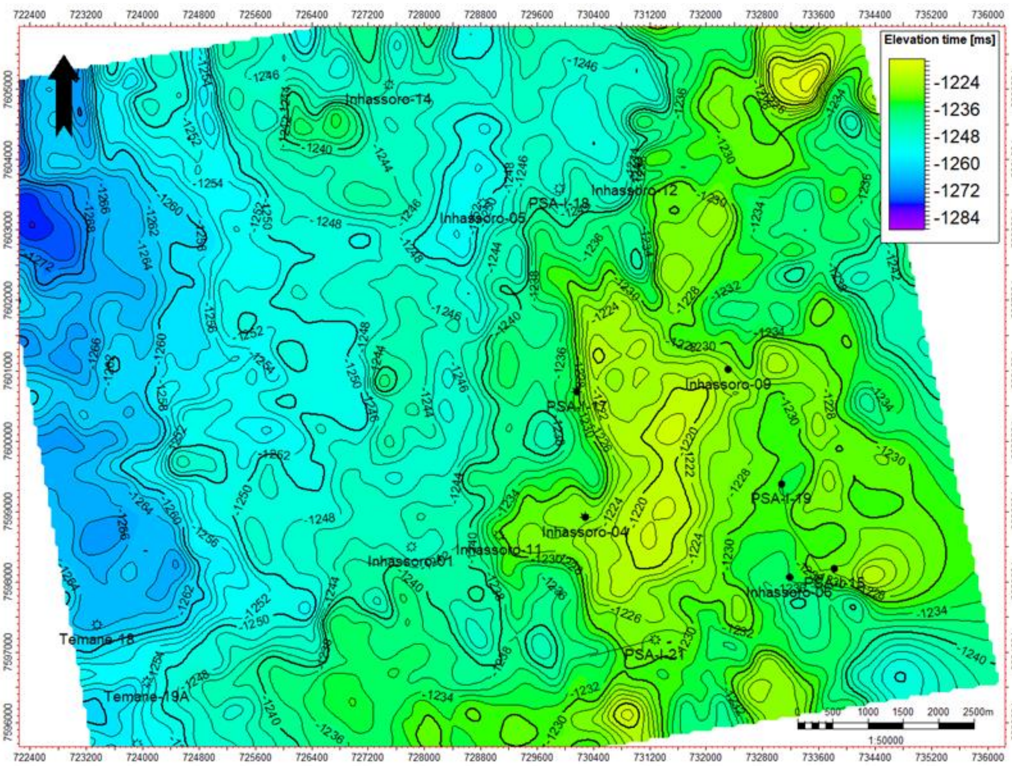

Figure 4-27. G12 two-way time structure map. This map is produced by convergent gridding of the G12 horizon that was mapped on a two-way time seismic section. The G12 structure is between -1200 ms and -1300ms two-way time. Boreholes are shown in white. The shoreline is shown in aqua colour.

`

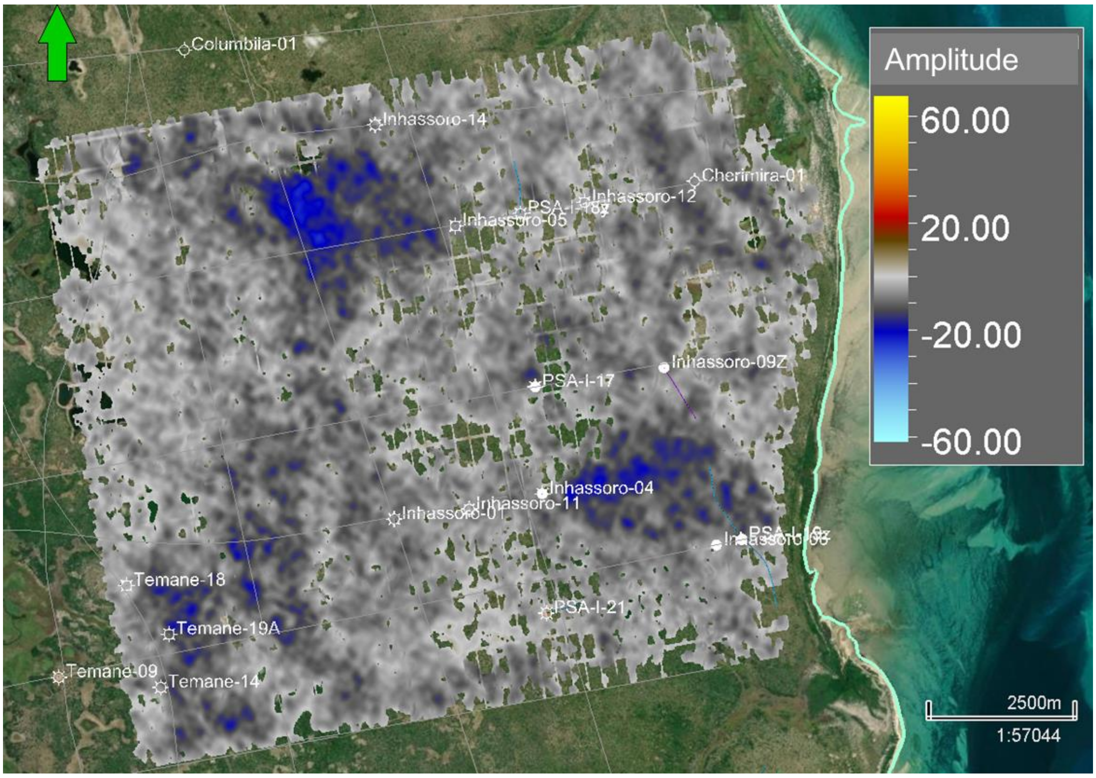

Figure 4-28. G12 auto tracked amplitude on full stack seismic data. Boreholes are shown in white and the shoreline on the right is shown in aqua colour. Boreholes are shown in white. The extracted amplitude qualitatively describes reservoir distribution and the likelihood of hydrocarbons. Hydrocarbon presence is related to soft facies, where amplitude response is low, represented by a trough and negative values on the colour bar.

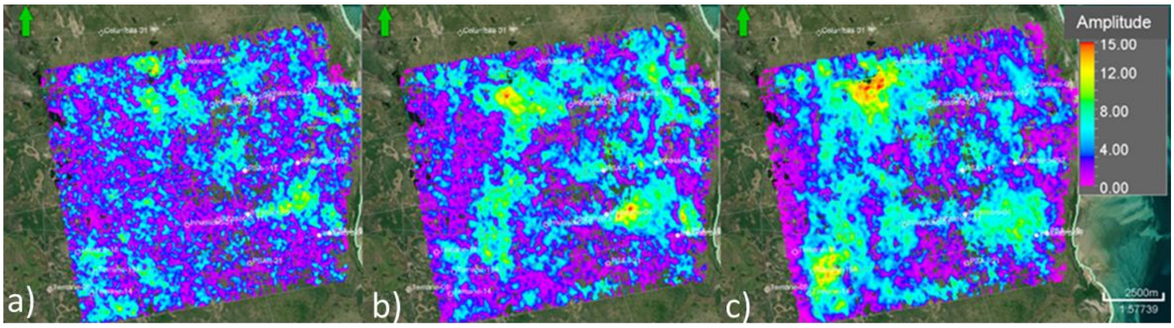

Figure 4-29. G12 surface attribute. a) Root Mean Square (RMS) amplitude information extracted from G11A horizon using seismic angles stack of (5 -15^0). b) Amplitude information extracted from G11A horizon using seismic angles stack (15-25^0). c) Amplitude information extracted from G10 horizon using angles stack (25-35^0).

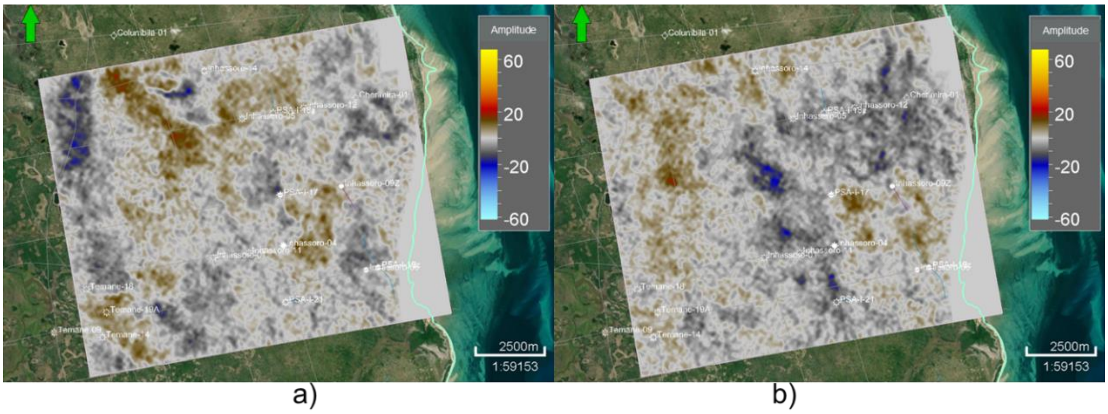

Figure 4-30. Time slice around the G12 reservoir. Time slices are useful displays to understand geologic facies and stratigraphy and bring a qualitative understanding of amplitudes around a reservoir a) Time slice at -1236 ms, and b) time slice at -1312 ms.

5 Quantitative Interpretation in the Mozambique Basin

5.1 Seismic analysis and inversion of Lower Grudja facies

Quantitative interpretation studies have been conducted in the Mozambique Basin, including post-migration, pre-stack seismic gather conditioning, and seismic inversion in the Pande field. These studies generated results from seismic inversion for rock properties using conditioned prestack data. As a proof of concept, amplitude-variation-with-offset (AVO) attributes were derived from conditioned pre-stack gathers using coloured seismic inversion to characterise both Grudja G6 and G10 reservoirs.

The seismic analysis and inversion of Lower Grudja Facies were useful to characterize AVO-related subsurface anomalies by conditioning pre-stack seismic gathers and performing quantitative data analysis beyond conventional data processing workflows used in subsurface imaging. Usually, seismic data are processed in offset (source-receiver distance) domain for stacking purposes, expecting that any residual noise is attenuated during stacking. However, seismic reservoir characterization requires preserved amplitude and frequency content in the offset domain to ensure quantitative amplitude interpretation of seismic wave propagation in the subsurface is bound by both structural and stratigraphic interpretations (Mbatha & Wells, 2014). Table 4 outlines the quantitative seismic data analysis workflow executed in this study.

Table 4: Quantitative seismic data analysis workflow.

1	Determine usable bandwidth of data (signal):
	• Apply a bandpass filter based on response at -20 dB
2	Determine critical angle from incidence angles using migration
	• Colour offset gathers by common incident angle
	• Determine average angle where residual NMO stretch develops
3	Determine S/N enhancements on data:
	• Estimate maximum CMP distance to gather (3 CMPs ~Fresnel zone) and super gather
	• Apply Radon transform to residual offset reverberations and non-coherent noise
	• Suppress noise
	• Apply Radon transform to remove residual long period multiples and converted waves
	• NMO-corrected gathers should show flattened offsets after Radon
4	Determine correlation between wells and seismic data
	• Select a key well and correct its TD curve using checkshot
	• Tie well to seismic using a statistical, zero-phase wavelet and align geologic tops and seismic horizons
	• Estimate wavelet using the amplitude and phase spectra and the well reflectivity
	• Tie well using estimated wavelet
5	Determine deconvolution operator for spectral balancing of data:
	• Apply wavelet deconvolution to dephase and balance amplitude spectrum using estimated wavelet from well
6	Calculate elastic-wave synthetic from well for conditioning QC:
	• Use well elastic logs to model the wave propagation through multilayer surfaces
	• Compare AVO response at key geologic tops between elastic-wave synthetic and conditioned gather
7	Generate angle stacks from conditioned gathers:
	• Estimate at least 4 angle ranges with no overlap below critical angle muted
	• Create angle and full stacks

`

In order to compare the quality of the seismic amplitude as a function of depth, a synthetic seismic model or seismogram was generated at one of the existing wells (P-21) by convolving the well reflectivity (e.g., a moving average representative of the contrast in acoustic impedance with depth, with acoustic impedance estimated as the product of p-wave velocity and bulk density logs) with a seismic wavelet (i.e., the autocorrelation of a seismic trace convolved with itself). For example, a well-to-seismic tie at the P-21 well location comparing the synthetic seismogram with a seismic trace from the 0-10 angle stack showed a correlation of 56.1% (Figure 5-1a, b). This tie used a statistical zero-phase seismic wavelet, which was adequate for the purpose of matching well information with full-stack seismic data dephased during data conditioning. A subsequent seismic inversion process requires a more accurate estimate of the seismic wavelet before applying wavelet deconvolution, spectral balancing, and dephasing. A seismic wavelet was therefore extracted from all angle stacks, and it was determined that the 10-20 angle stack was a stable representative estimate of the field seismic source to use in the wavelet deconvolution process. The amplitude spectrum of this wavelet showed a broad bandwidth (10-100 Hz), and the usable bandwidth determined at -20dB of amplitude threshold was in the 10-50Hz range. Therefore, a bandpass filter was applied to all seismic input gathers based on the usable bandwidth recovered.

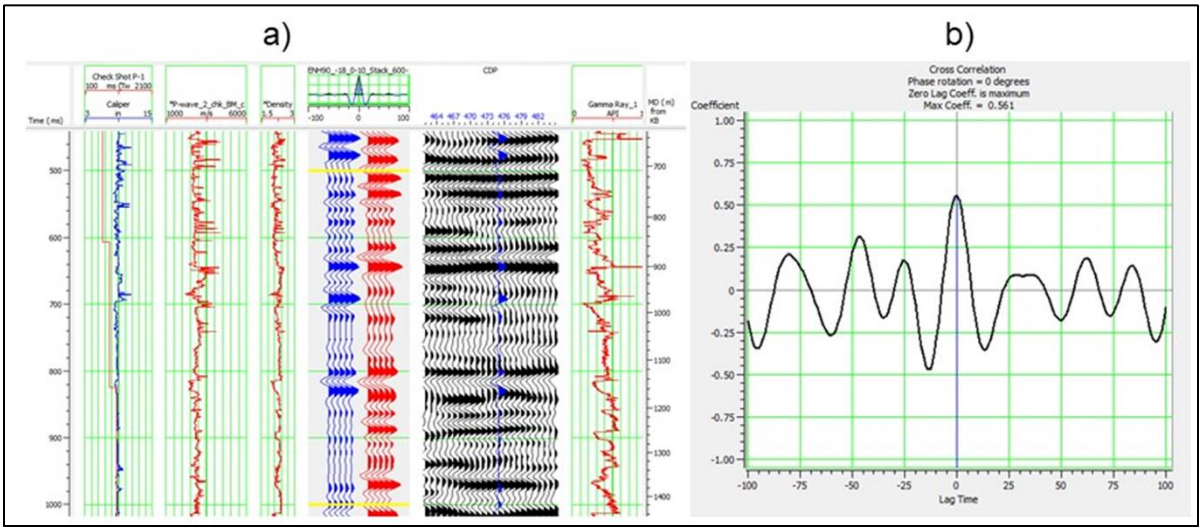

Figure 5-1. a) Well-to-seismic tie from P-21 well. The tie was achieved using calibrated sonic (2nd column) and density (3rd column). The Gamma Ray on the last column was used for comparison purposes and was not part of the well-to-seismic tie process. b) Cross-correlation. This plot indicates the level of correlation between the synthetic seismogram and the post-stack seismic at well location, within the window of interest. The window of interest above is 500-1000ms as indicated by yellow horizontal lines.

`

Pre-stack seismic gather conditioning also improved the correlation of the seismic gather amplitude variation with offset (AVO) compared against plane-wave solutions to the seismic wave equation, including Zoeppritz and Aki and Richards approximations (Zoeppritz, 1919; Ostrander, 1984; Aki & Richards, 2002). For example, at the P-21 well location, the original input seismic gather showed a 38% correlation against the Aki and Richards approximation before data conditioning. This correlation was then improved to a staggering 94% after performing prestack gather conditioning steps. As a reference, the maximum expected correlation obtained from an elastic wave AVO synthetic generated based on log data at this well location was 98.7% against the Aki and Richards approximation.

Figure 5-2 shows the improvement in well seismic AVO correlations at each step of the seismic gather conditioning process.

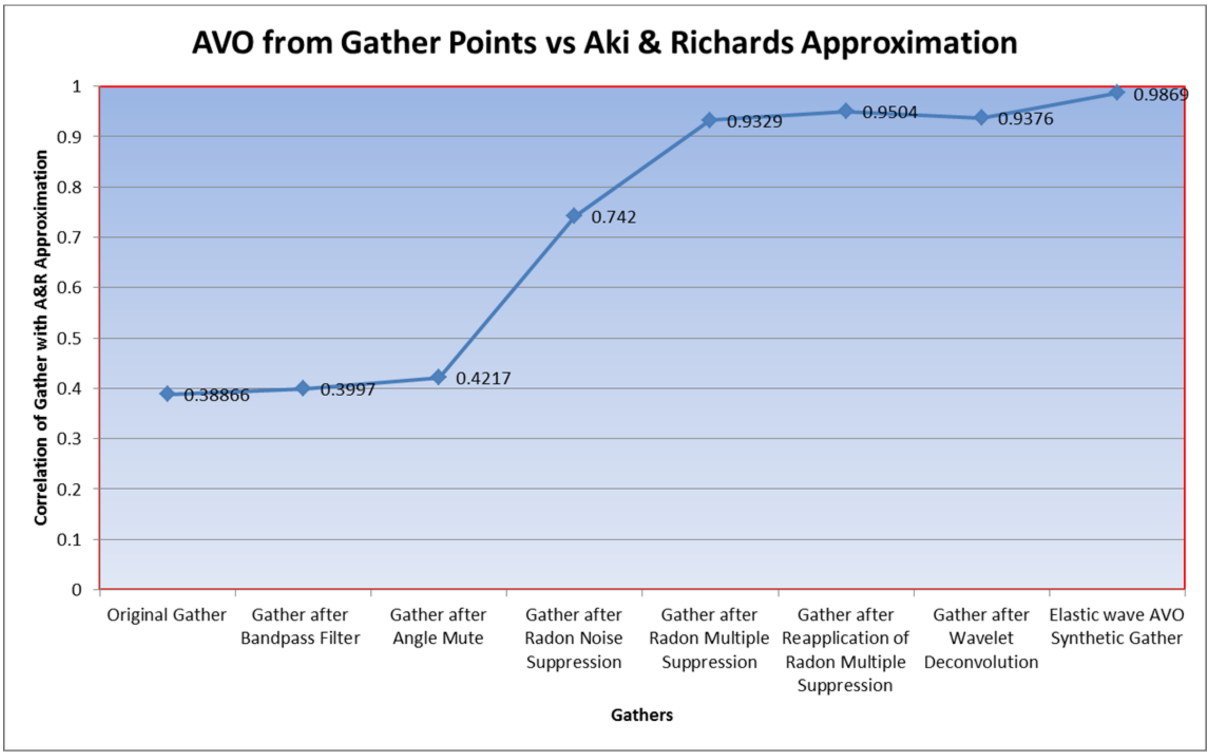

Figure 5-2. Amplitude Variation with Offset (AVO) correlations between conditioned seismic gather and Aki and Richards approximation. AVO extracted from post-migration pre-stack seismic gather only had a 38% correlation with Aki and Richards approximation. Seismic gather conditioning processes improved the seismic gather and made it AVO compliant. AVO extracted from the conditioned seismic gather had a 94% correlation with Aki and Richards approximation. A synthetic gather created using P-21 well logs was computed for comparison. AVO from synthetic gather points has a 99% correlation with Aki and Richards approximation.

Figure 5-3 shows the difference between the conditioned pre-stack seismic gather (Figure 5-3a) and the raw seismic gather (Figure 5-3b) at the P-21 well location. Figure 5-3c shows the amplitude vs. offset (AVO) response at two different depth locations. For example, blue triangles show the AVO response of the event from the raw gather at 820 ms two-way time (TWT), and the blue line shows the expected AVO response of such an event based on the Aki and Richards model. The correlation between these two AVO responses is 38.7%, showing a significant deviation from the expected response as the angle (x-axis) increases. However, after applying the prestack gather conditioning steps summarized in Figure 5-3, the dark green squares show the new AVO response of the same event at 820 ms on the conditioned gather, and the dark green line shows its expected AVO response based on the Aki and Richards model. The new correlation achieved between both AVO responses is now 95.0%, thanks to the pre-stack gather conditioning steps applied. Note that the expected AVO response according to the Aki and Richards model using well logs is a class IV response (Rutherford & Williams, 1989). A class IV AVO response is characterized by a negative intercept with the Y axis (e.g., a strong negative zero-offset amplitude) and a positive AVO gradient (e.g., an upward trending amplitude variation with offset showing less negative amplitude values as offset increases).

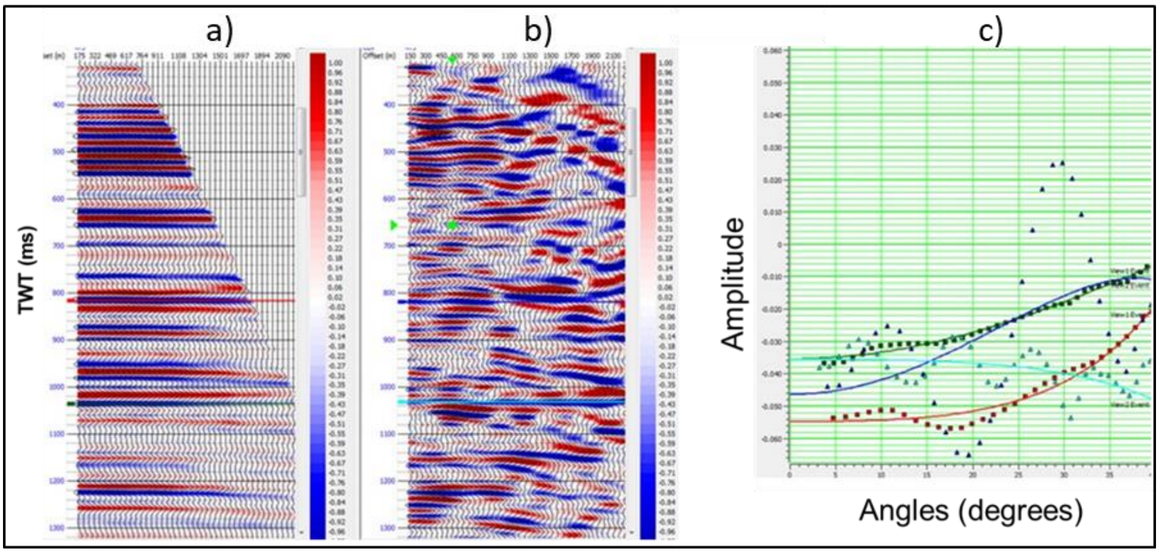

Figure 5-3. A comparison of a conditioned seismic gather and the raw gather. a) Conditioned seismic gather, b) raw seismic gather, and c) AVO responses – red points represent AVO seismic response at the G6 level on the conditioned seismic gather. Green points in (c) represent the AVO seismic response at the G10 level on the conditioned seismic gather, blue points represent the G6 AVO response from the raw seismic gather, and light blue points represent AVO points from raw seismic gather at the G10 level.

Once all prestack seismic gathers across the survey were conditioned, a seismic inversion study was conducted to characterize the Grudja reservoirs. In this case, AVO attributes extracted from partial angle stacks were used to derive elastic and petrophysical property proxies. These attributes were used to predict absolute reservoir properties after calibration at reservoir levels.

`

Reservoir property proxies produced from this study included porosity, volume of shale, and water saturation (Figure 5-4).

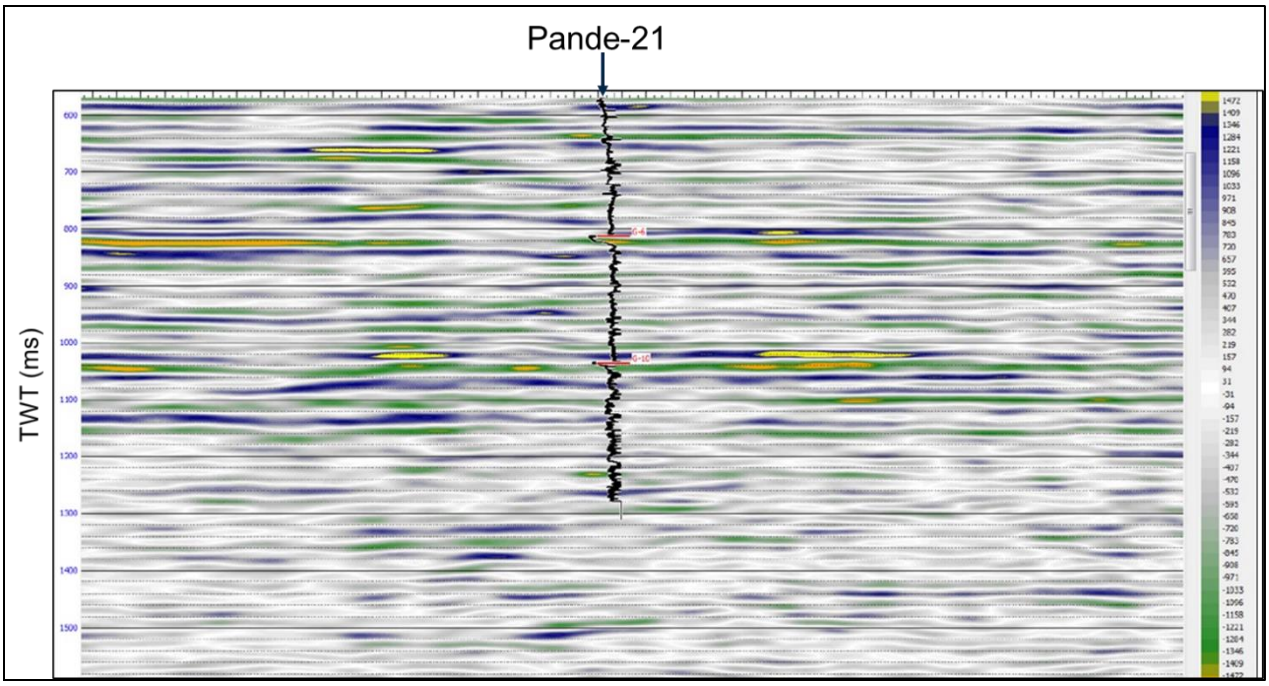

Figure 5-4. Water saturation proxy derived from a combination of Amplitude Variation with Offset (AVO) attribute projections. P-21 well is projected, with a water saturation curve inserted on the section. The formation tops (G6 and G10 levels) are shown in red on the projected water saturation curve.

Results from this seismic inversion study showed that the Pande G6 reservoirs exhibit a class IV AVO response, which is characterized by a negative intercept and a positive gradient (similar to the AVO trends shown in Figure 5-3c) associated with high-porosity, gas-filled sands capped by a relatively stiff rock. To correctly assess and obtain AVO-compliant gathers, a similar prestack gather conditioning workflow was applied to line ENH90-18. This process included bandpass filtering to remove noisy low-amplitude, high-frequency data. Using seismic migration velocities, a normal moveout (NMO) stretch observed on the data was muted. The signal-to-noise ratio (S/N) was enhanced through supergathering (e.g., combining multiple adjacent gathers into a single super gather). Coherent noise and residual multiples were suppressed using a 10 to 100 ms Radon transform parabolic function. Lastly, wavelet effects on the resulting gather were removed through wavelet deconvolution. Angle stacks and AVO products were created from these conditioned gathers. The seismic inversion of AVO attributes was computed through the coloured inversion process. This process allows for quick

`

computation of inversion products and avoids biasing of the results inherent to other conventional, model-based inversion methodologies.

5.2 Temane PSA-T-27 quantitative interpretation modelling

In the Temane field, a quantitative interpretation study was performed focused on a new well, PSA-T-27, with reliable well logs and VSP data. The study was two-fold: firstly, by forward modelling (fluid substitution modelling for gas and oil), seismic amplitude responses from G6a, G10, G11, G11a, and G12 reservoirs were interpreted to identify contrasts as a function of fluid saturation at seismic scale and bandwidth. Secondly, by reviewing seismic amplitude response from angle stacks, amplitude maps were superimposed on depth maps to assess conformance to structure as potential fluid-related anomalies.

The quantitative interpretation workflow followed included rock physics, AVO analysis, and seismic inversion. The rock physics workflow assists in identifying trends of reservoir rock properties independent of fluid saturation (e.g., mineral content, porosity) that might influence seismic response derived from elastic properties (Mbatha et al., 2017). This workflow also identifies trends of non-reservoir facies (bounding rocks) that may also influence seismic contrasts (reflectivity). Once both reservoir and non-reservoir responses are understood, a fluid substitution modelling (e.g., from water to gas and oil) is executed to identify seismic contrasts as a function of fluid saturation at seismic scale and bandwidth. For this study, reservoir sections were defined based on ranges of photoelectric and gamma-ray logs (PEFZ < 2.85 b/e and GR < 90 API), and non-reservoir sections followed a complementary range (PEFZ > 2.85 b/e and GR > 90 API).

The AVO modelling of Lower Grudja reservoirs involved the calculation of AVO intercept, gradient, curvature, and near/mid/far angle reflectivity from well logs as a function of fluid saturation. This step required a well-to-seismic tie to identify signal bandwidth from existing seismic and corrections against seismic models at in-situ conditions. Calculated AVO properties were bandlimited to match the bandwidth of the existing seismic data at the well location.

The seismic inversion workflow involved the estimation of bandlimited elastic reflectivities from well logs and depth trends from seismic AVO reflectivities. Bandlimited petrophysical

`

properties were estimated from elastic reflectivities using both well and seismic elastic reflectivities. This approach enables to identify the highest correlation between petrophysical and elastic properties at the well (1D) along adjacent seismic lines (2D). Figure 5-5 shows a crossplot between bulk modulus (K) and total porosity (PHIT) at the G6 reservoir level using well logs. Note the hydrocarbon effect caused by a drop in bulk modulus (e.g., an increase in rock compressibility) over a similar porosity range.

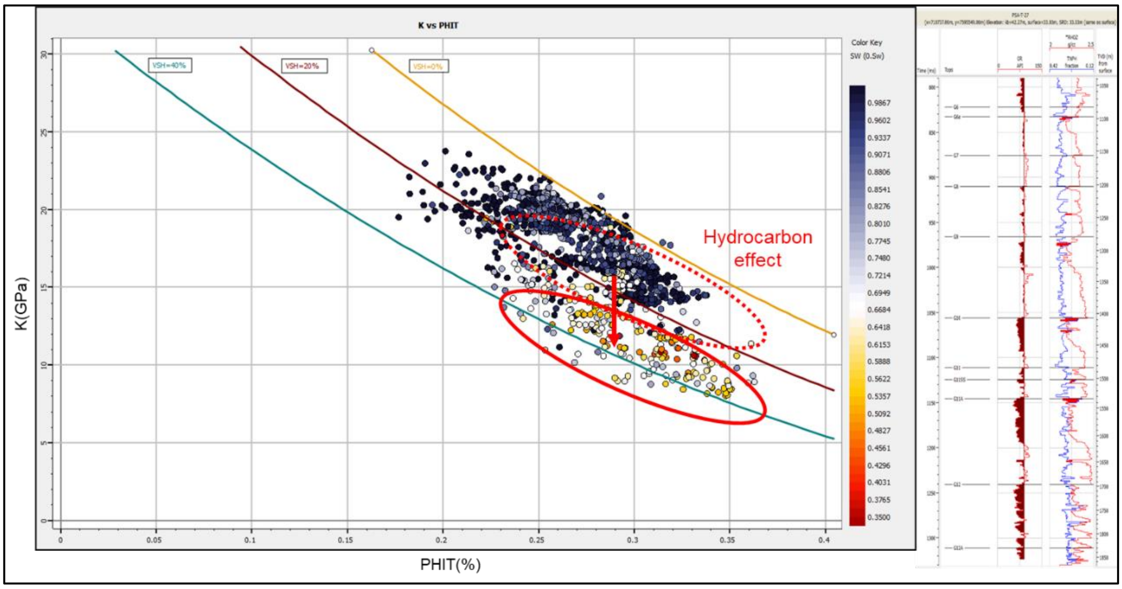

Figure 5-5. Rock physics crossplot of bulk modulus (y) vs. porosity (x). Reservoir facies saturated with hydrocarbon (light colours) exhibit lower bulk modulus (K) values than those expected from the constant shale-volume trends.

To characterize the expected response of hydrocarbon saturations at multiple Grudja reservoir levels, a set of cross plots compared water saturation and elastic properties (Rho or bulk density, Vs or S-wave velocity, K or bulk modulus, and Vp or p-wave velocity) at the well location, and extended to other water saturation values based on trends estimated using combinations of minerals and fluids based on the material-balance equations for density & porosity (Figure 5-6) and extensive to geophysical properties including AI (acoustic impedance or the product of p-wave velocity and bulk density), SI (shear impedance or the product of s-wave velocity and bulk density), Vp/Vs (the ratio of p-wave and s-wave velocities), and GI (gradient impedance defined as the extended elastic impedance as a function of p-wave velocity, s-wave velocity, and bulk density when the chi angle is equal to 90 degrees) (Figure 5-7) (Whitcombe, 2002).

`

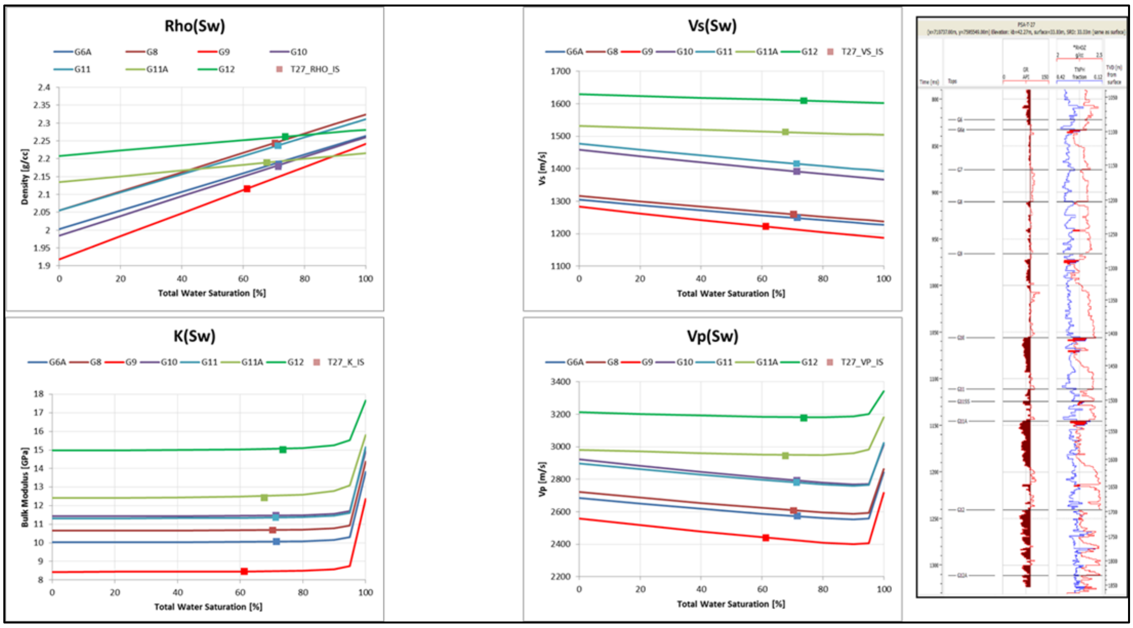

Figure 5-6. Elastic properties and water saturation for all Grudja reservoirs. The top left plot shows a plot of density versus total water saturation for all lower Grudja reservoirs, G6A, G8, G9, G10, G11A, and G12. G11A and G12 contained liquids and exhibit a different trend to the rest of the reservoirs which contained only gas. On the top right, fluids do not affect the shear velocity trend. The bulk modulus (bottom left) and compressional velocity (bottom right) exhibit a similar trend when plotted against total water saturation.

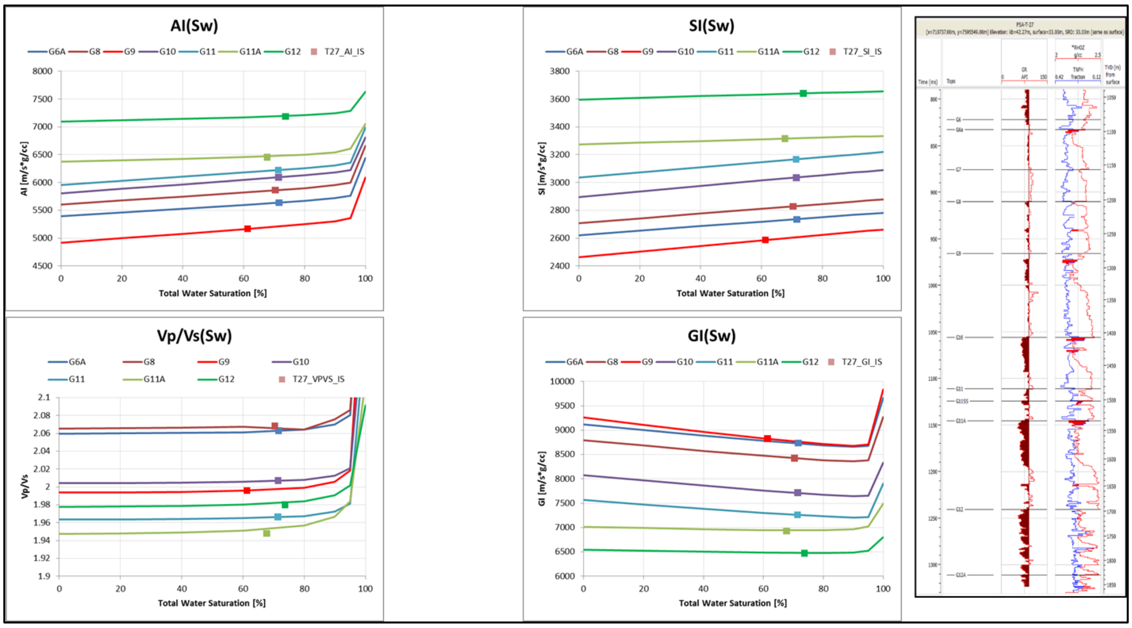

Figure 5-7. Geophysical properties and water saturation for all Grudja reservoirs. The geophysical property less sensitive to fluid saturation is shear impedance. Acoustic Impedance (AI), P-wave and S-wave ratio (Vp/Vs), and Gradient Impedance (GI) are all sensitive to fluids, especially when gas is introduced. They have less effect as gas/oil saturation increases.

A seismic wedge modelling of Lower Grudja reservoirs at PSA-T-27 assisted in determining the effects of amplitude response as a function of apparent thickness given seismic bandwidth

`

limitations to properly differentiate thin (e.g., less than 15 m) reservoir sections. This model assists in differentiating true positive and false positive amplitude responses associated with different fluid saturations. An example of a G9 wedge model for 100% wet reservoir or SW100 (Figure 5-8a), in-situ water saturation (Figure 5-8b), and 80% oil saturation or SW20 (Figure 5-8c) is shown in Figure 5-8. Note the similarity in the amplitude vs. thickness crossplot in the lower section of these panels between the in-situ water saturation (61% or SW61) and the saturated oil model (20% or SW20).

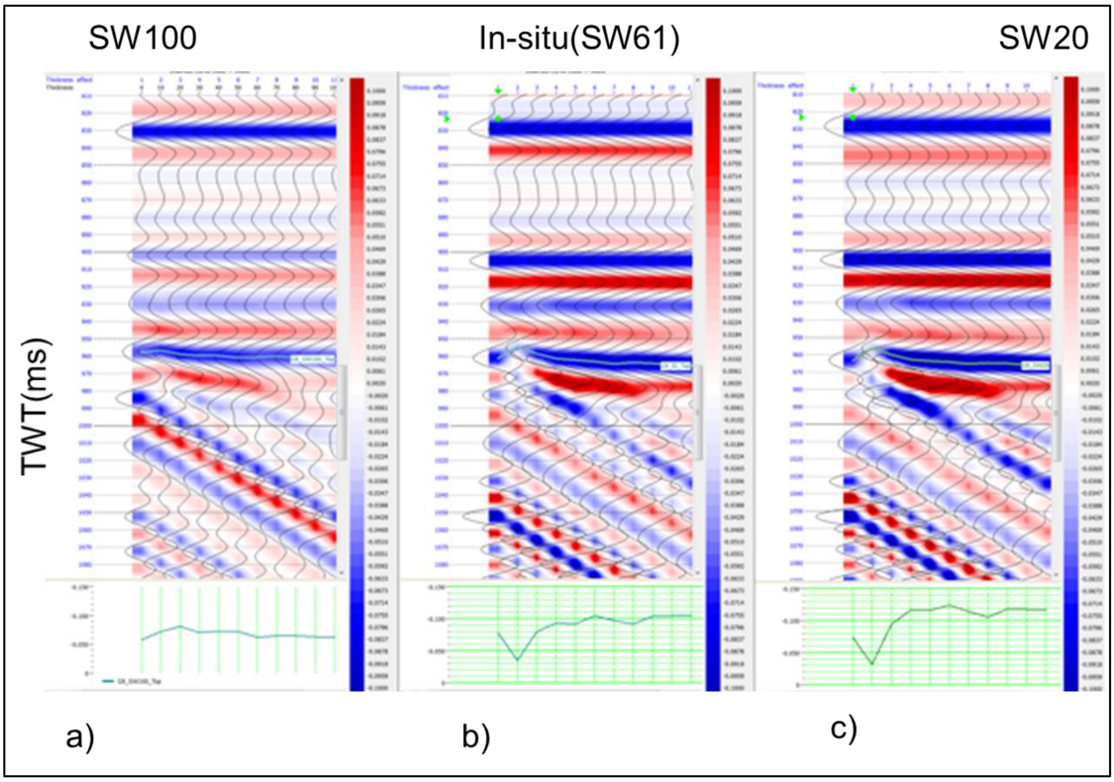

Figure 5-8. G9 reservoir seismic wedge model. a) G9 reservoir seismic wedge model when the reservoir is saturated with 100% water. b) G9 reservoir seismic wedge model with reservoir showing in-situ conditions, that is 61% saturated with water, meaning it is 39% saturated with hydrocarbons. c) G9 reservoir seismic wedge model with 20 % water saturation.

Lastly, petrophysical predictions from elastic properties at Grudja G6 to G12 reservoir levels were investigated. This analysis provided some valuable relationships between elastic rock properties and the reservoir's petrophysical properties:

- Bulk density is a proxy for relative porosity and relative fluid saturation.
- Shear modulus is a proxy for relative shale volume.

An example of the relative fluid saturation from the density proxy relationship is shown in Figure 5-9. Note the contrast between the G8 and G9 reservoir sections, both gas-saturated with similar porosity values but different fluid saturation profiles. Also, note the increase in hydrocarbon saturation observed along the G11 reservoir sections; although it shows a scattered distribution of hydrocarbon-related anomalies, it might inform of changes in fluid phase along these deeper and tighter Grudja reservoir sections.

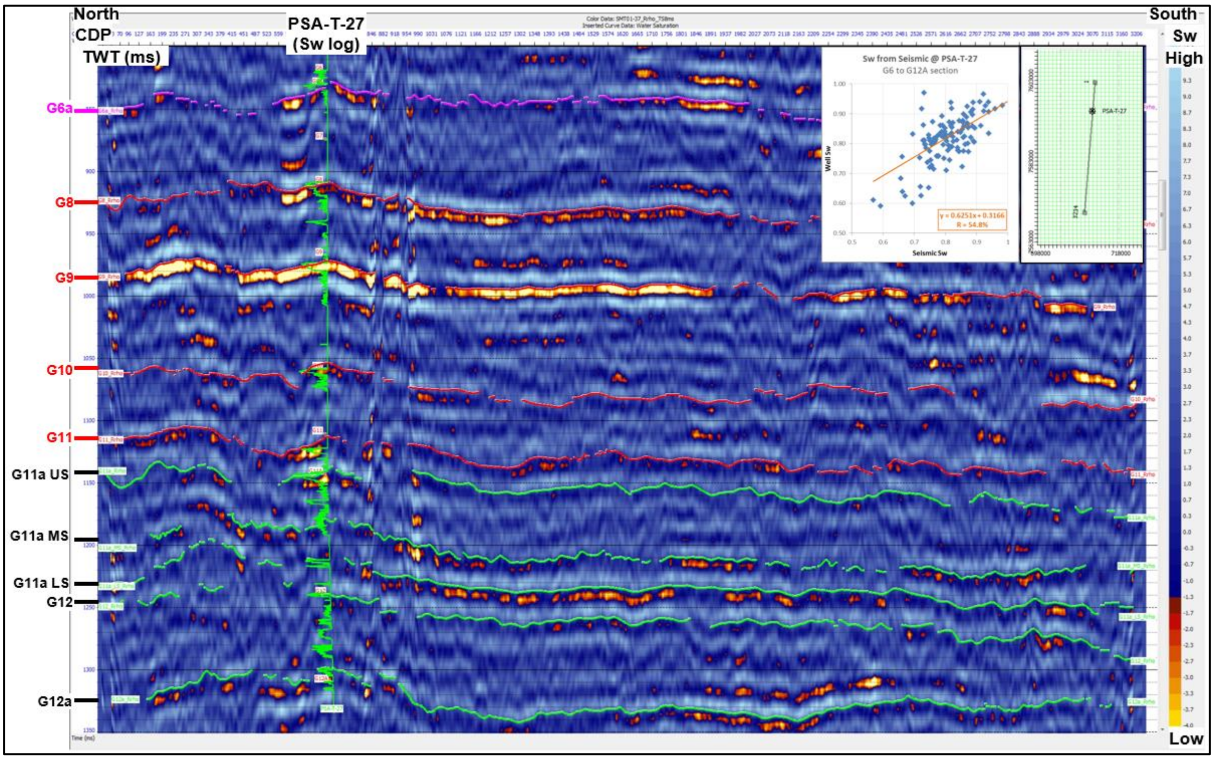

Figure 5-9. Water saturation prediction from seismic at G6 to G12a reservoirs. Seismic section inversion results showing water saturation. A water saturation well log is plotted along the borehole. These results enable prediction away from the well location, showing areas more likely to contain hydrocarbons.

5.3 Seismic AVO attributes

Seismic exploration's primary role is to identify pore fluids at depth to map hydrocarbon deposits (Batzle & Wang, 1992). Fluids within sedimentary basins strongly influence the seismic properties of rocks. "Pore fluids vary substantially, but systematically, with composition, pressure, and temperature", and "gas in solution in oils can drive their modulus so far below that of brines that seismic reflection bright spots may develop from the interface between oil saturated and brine saturated rocks" (Batzle & Wang, 1992). In this regard, seismic attributes assist in identifying areas of interest before conducting an AVO study. Figure 5-10 shows an RMS amplitude surface attribute extracted from the seismic data in the Inhassoro G6 reservoir. Higher RMS amplitude values show the G6 amplitude response, and areas more likely to have good reservoir properties and possible hydrocarbons. Root Mean Square (RMS) Amplitude “is the square root of the average of the squares of a series of measurements” (Sheriff, 2002). It is a commonly used technique to display amplitude values in a specified window of stack data. Anomalous RMS amplitudes may be associated with gas accumulations, although these may be uncommercial. Anomalous RMS amplitude may also be associated with sharp lithologic changes between adjacent rock layers, such as unconformities and boundaries associated with sharp changes in sea level or depositional environments (Taner et al., 1979). The RMS is computed from instantaneous traces on a specified window and displayed on a seismic section as an attribute, or as a seismic surface (see Figure 5-10). At G6, the extraction used a narrow window of 10ms TWT to ensure that the response captured the soft reservoir facies in G6.

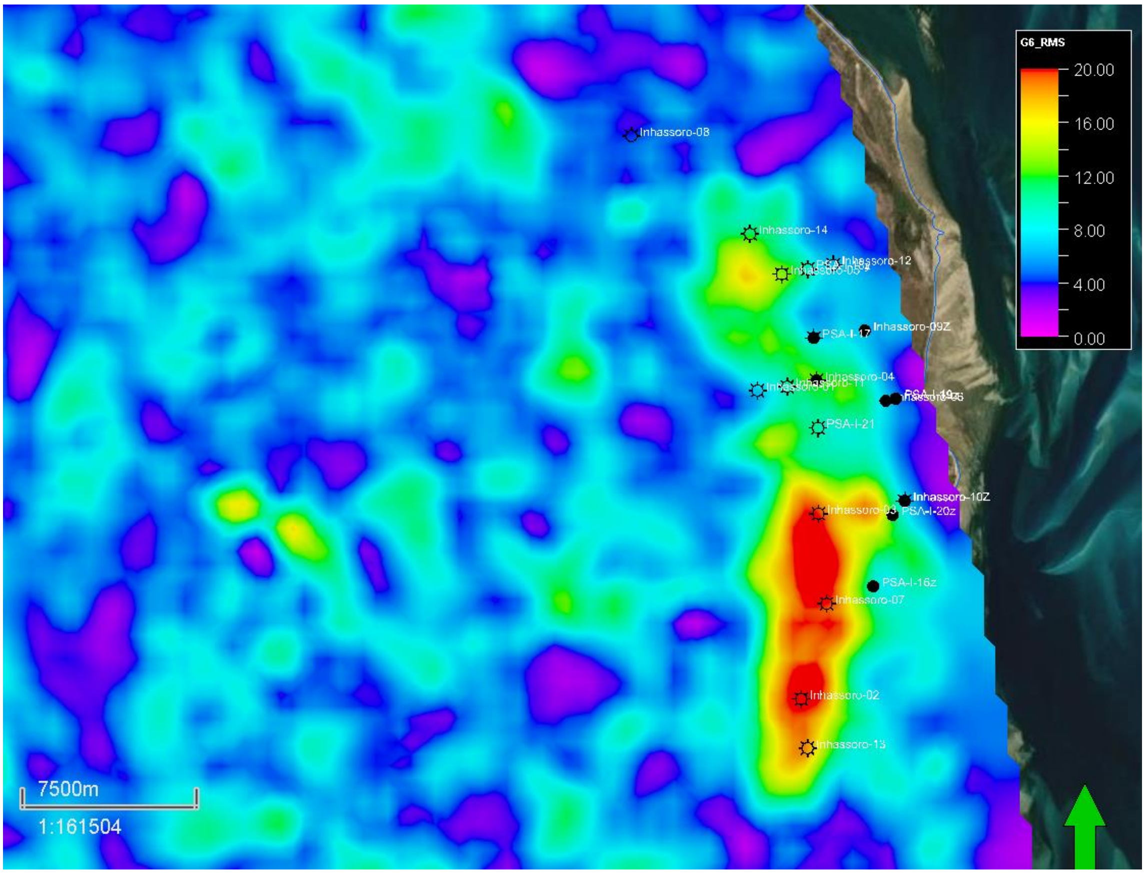

Figure 5-10. G6 RMS amplitude surface attribute. RMS extracted on a 10 ms window (5 ms above the G6 horizon and 5 ms below the G6 horizon). Higher RMS amplitude values show the G6 amplitude response, and areas more likely to have good reservoir properties and possible hydrocarbons.

Figure 5-11 shows the instantaneous amplitude attribute computed for the G6 reservoir. The Instantaneous amplitude is an amplitude extraction based on the single horizon exactly where the surface is mapped. This amplitude extraction captures what the interpreter has mapped on a seismic section. Furthermore, the instantaneous amplitude was extracted from angle stacks (5 to 35 degrees) as shown in Figure 5-12a-c. Figure 5-12 suggests that amplitude varies with the angle of incident. Figure 5-13 shows the computation of the minimum amplitude. This attribute captures the minimum value of the amplitude within the chosen window (10 ms in this case), and it is associated with soft facies since it represents a negative reflectivity or a contrast between a hard impedance on top and a soft impedance below the seismic horizon.

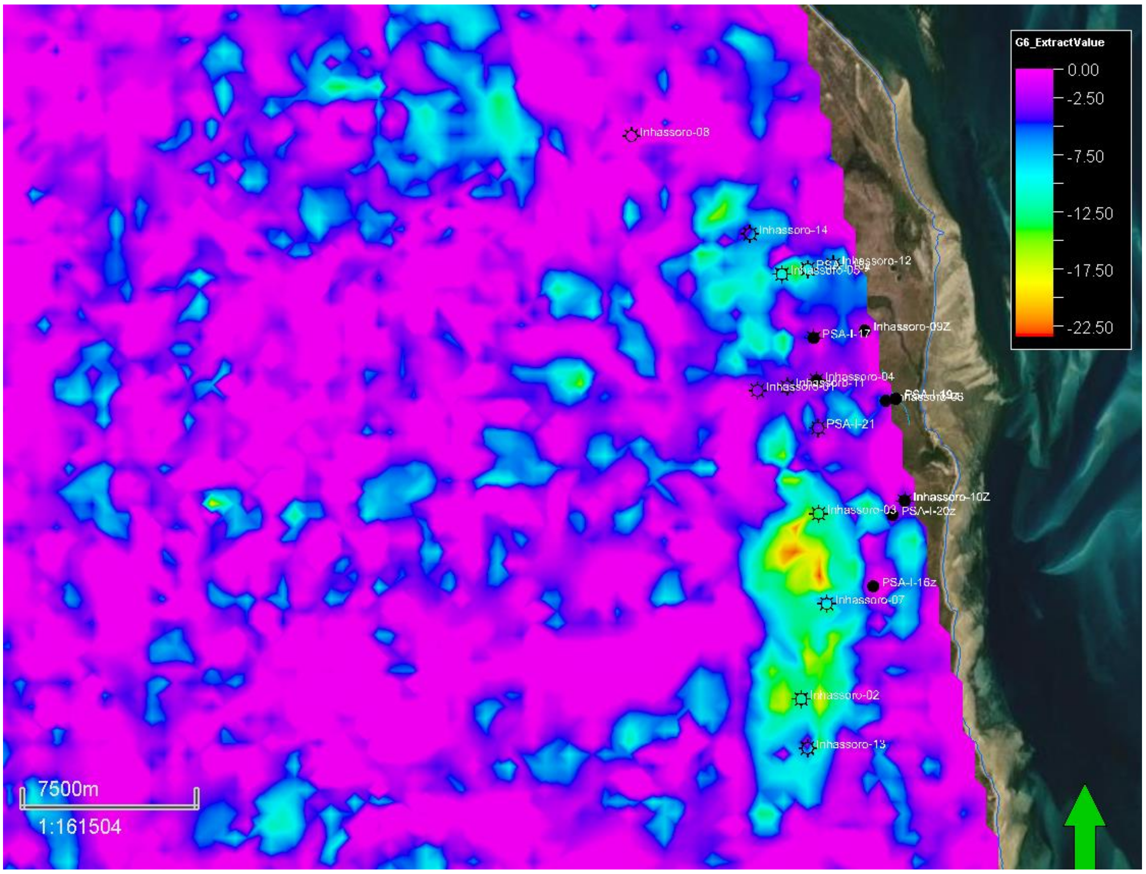

Figure 5-11. G6 Instantaneous amplitude. The G6 is mapped on a soft amplitude response, and that is where the amplitude surface attribute on the figure is extracted.

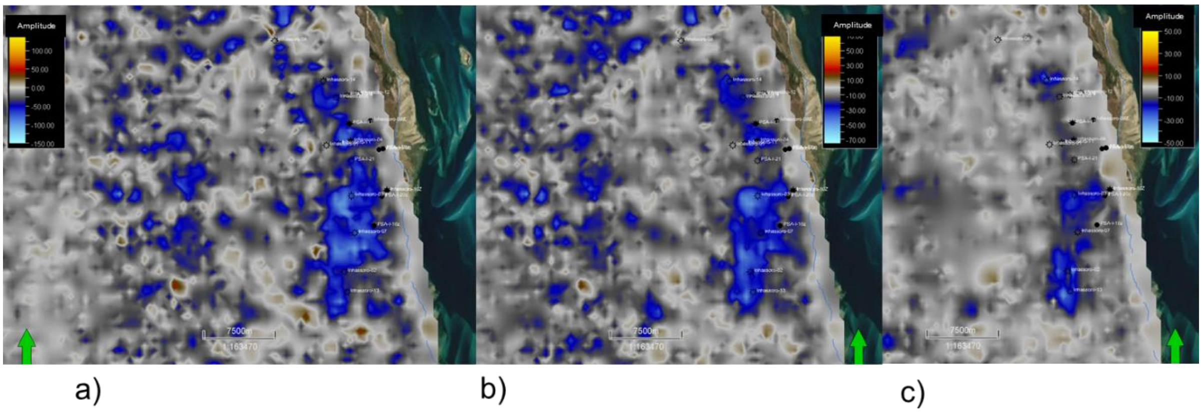

Figure 5-12. Extract value attribute extracted from angle stacks. a) Low-angle extract value, b) mid-angle extract value, c) high-angle extract value.

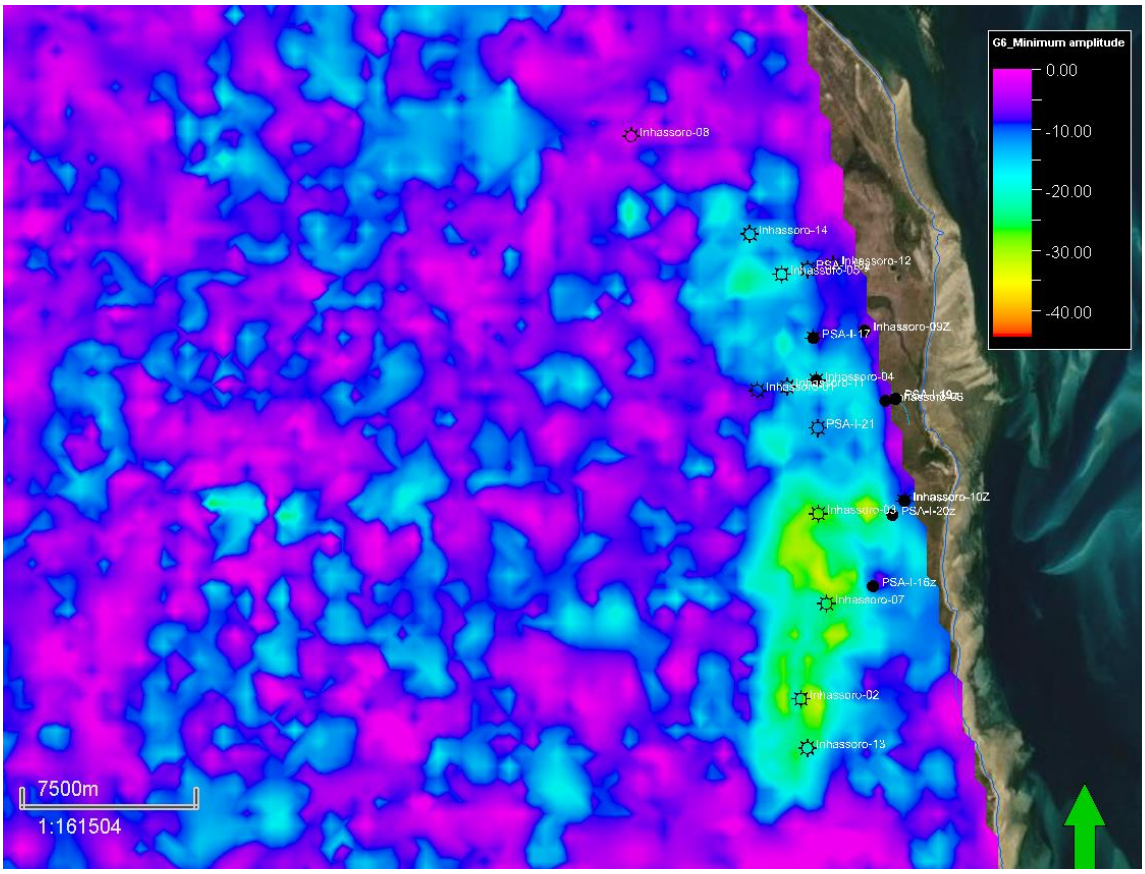

Figure 5-13. G6 Minimum amplitude. This amplitude extraction delineates the seismic amplitude response around the Inhassoro field. Minimum amplitudes only focus on the trough, therefore positive values are on background, shown in purple. Anomalous amplitude in Inhassoro is related to hydrocarbon presence, mainly the gas cap that overlies the oil rim. Wells/Boreholes are shown in black.

The gas indicator attribute was also computed as demonstrated in Figure 5-14 to Figure 5-17. The attribute is an AVO product designed to highlight gas in sands (e.g., Figure 5-14, Figure

`

5-16, and Figure 5-17). It was originally designed for the Gulf of Mexico (Petrel software, SLB). It is essentially an AVO product and can be computed from both pre-stack and post-stack seismic data. The AVO method used in this study is the Shuey 2-term approximation (Figure 5-15a, b). This is a “linear approximation that can be used to invert amplitude information to provide rock elastic properties” (SLB Software definition, 2021). The primary attributes of AVO are Intercept and Gradient. The gas indicator is derived from these two attributes. The AVO reconnaissance process can be executed using both pre-stack and post-stack data, but if only post-stack data is available, partial angle stacks should be used (Figure 5-15).

One of the advantages of using this gas indicator is that it does not rely on wells to be implemented. It can be calibrated using existing well information and wells with known hydrocarbon accumulation to confirm its validity. The blind well test can also be applied to confirm the robustness of the method. Gas indicator can be displayed on a vertical seismic section (Figure 5-16 and Figure 5-17) as well as along a reservoir horizon in a map view.

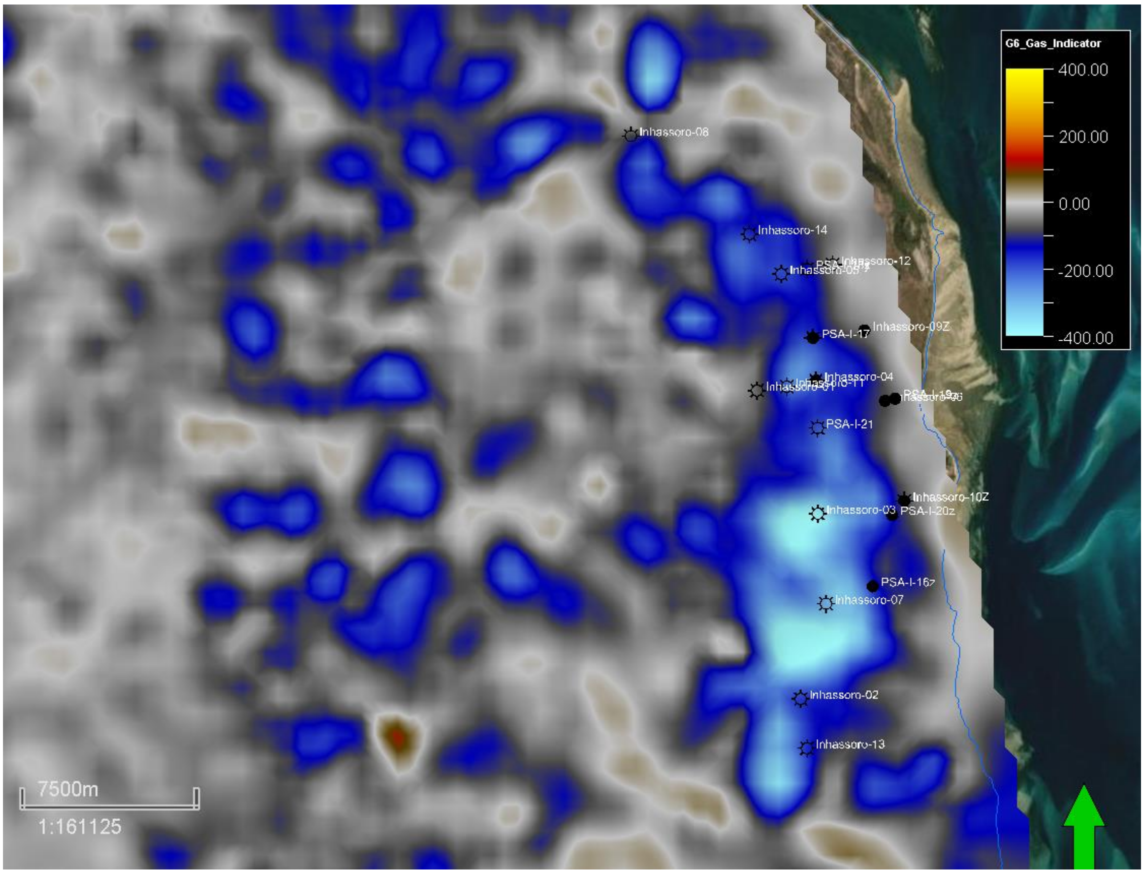

Figure 5-14. G6 Seismic gas indicator. This attribute is a product of AVO attributes and highlights gas in sands.

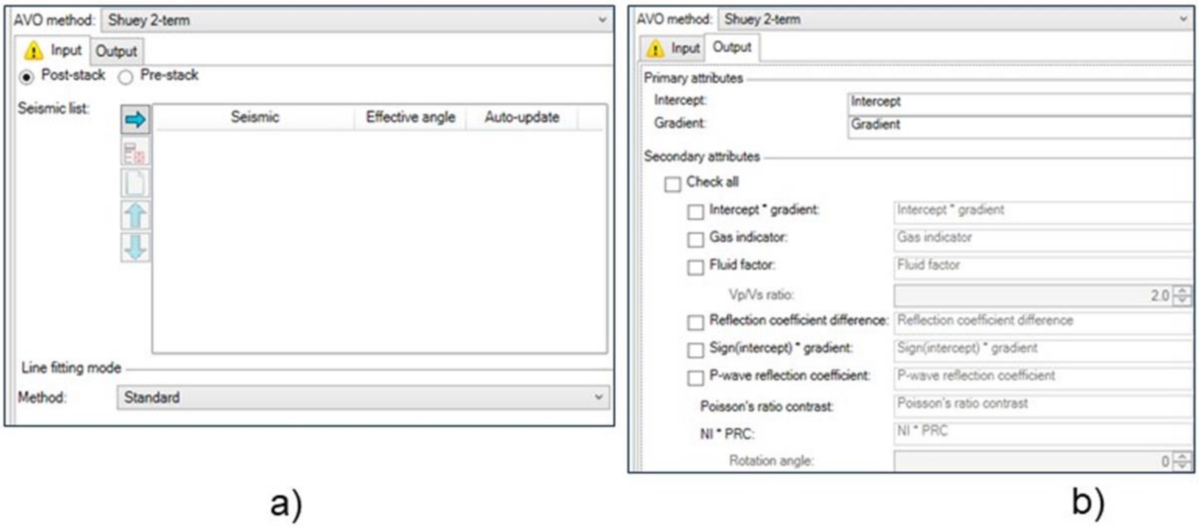

Figure 5-15. a) Amplitude Variation with Offset (AVO) Reconnaissance input dialog. 2D seismic partial angle stacks were used as input to the AVO Reconnaissance. b) AVO Reconnaissance output dialog.

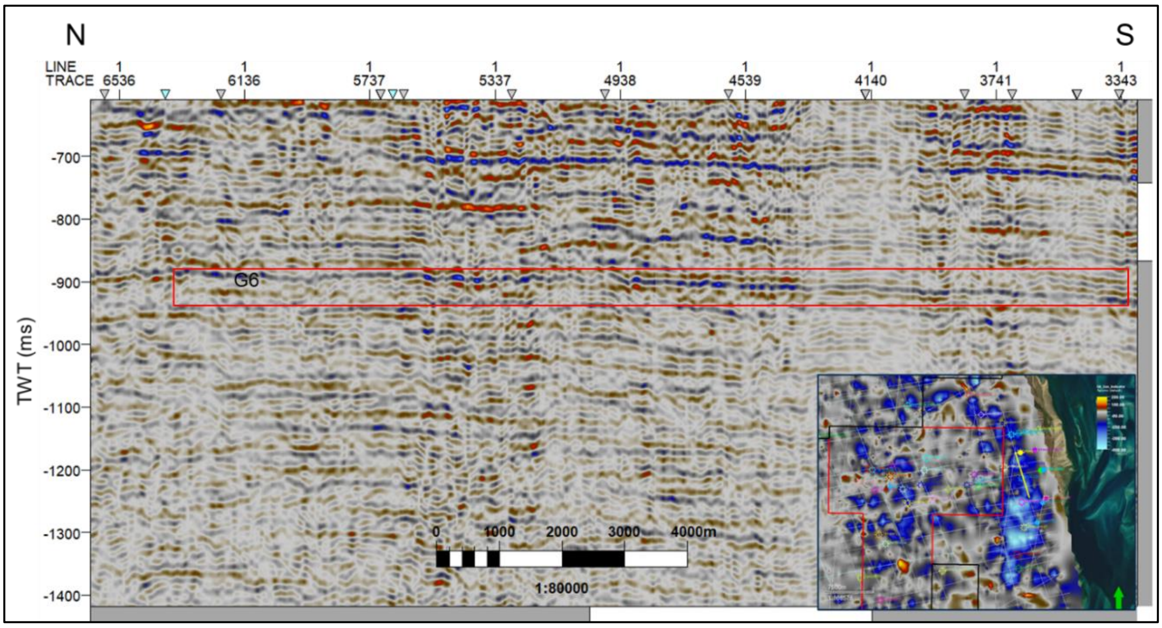

Figure 5-16. G6 gas indicator seismic section and a base map of gas indicator surface attribute. Seismic line SME05-26 gas indicator, with G6, indicated with the red box around -900 ms.

`

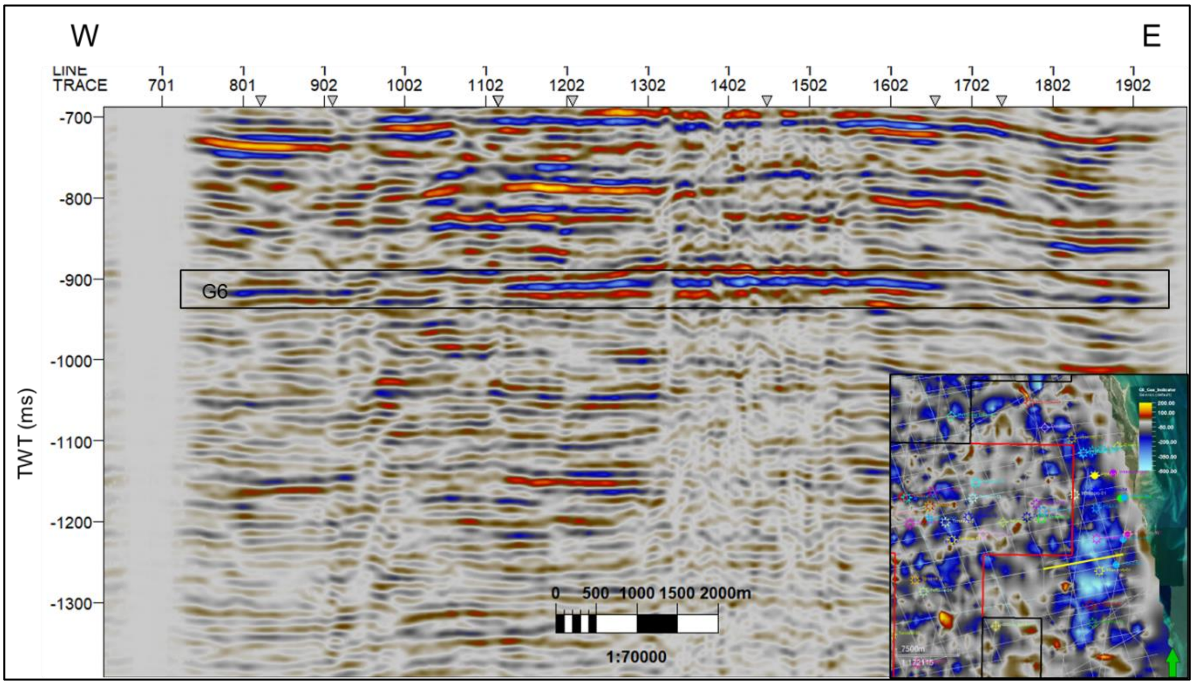

Figure 5-17. G6 Gas indicator. a) G6 Gas indicator surface. b) East-west line, AMT90-10 gas indicator seismic section.

5.4 Inhassoro area AVO analysis

Seismic line SME05-26 (Figure 5-16) was one of the lines identified to have gather conditioning and extracted quantitative properties from. The well, PSA-I-21, was projected into this line to compare pre-stack seismic gather responses against well AVO synthetics. The workflow for seismic gather conditioning is presented in Figure 5-18.

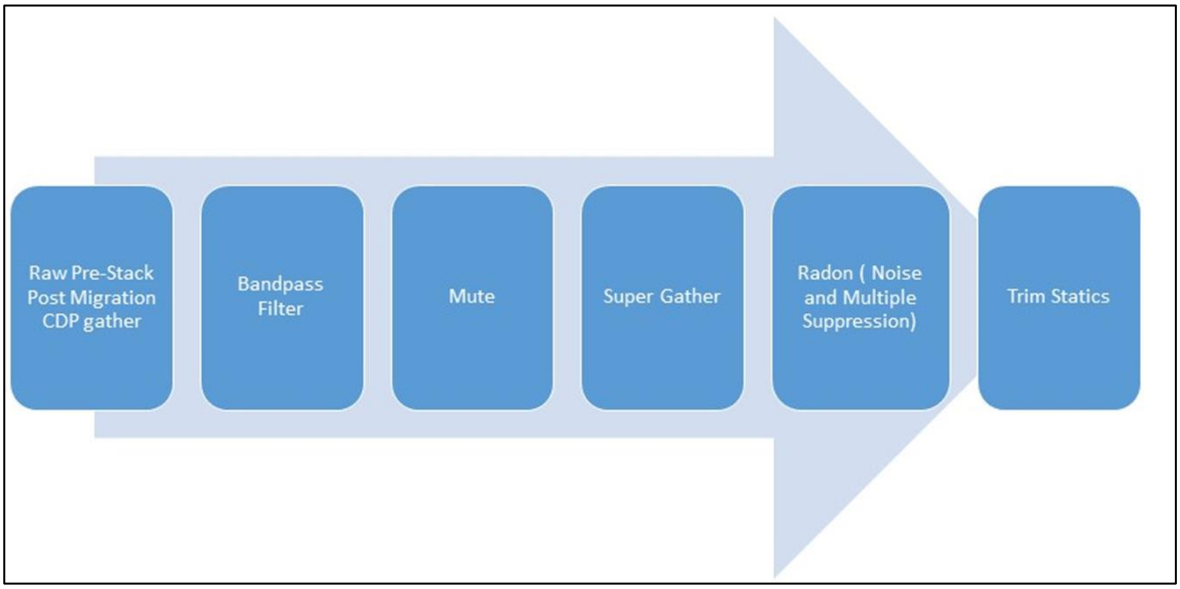

Figure 5-18. Seismic gather conditioning workflow.

`

The post-migration prestack seismic gather amplitude spectrum was inspected and found to be usable up to 60 Hz. Beyond 60 Hz, it is a high frequency and low amplitude signal and not desirable for subsequent processes in the workflow (Figure 5-19a, b). After inspecting the usable amplitude spectrum, a bandpass filter was designed to eliminate spurious and noise-dominant events in the seismic data (Figure 5-19b).

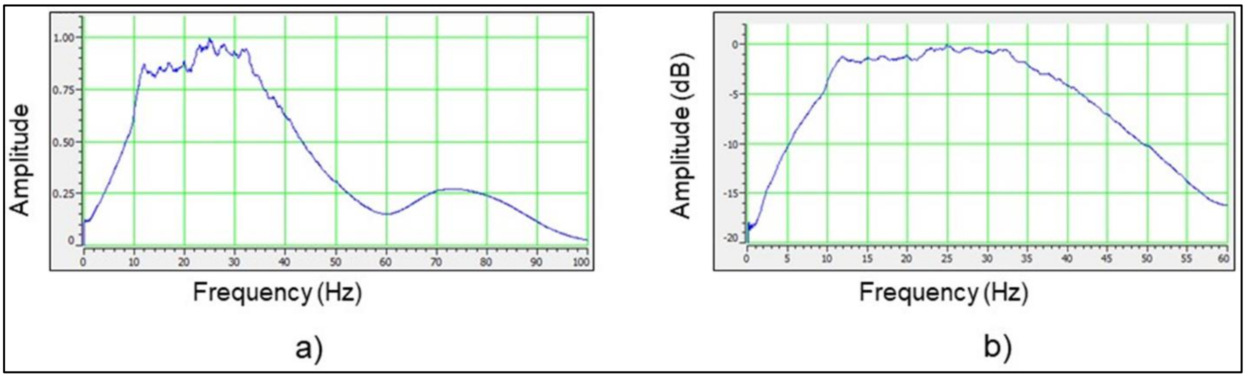

Figure 5-19. a) SME05-26 seismic gather Amplitude Spectrum, and b) SME05-26 Seismic Gather Amplitude Spectrum limited to 60 Hz, and in dB amplitude scale.

Velocity information from the PSA-I-21 well is used in determining angle information from the gather and assist in choosing a competent mute function to filter out events beyond the critical angle. A mute function can be picked manually or can be based on angle ranges (Figure 5-20). An inner and an outer mute can be chosen. In most cases, an outer mute is adequate (Figure 5-21). A super gather (Figure 5-22) was estimated by stacking traces in offset ranges to increase the signal-to-noise ratio of the original prestack gathers. In this case, using fifteen angle bins between 1 and 34 degrees, the super gather stacked three adjacent traces centered at 2, 4, 7,…29, 31, and 33 degrees. Radon transform (Figure 5-23) was used to remove unwanted noise from meaningful reflection signals. Radon transform (Figure 5-24a-c) was used to remove seismic multiple energy related to reverberations in the seismic signal that create “false” geological reflectivity in the data. Trim statics correction (Figure 5-25) was applied to correct the TWT response of similar seismic events across offset traces by using a pilot trace as a reference and ensuring all other traces are aligned in TWT accordingly. This method is more successful when using a long TWT window as a reference to avoid distorting AVO effects, particularly AVO classes that exhibit phase reversal in the offset domain (i.e., Class IIp or IVp). Class II sands according to (Castagna et al., 1998), have low normal-incidence reflectivity, meaning it has small impedance contrast. The introduction of gas in class IV sands

`

causes its reflection coefficient to become more positive with increasing offset (Castagna et al., 1998). The "p" in Class IIp and Class IVp stands for polarity. Before AVO gradients are performed, it is important to position well tops at correct two-way time positions. Subsequently the data were conditioned (Figure 5-26) and muted by manual picking (Figure 4-27a, b) to enhance the reflectivity and improve well-to-seismic tie. A well-to seismic tie at PSA-I-17 is shown in Figure 5-28.

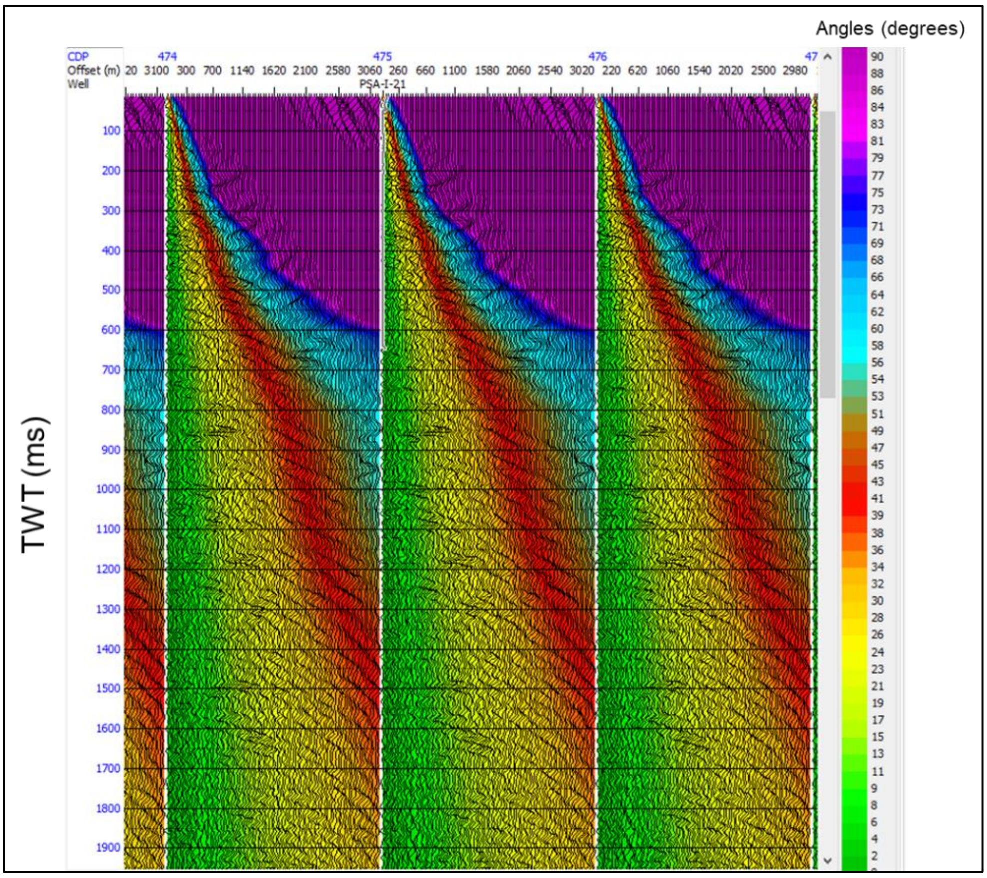

Figure 5-20. SME05-26 seismic gather after bandpass filter, with angle information overlain.

`

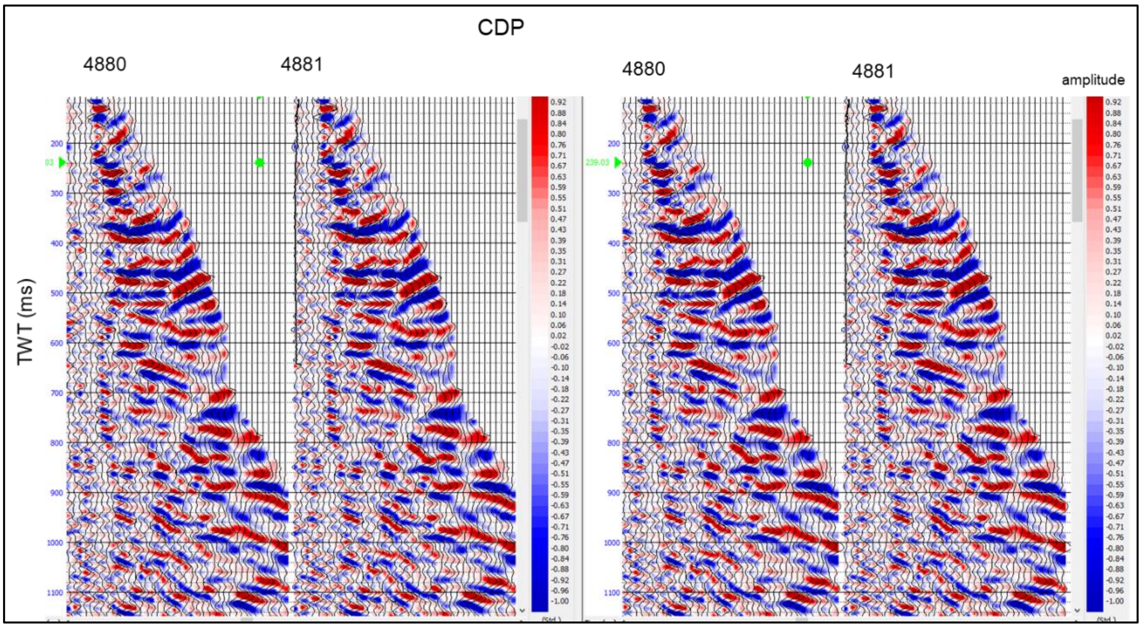

Figure 5-21. SME05-27 mute gather. The mute was manually picked, based on the angle obtained through PSA-I-21 well velocities.

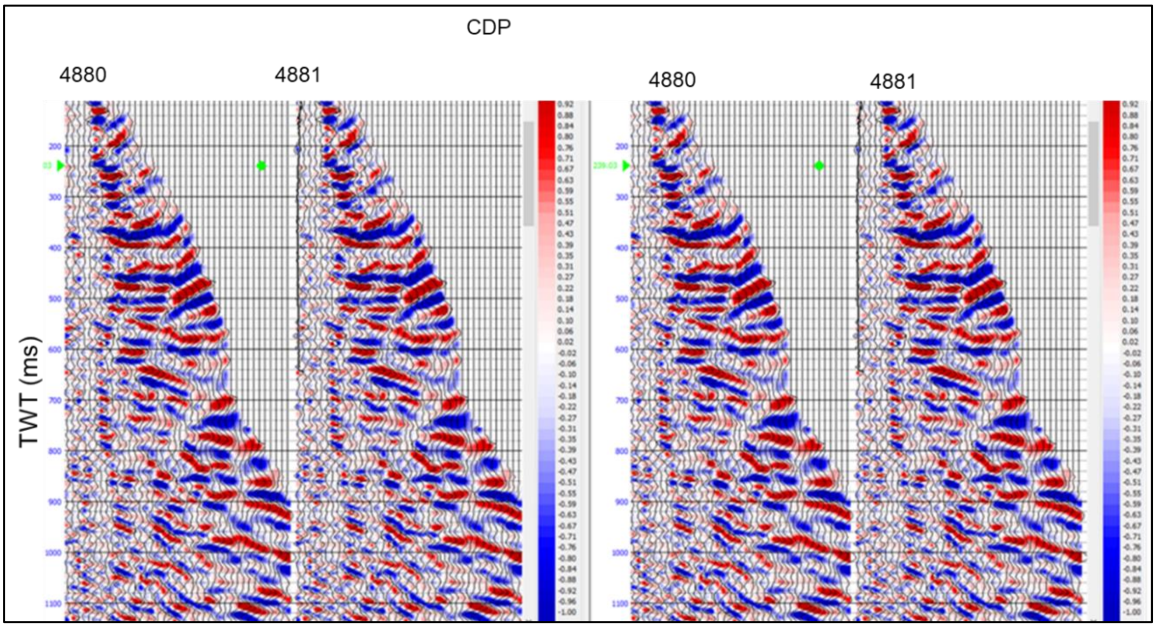

Figure 5-22. Super gather. A super gather is created by stacking 3 CDPs.

`

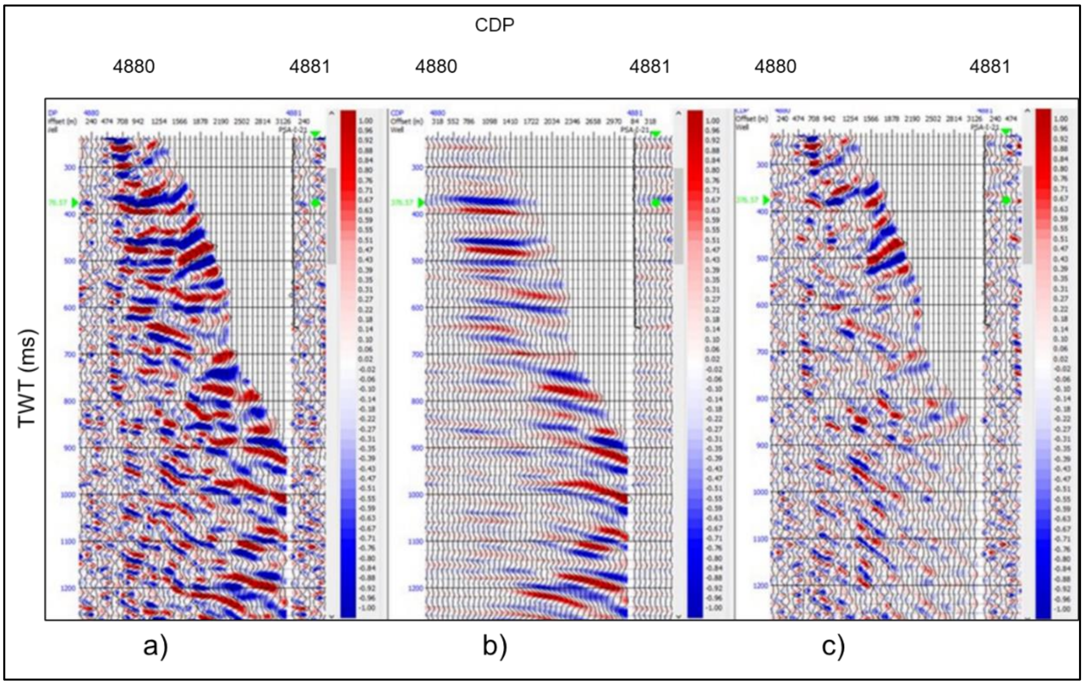

Figure 5-23. a) Super gather, b) seismic gather after radon noise attenuation, and c) noise attenuated from the seismic gather.

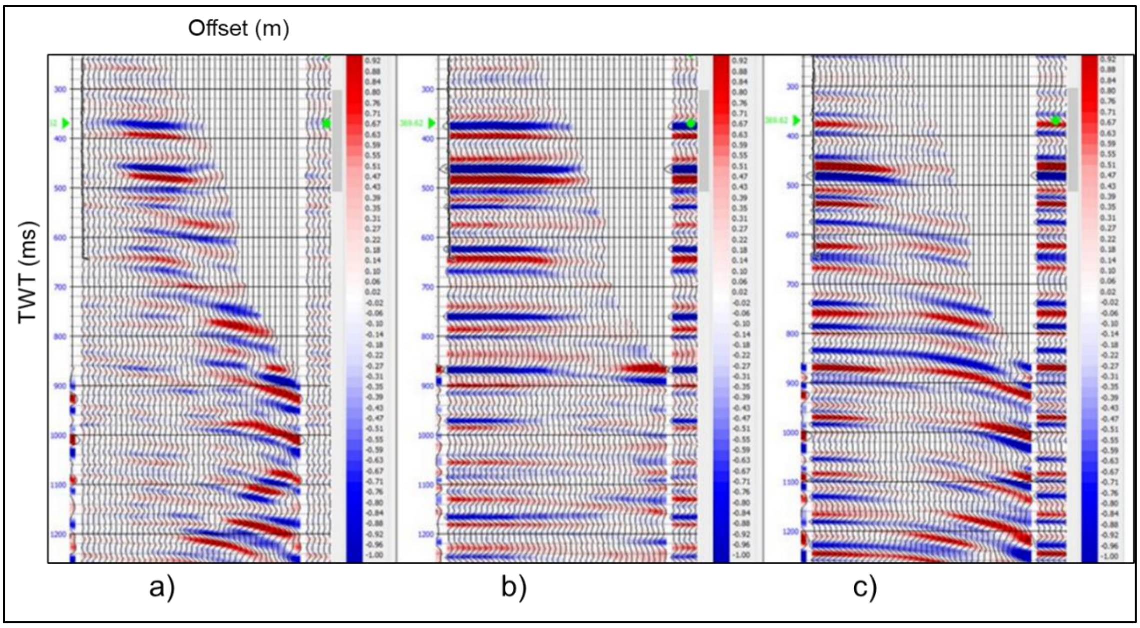

Figure 5-24. a) Input gather, b) gather after radon multiple Suppression, and c) noise removed using the radon operator.

`

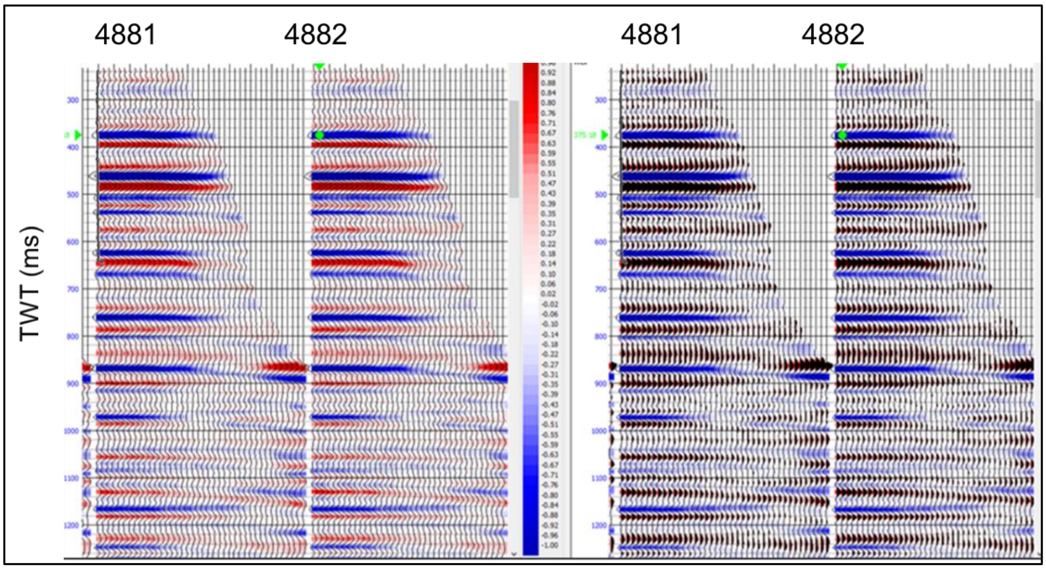

Figure 5-25. Seismic gather after Trim Statics operator.

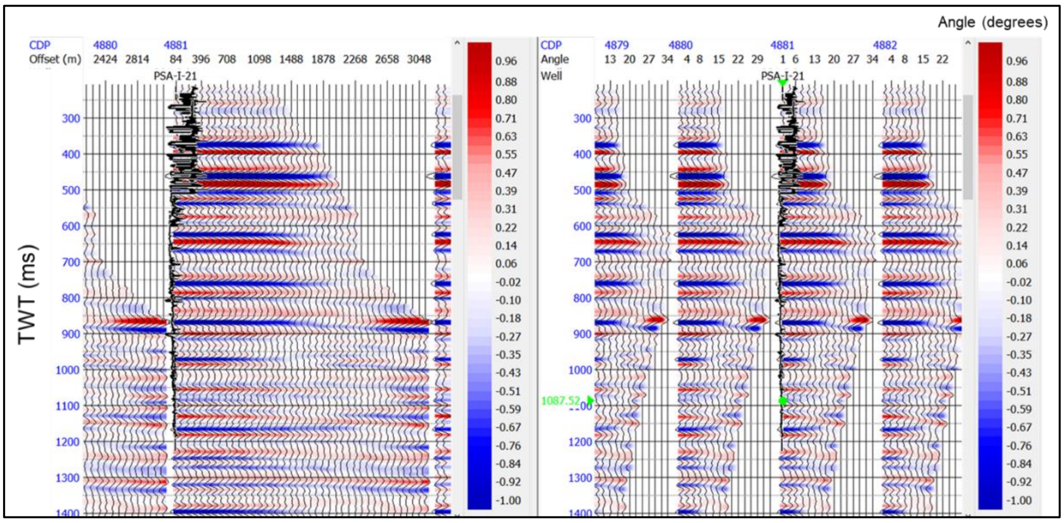

Figure 5-26. Conditioned seismic gather showing G6 around 900 ms.

`

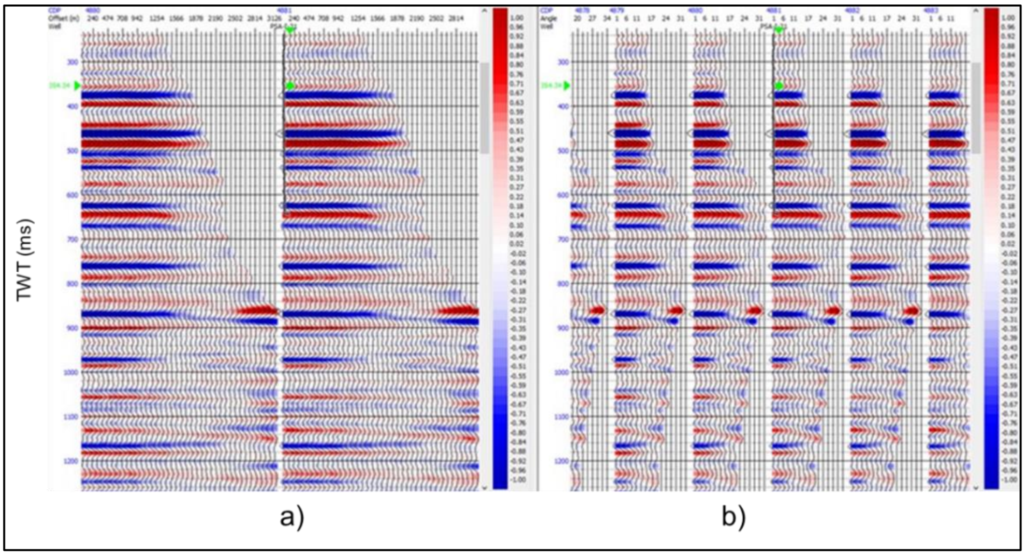

Figure 5-27. a) Seismic gather muted by manual picking, and b) Seismic gather after an angle mute was applied on SME05-27 seismic gather.

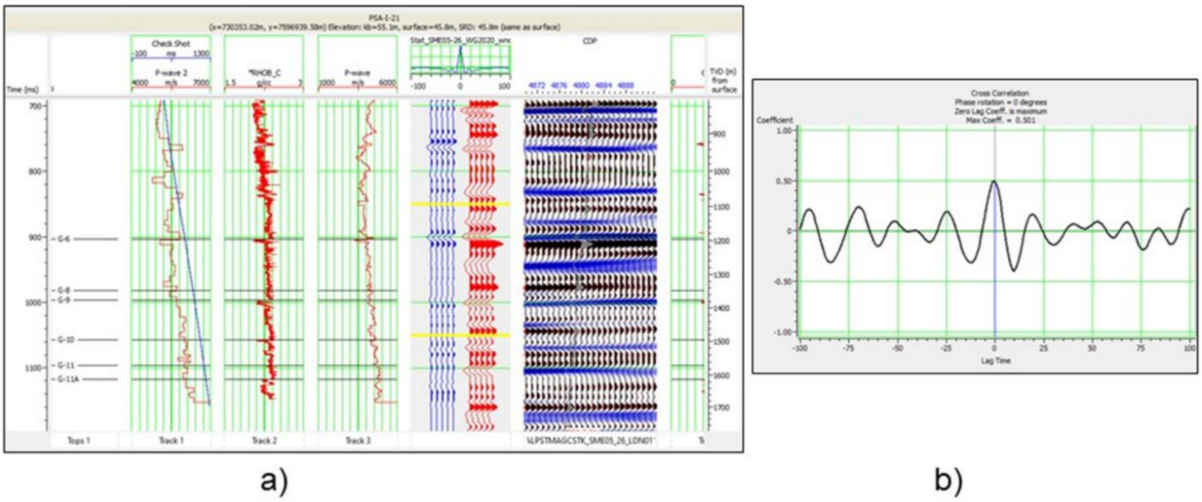

Figure 5-28. PSA-I-17 well to seismic tie. a) A well to seismic tie created by convolving the reflection coefficient and a statistical wavelet extracted from the SME05-26 seismic section within the lower Grudja section, b) cross correlation between the synthetic seismogram and SME-05-26 seismic section.

`

AVO gradient analysis

To characterise reflection at an angle of incident, intercept and gradient parameters are used. AVO interpretation may be facilitated by cross plotting AVO intercept and gradient (Castagna et al., 1998). The two-term version of equation 1 shows that the main factors that contribute to the AVO behavior of hydrocarbon-filled sands are amplitude (A), gradient (B), and the angle of incident (θ). A plane-wave reflection at the top of a gas and can be analysed through a plot of the reflection coefficient, R(0), versus incidence angle, θ (Figure 5-29).

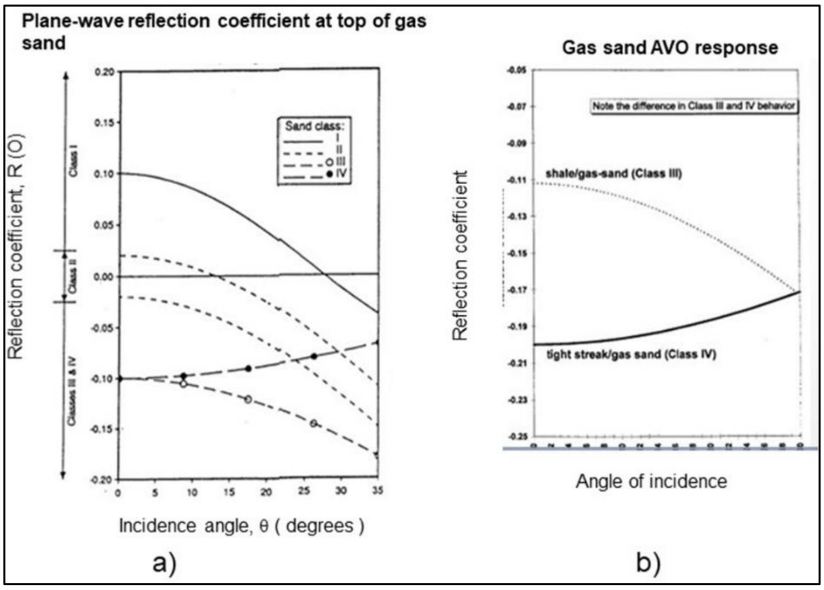

Figure 5-29. AVO response indicated through plotting reflection coefficient and incident angle. a) Plots the reflection coefficient versus incident angle and indicates all possible AVO classes, and b) a special AVO case where a reservoir is a gas sand (Castagna & Swan, 1997).

According to (Castagna et al., 1998), AVO interpretation is facilitated by cross-plotting intercept and gradient. Brine-saturated rocks generally follow a “background” trend in the A-B plane (Figure 5-30). Deviations from the background indicate hydrocarbon saturations or anomalous elastic properties from lithology (Foster & Keys, 1999). In the Mozambique Basin, gas sands were analysed, although there are liquids in G6 Inhassoro.

What is evident from the Figure 5-30 plot is that in the intercept vs gradient crossplot, gas sands are heavily influenced by the porosity of the reservoir. What differentiates class III and IV AVO, is the porosity. Reducing the porosity of the gas reservoir can result in class III and

`

increasing porosity moving in the opposite direction, towards quadrant II, class IV AVO response.

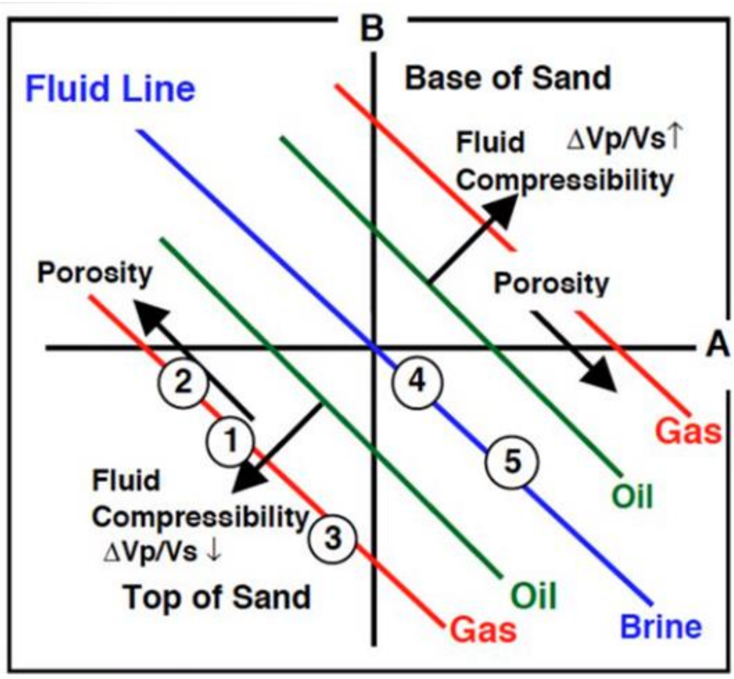

Figure 5-30. Fluid line, Gas Sands, and Rock Properties. The plot demonstrates that if starting with a class 3 sand at point 1, and porosity is increased, the AVO response moves to point 2, which after crossing into the second quadrant becomes a class V AVO response. Alternatively, if porosity is reduced from point 1, the response would be point 3. If gas is replaced with brine, the resulting plot is point 4. Reducing porosity in a brine-saturated reservoir would move the plot to point 5 (Foster & Keys, 1999).

Figure 5-31a shows a conditioned gather where angle and amplitude information can be extracted from. Figure 5-31b plots amplitude versus the angle of incident. This process enables the picking of surfaces/horizons and analysis of resulting AVO responses. Ideally, a conditioned gather should result in the flattening of events. In cases where events on a gather are not completely flat, a horizon pick may be a better representation of how the amplitude behaves as a function of angle. The G6 in Inhassoro exhibits a class IV AVO response. This is characterised by a negative intercept (Amplitude) and a positive gradient. This is consistent with an observation made in Pande at the G6 and the G10 levels. AVO gradient responses from analysis done at the G6 level of SME05-26 gather at CDP corresponding to PSA-I-21 well is shown in Figure 5-32, indicating that it plots in the second quadrant, typical of class IV AVO response.

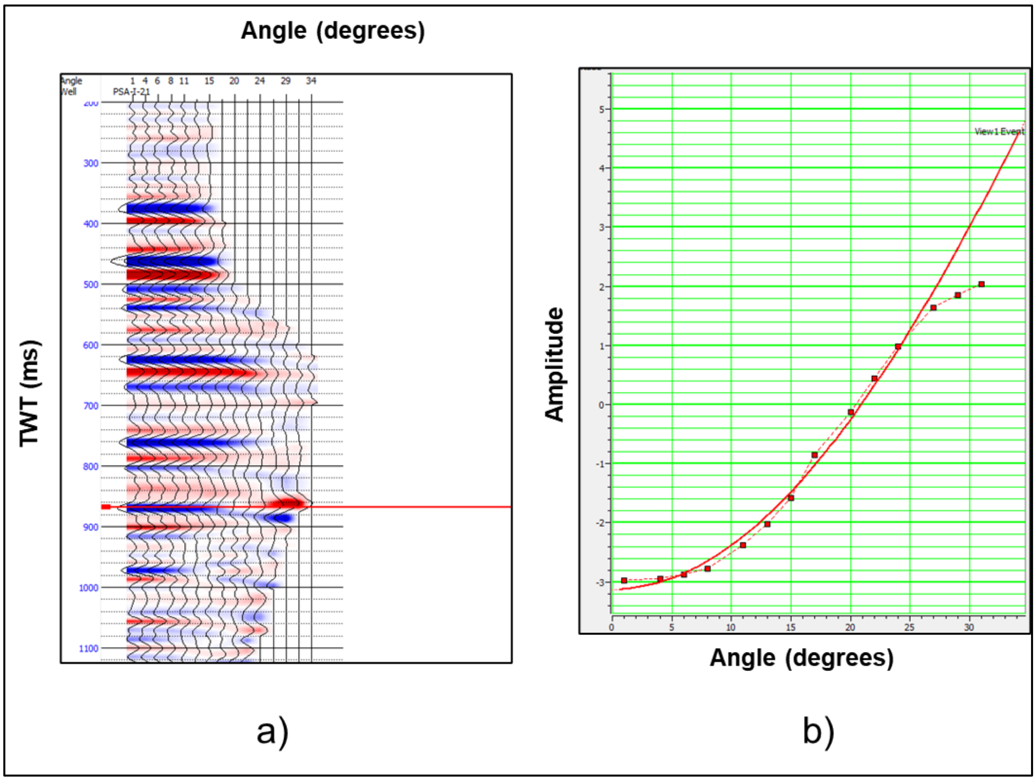

Figure 5-31. AVO Gradient on line SME05-26. a) Conditioned seismic gather and G6 pick shown in red, b) AVO response – red dots represent AVO points from the seismic gather and the red line shows Aki & Richards approximation.

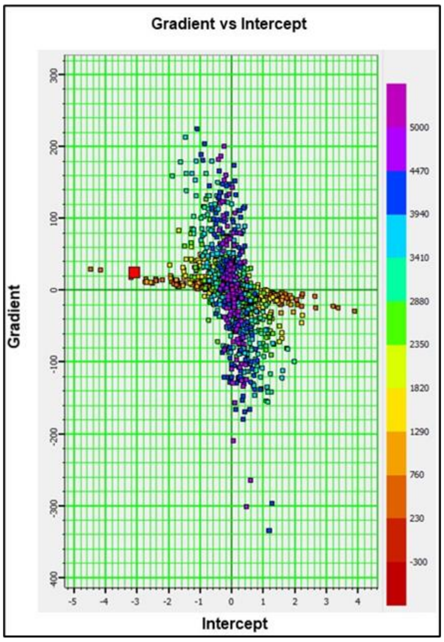

Figure 5-32. AVO gradient analysis on SME05-26, at the CDP corresponding to PSA-I-21. The AVO response at G6 at the Inhassoro well location exhibits a class IV AVO response. Class IV AVO response in the gradient/intercept domain plots in the second quadrant.

`

SME05-19 and Inhassoro 14

The Inhassoro 14 well is covered by the Inhassoro 3D seismic data and on the SME05-19 2D seismic line. SME05-19 seismic gather, Figure 5-33, was conditioned through radon and trim statics application. A conditioned SME05-19 gather with most of the noise removed to enable AVO attributes analysis is presented in Figure 5-34. Amplitude behaviour at the CDP corresponding to the Inhassoro 14 well location and at the G6 horizon is shown in Figure 5-35. Gradient analysis of the G6 reservoir on SME05-19 at the Inhassoro 11 well location is plotted in Figure 5-36.

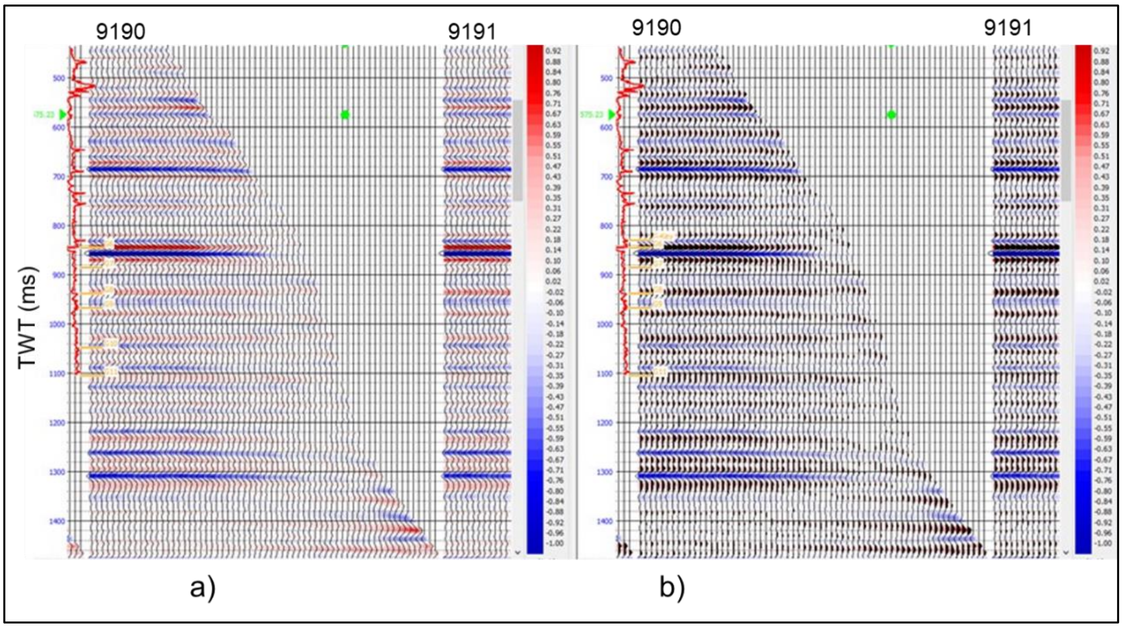

Figure 5-33. SME05-19 Seismic gather. a) Seismic gather after radon transform application, and b) seismic gather after trim statics application.

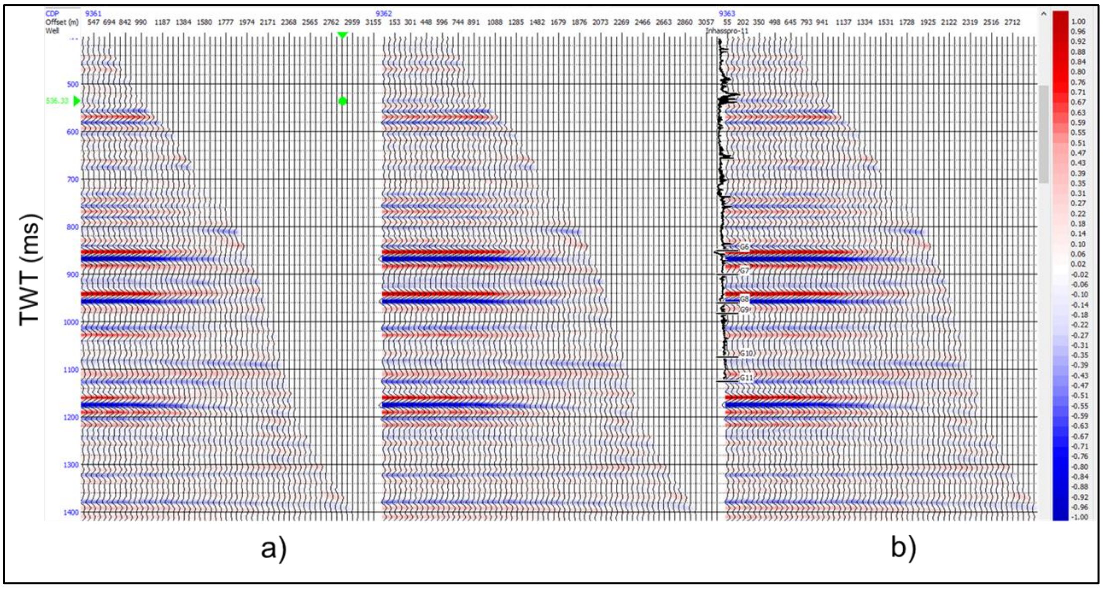

Figure 5-34. SME05-19 seismic gather after conditioning (a). Most of the noise has been attenuated and it's now AVO compliant (b).

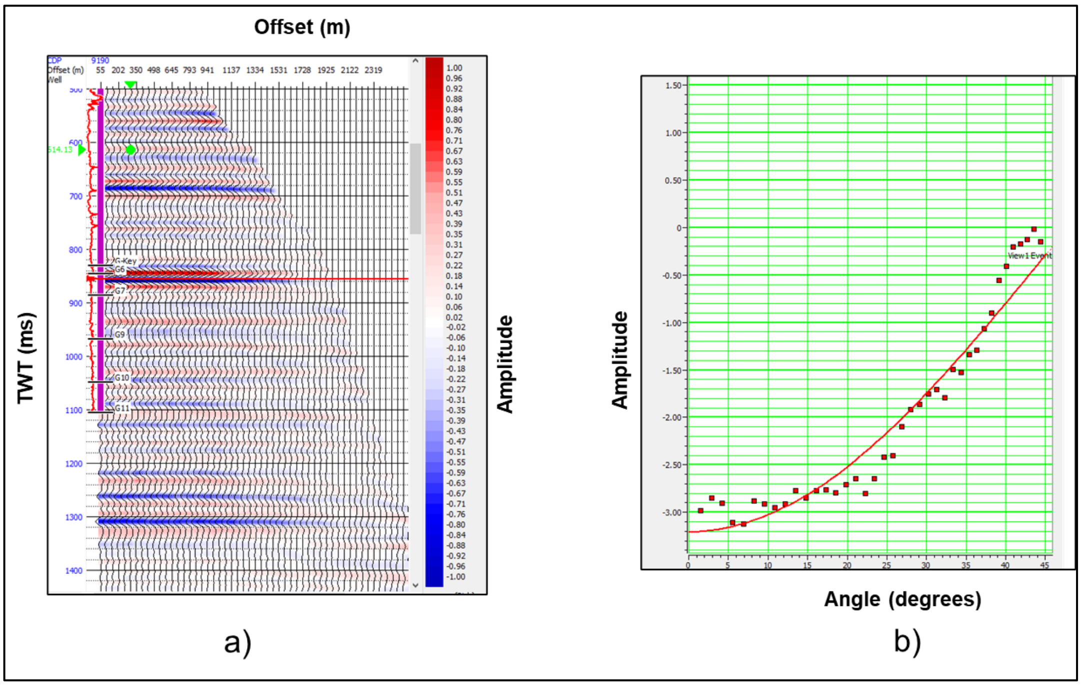

Figure 5-35. SME05-19 gradient analysis at G6 level on the location of Inhassoro 11 CDP. a) SME05-19 seismic gather in the offset domain. A G6 pick is shown in red. b) AVO response from the picked points. The red line represents Aki and Richards's approximation.

`

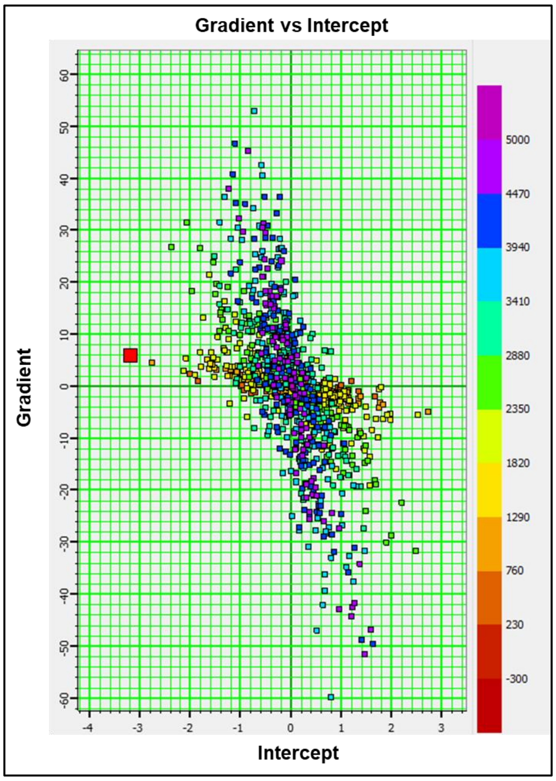

Figure 5-36. SME05-19 gradient vs Intercept at Inhassoro 11 CDP location at G6. The AVO response at G6 at the Inhassoro well location exhibits a class IV AVO response. Class IV AVO response in the gradient/intercept domain plots in the second quadrant.

AMT98-06 and Inhassoro 9.

Inhassoro 9 G6 AVO behaviour was also investigated through the use of conditioning seismic gathers, this is through extraction amplitudes at reservoir level (Figure 5-37a) and plotting reflection coefficient versus angle of incident (Figure 5-37b) and through cross plotting intercept versus gradient (Figure 5-38).

`

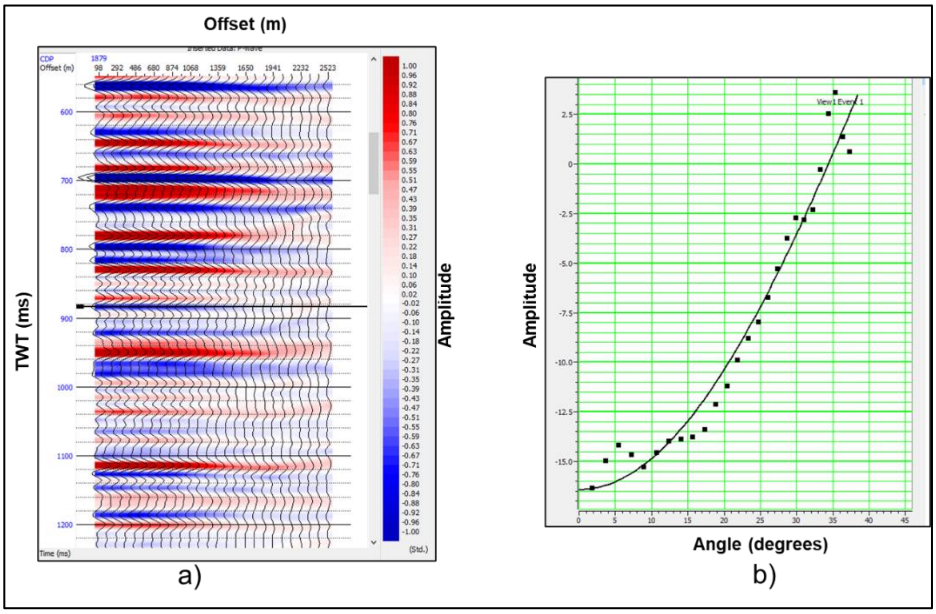

Figure 5-37. G6 line (a) and (b) AVO gradient analysis at AMT98-06, at Inhassoro 9 CDP location (b).

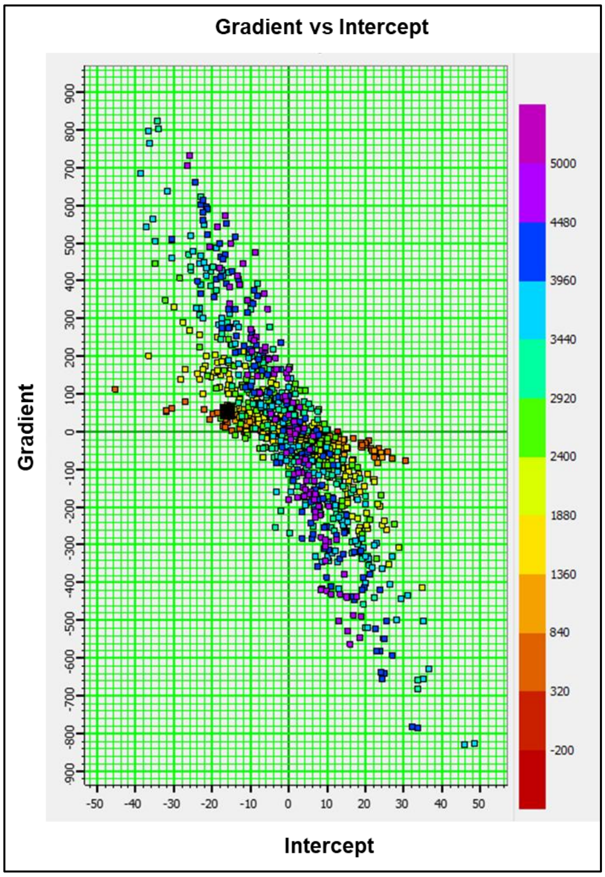

Figure 5-38. AMT98-06 Gather. AVO Gradient analysis at Inhassoro 9 gather location. The AVO response at G6 at the Inhassoro 9 well location exhibits a class IV AVO response. Class IV AVO response in the gradient/intercept domain plots in the second quadrant.

SME05-27 and Inhassoro 13

A standard procedure of analysis, that is, conditioning a seismic gather and extracting reservoir properties at well location CDP and reservoir level was also conducted on 2D line SME05-27. The input gather, Figure 5-39a, contains a lot of noise and was produced mainly for subsequent data processing processes that prioritised structural analysis. The display in Figure 5-39b shows the robustness of the seismic conditioning process that ensures that the resulting gather is AVO compliant. Class IV AVO for G6 is confirmed by Inhassoro 13 well on Figure 5-40a extraction and plot on Figure 5-40b. Gradient analysis through cross plotting intercept versus gradient of G6 reservoir on line SME05-27, on CDP corresponding Inhassoro 13 well is presented in Figure 5-41 and Figure 5-42.

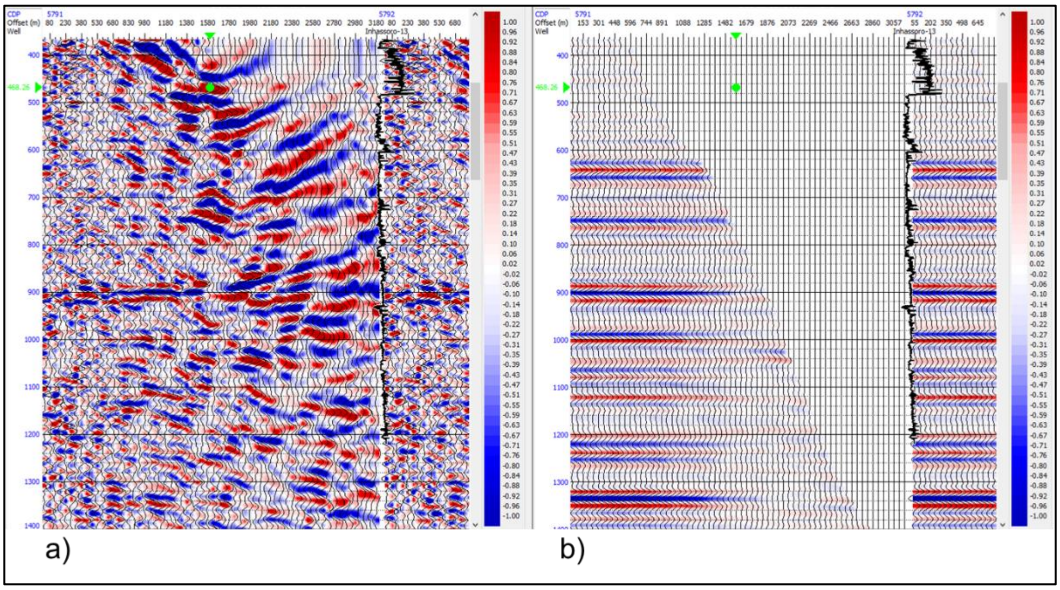

Figure 5-39. a) SME05-27 input vs b) conditioned seismic gather at Inhassoro-13 CDP location. The conditioned gather demonstrates the robustness of the conditioning process, which results in AVO-compliant gathers.

`

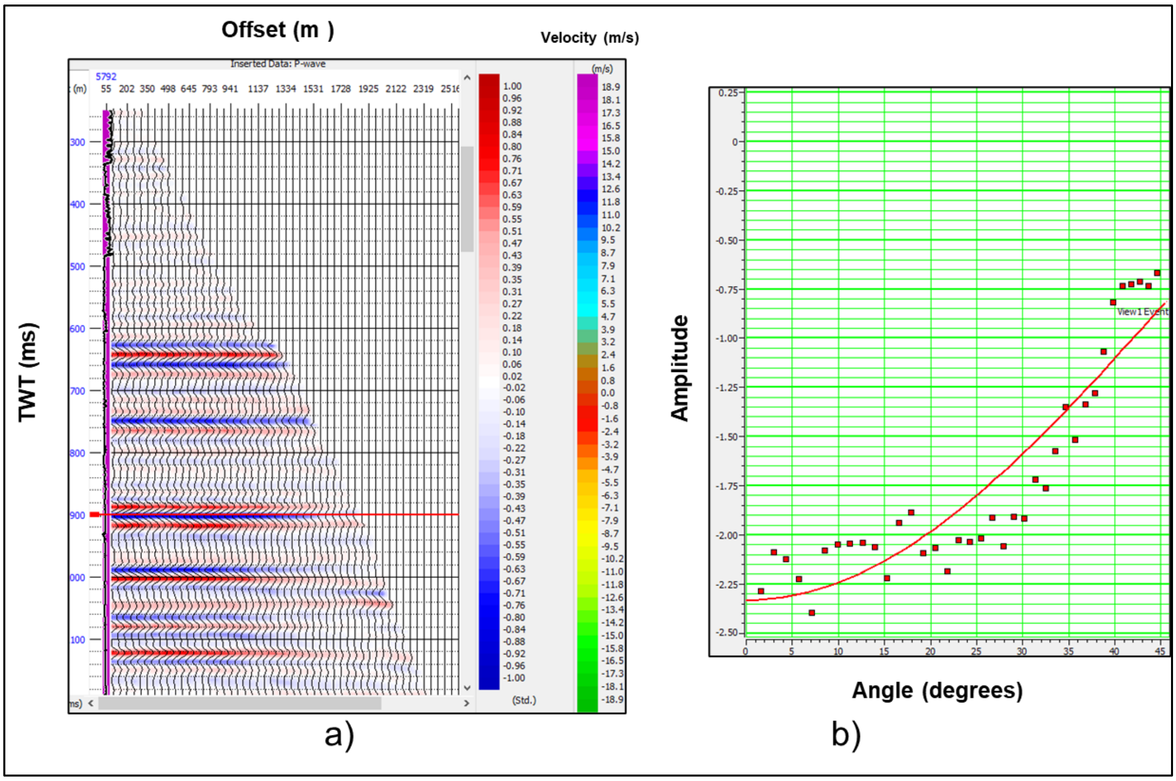

Figure 5-40. SME05-27 conditioned gather AVO gradient analysis. a) Seismic gather at the CDP corresponding to the Inhassoro-13 well. b) AVO points from the G6 levels, red dots. The red line is Aki and Richards's approximation. The crossplot exhibits a class IV AVO behaviour.

`

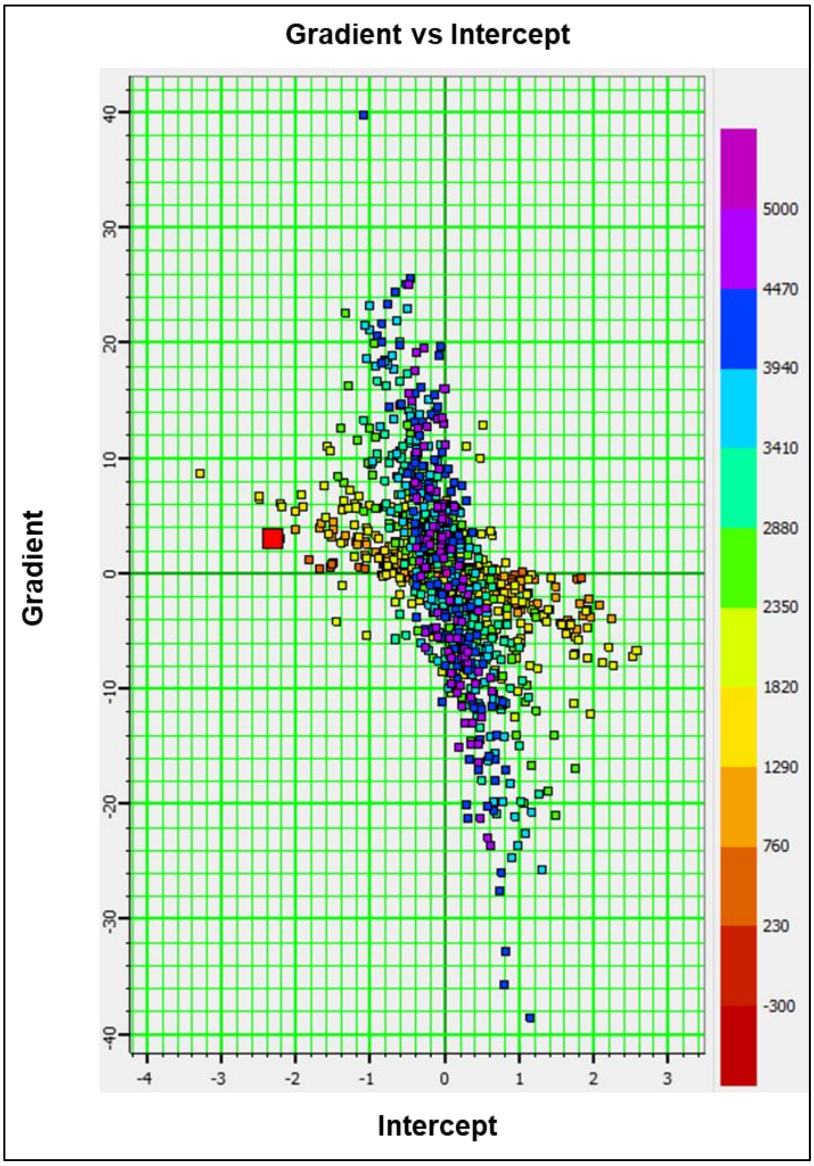

Figure 5-41. SMEO5-27 gather gradient vs intercept crossplot. Class IV AVO in the gradient vs intercept domain at the G6 level.

`

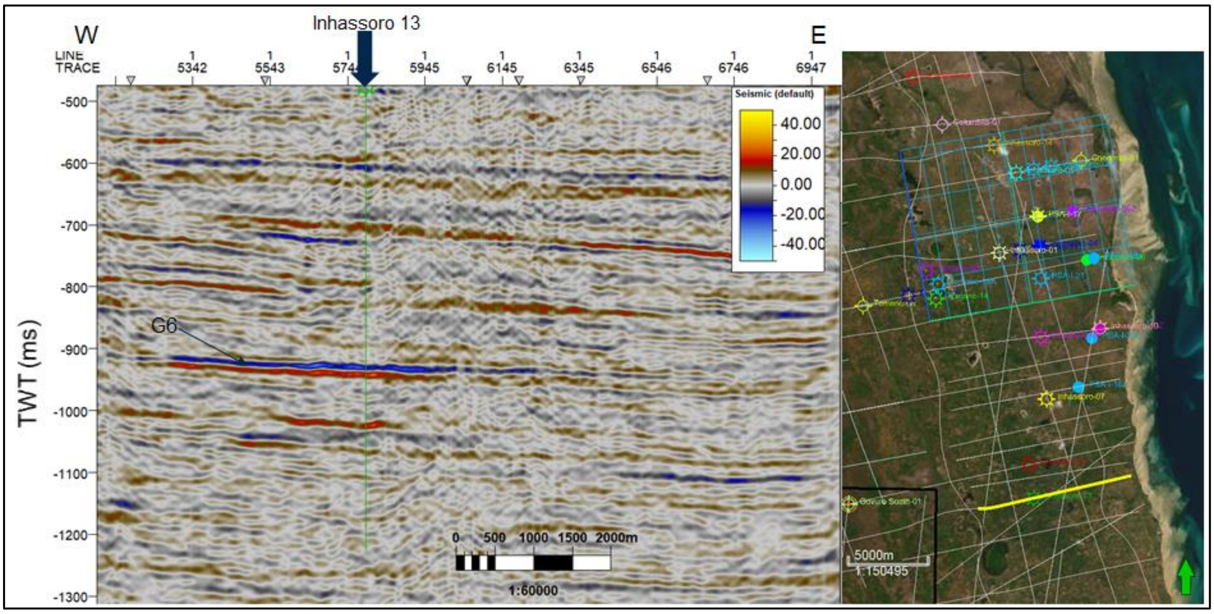

Figure 5-42. Inhassoro G6 on SME05-27 at around 900 ms. Inhassoro 13 well is projected on the seismic section. The G6 reservoir is a soft event, a negative amplitude which plots as a blue over red on the seismic section.

5.5 Rock physics trends of Mozambique Basin

Rock physics analysis links the response of elastic rock properties (elastic moduli and density) and petrophysical properties (porosity, mineral volume, and water saturation) to characterise reservoir and non-reservoir facies (Figure 5-43) (Dvorkin, 2001).

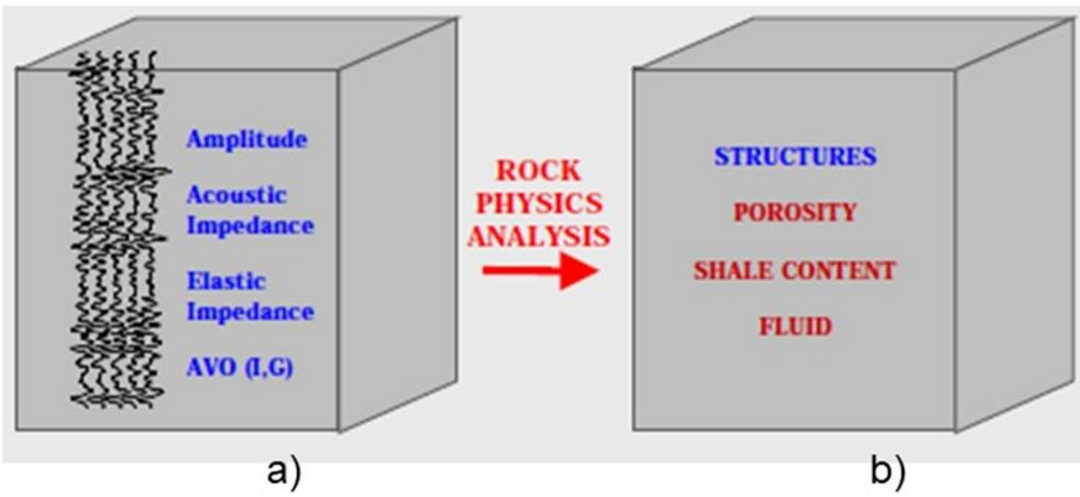

Figure 5-43. Rock Physics Reservoir Characterization. The goal is to create a 3D image of volumetric rock properties from seismic data (a). This is achieved through the transform function between rock elastic properties and rock volumetric properties (b). Measurements from well logs and laboratory studies are used (Dvorkin, 2001).

`

A rock physics model is built from crossplots involving velocity-porosity relations for the entire log, and where appropriate depth intervals and depositional sequences are assigned (Dvorkin, 2001). Crossplots are not limited to showcasing AVO behaviour. A rock physics diagnostic can be done using well log and core data. Relationships obtained from cross plots can be used to relate petrophysical properties like porosity, shale content, saturation, and pore fluids to elastic rock properties (Dvorkin, 2001). Well log information typically included: sonic, shear, density, gamma ray, and neutron porosity. If a core was collected, its analysis typically includes information about density, velocity, mineralogy, and porosity. If good log data are available, these cross plots can be used to describe lithology, porosity distribution, reservoir quality, pore pressure, cementation, and gas saturation. Figure 5-44 presents these conceptual Vp/Vs vs P-Impedance trends for siliciclastic lithologies at constant confining pressures (Odegaard & Avseth, 2004). These crossplots act as Rock Physics Templates (RPT) to assist geoscientists in the understanding of (i) vertical variability of elastic and petrophysical properties across stratigraphic columns, and (ii) lateral variability of such properties creating facies heterogeneities. Rock physics templates can also be used for “interpretation and quality control of well log data”, given that they can be used to detect different fluid and lithology scenarios (Odegaard & Avseth, 2004).

`

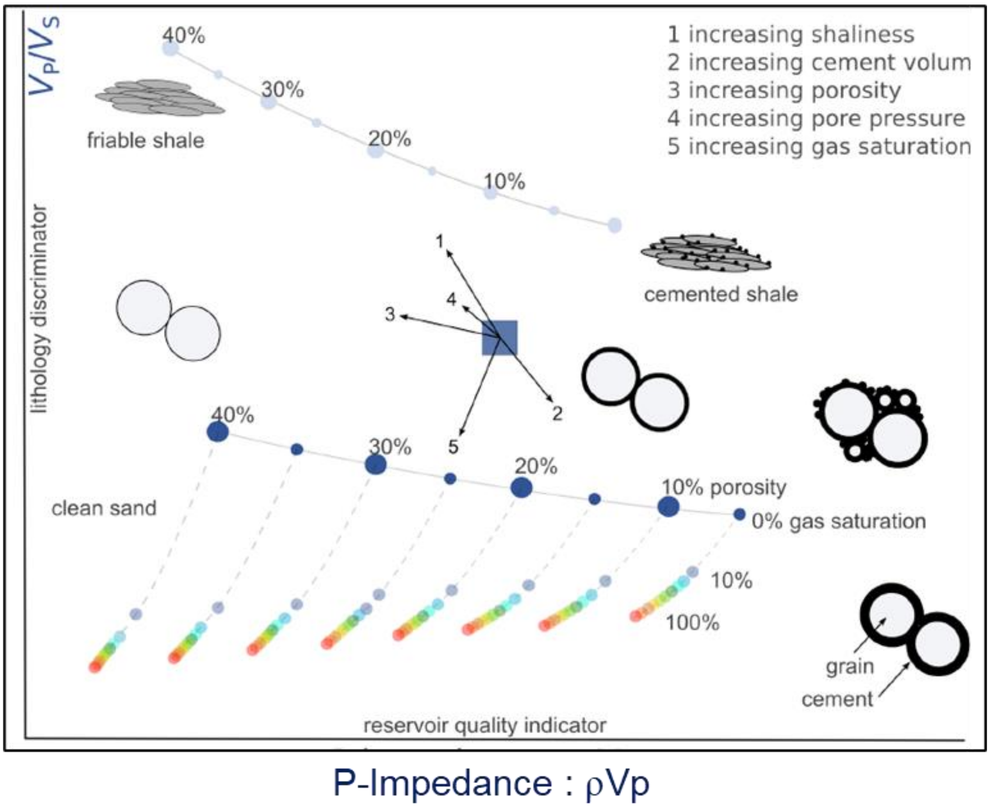

Figure 5-44. Vp/Vs vs P-Impedance. Conceptual trends for siliclastic lithologies at constant confining pressure (Odegaard & Avseth, 2004).

The Vp/Vs vs AI cross-plot is useful to describe variations in a reservoir and non-reservoir facies based on typical outputs from elastic inversion of seismic data (Odegaard & Avseth, 2004). A Rock Physics Template trend for the Mozambique Basin can be created to capture basin information about burial depth (given that reservoirs of interest are typically compacted at 1000 to 1500m TVDSS), mineralogy (to characterize differences between quartz, feldspar, and clay-rich facies) at multiple pressure and temperature conditions. Likewise, the seismic response of hydrocarbon-saturated facies can also be assessed using these RPTs, particularly given that the presence of oil in these facies is usually subtle and not as anomalous as gas saturated facies.

`

5.6 Inhassoro reservoir characterization

PSA-I-17 Crossplots

The crossplot of VpVs vs P-Impedance on well PSA-I-17 (Figure 5-45) in Inhassoro exhibits the same trends as described by (Odegaard & Avseth, 2004). Most of the data, representing shaly and brine saturated sands, plot in a trend higher than those gas-saturated porous rocks (lower left data points). The data in Figure 5-45 is from PSA-I-17 well and can be viewed in cross section as shown in Figure 5-46.

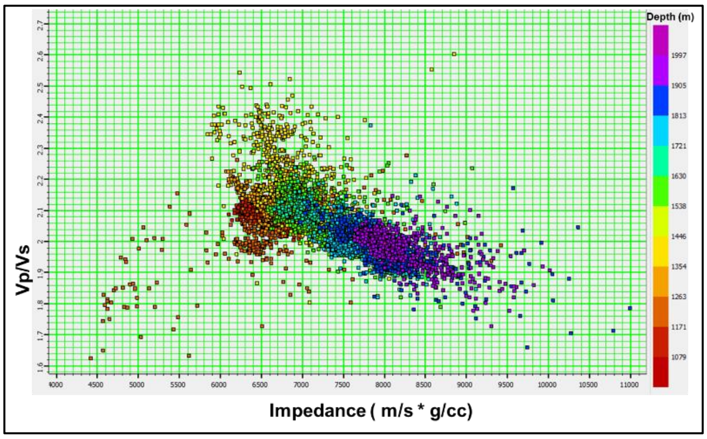

Figure 5-45. PSA-I-17 P-Impedance vs Vp/Vs Ratio. Gas-saturated porous rocks plot on the lower left section of the cross-plot. Well log data from Lower Grudja to deeper as shown on the plot on Figure 5-46.

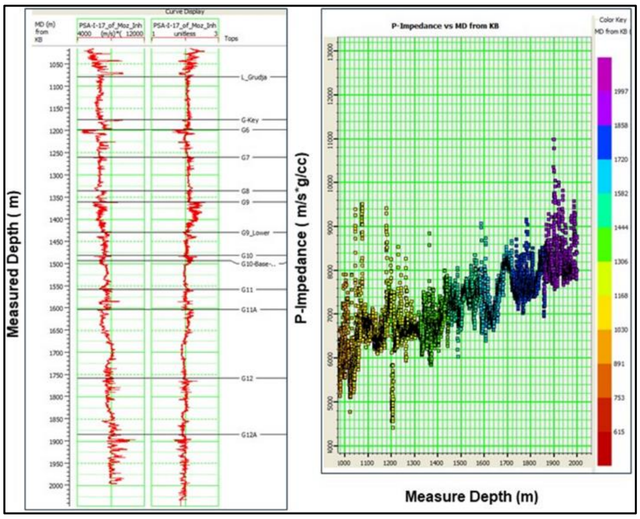

Figure 5-46. PSA-I-17 Vp/Vs vs P-Impedance Cross Section. The cross-section plots the cross-plot data from Figure 5-45 as well as logs.

`

Lamé petrophysical properties as fluid indicators

In full stack seismic or in well log elastic properties, the main parameters considered are Vp – compressional velocity, Vs – shear velocity and ρ – density. Vp given in equation 1 is given by,

$$Vp = \left(\frac{k+\frac{4}{3}\mu}{\rho}\right)^{1/2} = ((\lambda + 2\mu)/\rho)^{1/2}$$

And $Vs = (\frac{\mu}{\rho})^{1/2}$

Lambda (λ) and Mu (μ) are Lamé elastic constants, named after the French mathematician Gabriel Lamé (Sheriff, 2002). Lambda (λ) is associated with fluid incompressibility and is the most sensitive fluid indicator. This is often not apparent since it is embedded in the Vρ equation and its effects not fully appreciated or diminished by other parameters (Goodway et al., 1997). This applies to bulk modulus or K, when the compressional velocity equation is expressed in terms of bulk and shear modulus. Advantages of using this crossplot include improved petrophysical discrimination of rock properties over conventional Vp, Vs analysis by isolating reservoir rock properties between pore fluid and lithology based on Lame parameters (Goodway et al., 1997).

The clean, gas saturated sands in Figure 5-47 fall within 20 GPa*g/cc. At this point, a cut-off for the basin has not been established. Mu-Rho (μρ), rigidity x density, usually plots upper than it is plotting in this field. This is probably due to lower density values in the reservoir section. Nevertheless, lambda-Rho, the incompressibility x density function, can positively discriminate gas sands. The λρ vs μρ crossplot is orthogonal to Lame parameters or modulli. This offers a clear separation compared to acoustic impedance x density (Ip) vs shear impedance (Is) (Figure 5-48).

`

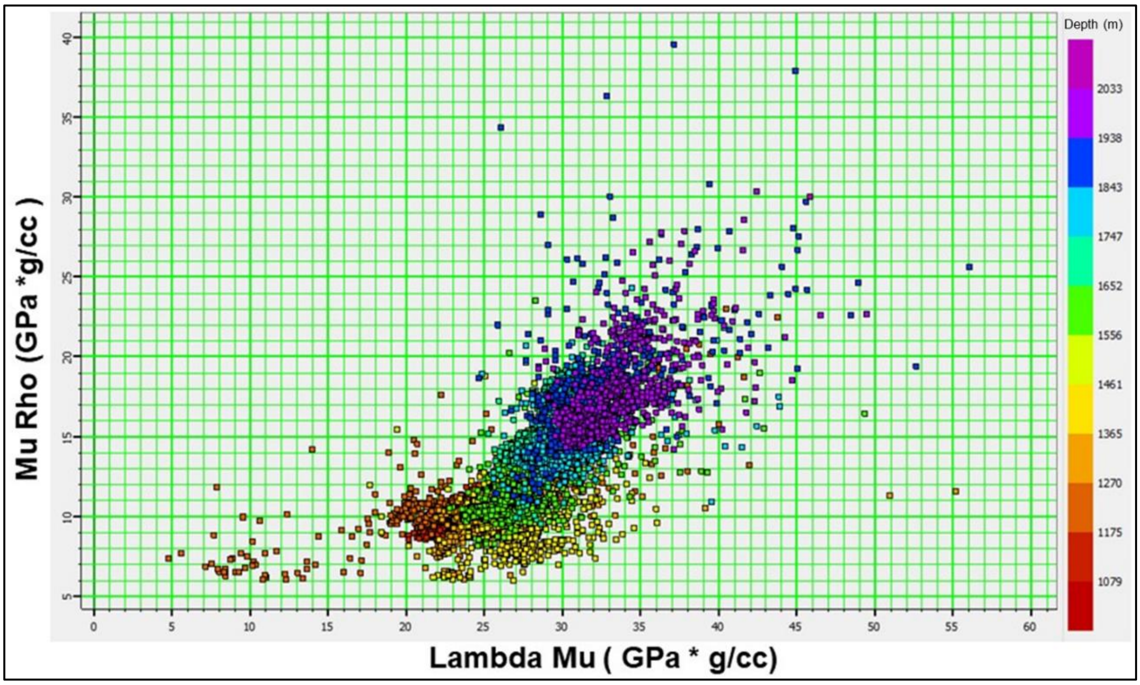

Figure 5-47. PSA-I-17 Lambda Mu Rho (LMR), Lambda-Rho vs Mu-Rho, lower Grudja to G12A. Lambda Rho is the incompressibility x density function. Mu-Rho is rigidity x density function.

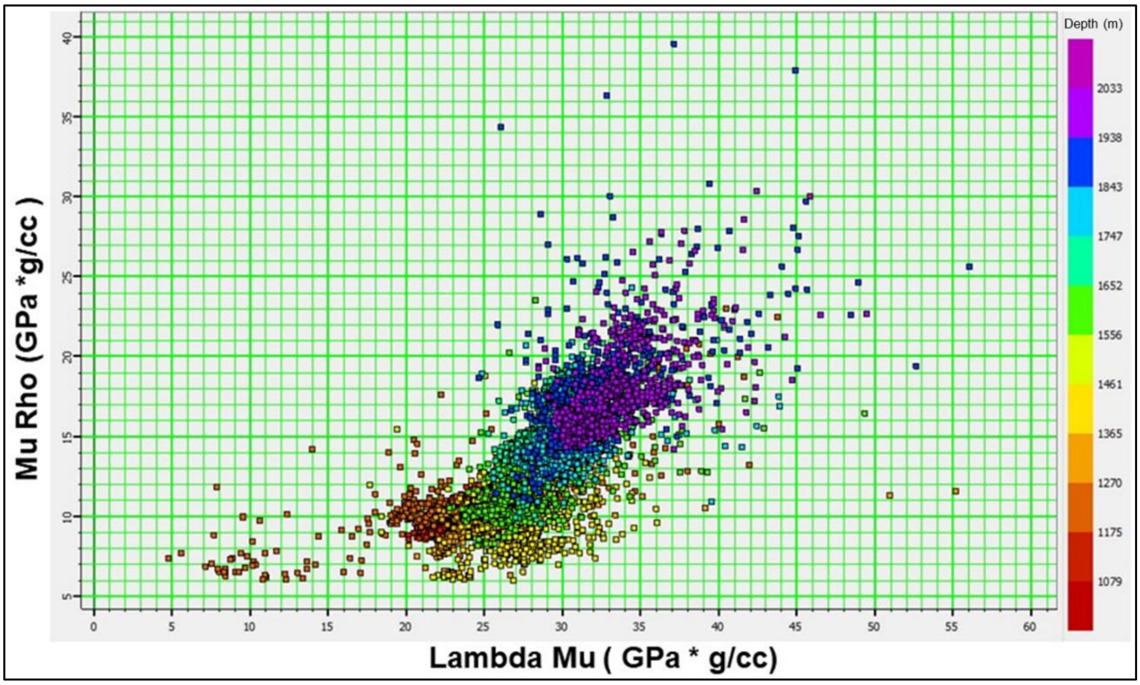

Figure 5-48. PSA-I-17 P-Impedance vs V-Shale, Lower Grudja to G12A.

`

Effects of porosity

Porosity is the percentage of void space in a rock, and it is one of the key factors when determining the amount of hydrocarbons contained in a reservoir. Porosity can be determined from cores, sonic logs, neutron logs, or resistivity logs. Figure 5-49 shows the tool and how porosity is measured in a borehole. Sandstone typically has higher porosity than a crystalline rock as visualised in Figure 5-50. The cross-plot in Figure 5-51 and other porosity cross-plots use neutron porosity (Figure 5-52).

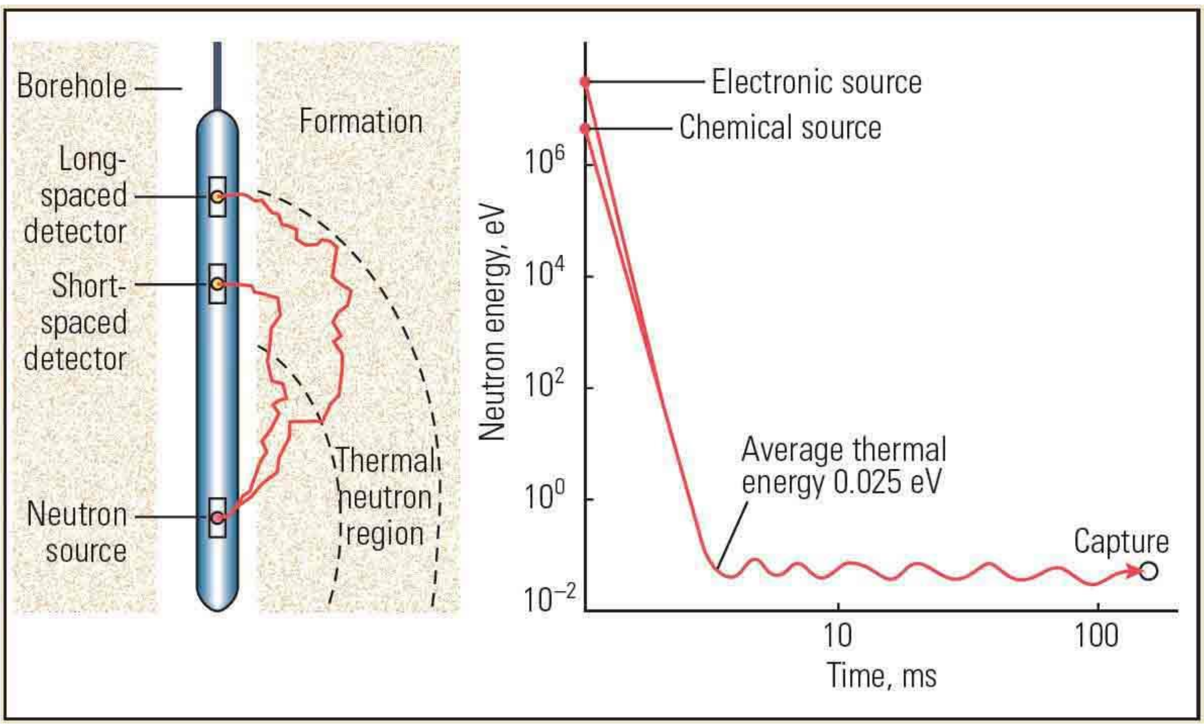

Figure 5-49. Neutron porosity tool showing how porosity is measured downhole.

Although useable for creating Rock Physics Templates for the Mozambique Basin, there are some shortcomings of neutron porosity. Gas has a much lower hydrogen density than oil or water, as a result, gas-filled porosity appears as low porosity (Smithson, 2015).

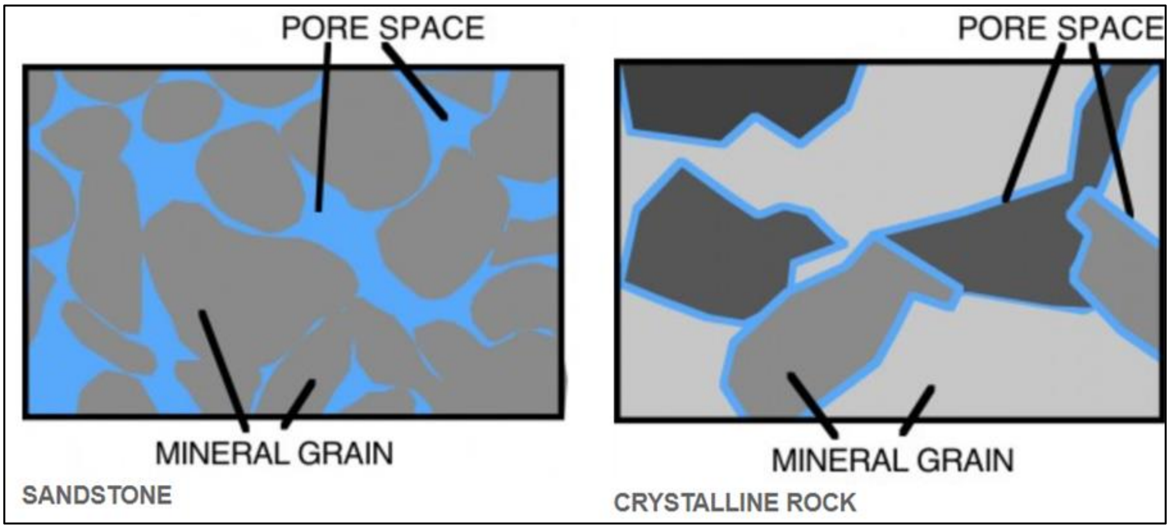

Figure 5-50. Porosity visualisation. Pores shown in blue (Wisconson Geological and Natural Survey , Univeristy of Wisconson-Madison, n.d.).

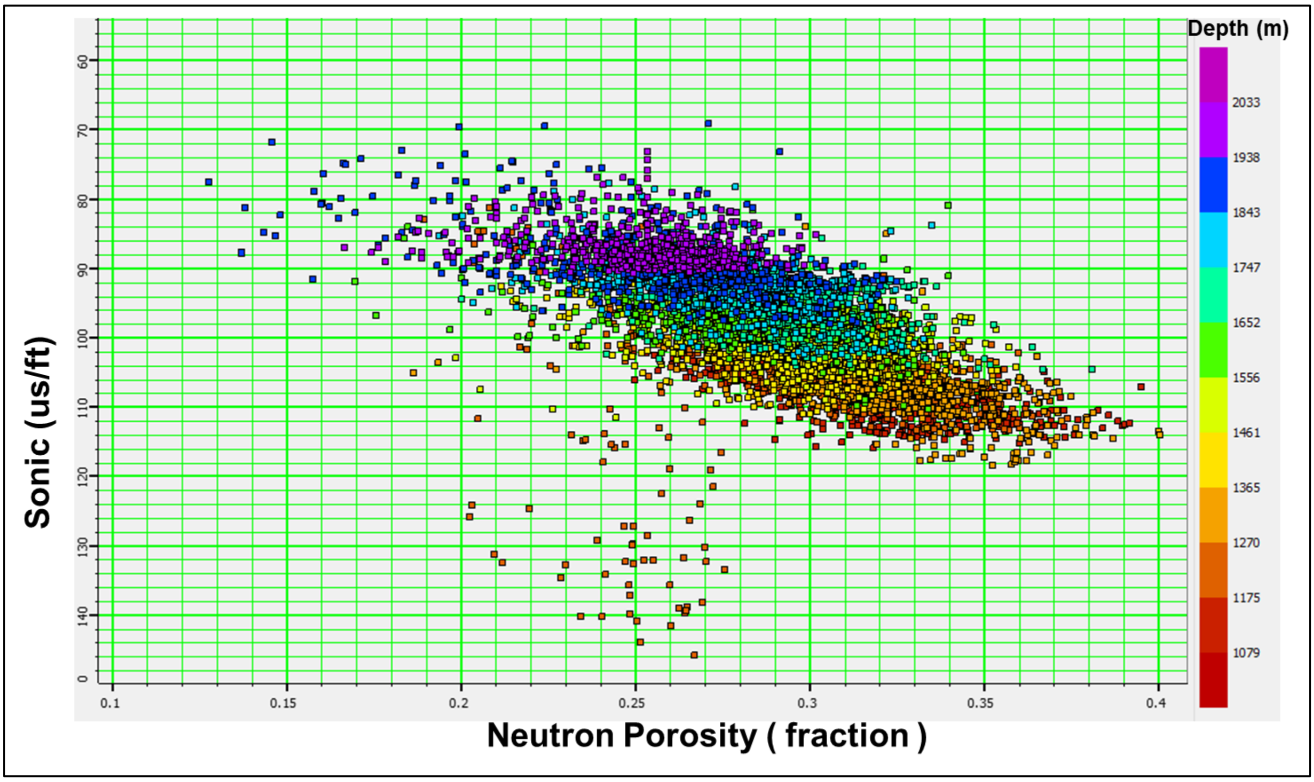

Figure 5-51. PSA-I-17 P-wave vs Neutron Porosity. P-wave plotted as sonic log response. Most points plot within an easily defined trend, but some points plot in relatively high porosity and low p-wave velocity regions.

`

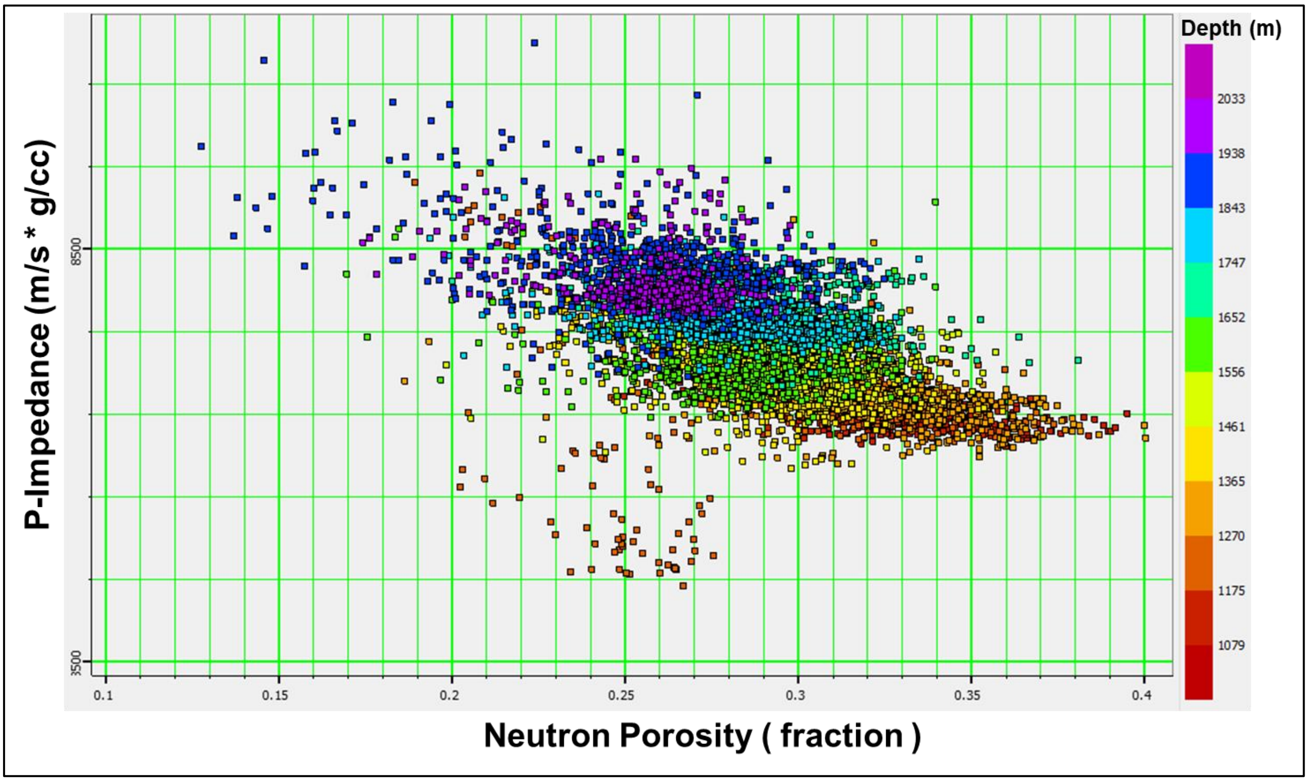

Figure 5-52. PSA-I-17 P-Impedance vs Neutron Porosity. G6 Gas sands plot away from the background, have lower p-impedance, and they are between 20% and 30% porosity.

An empirical impedance-porosity relationship developed from sonic, density, and porosity. According to (Dvorkin & Alkhater, 2004), the acoustic impedance of gas-saturated sands is much lower than that of oil and water-saturated sand. This difference allows for the identification of pore fluids from P-wave data. Acoustic impedance data can then be used to map pore fluids and porosity information from stacked seismic data (Dvorkin & Alkhater, 2004). In the data used by (Dvorkin & Alkhater, 2004), distinct acoustic impedance vs porosity

`

trends for gas and the other for liquids (oil and water) were identified. The general trend of porosity is that it reduces with burial depth due to packing, sorting, and compaction.

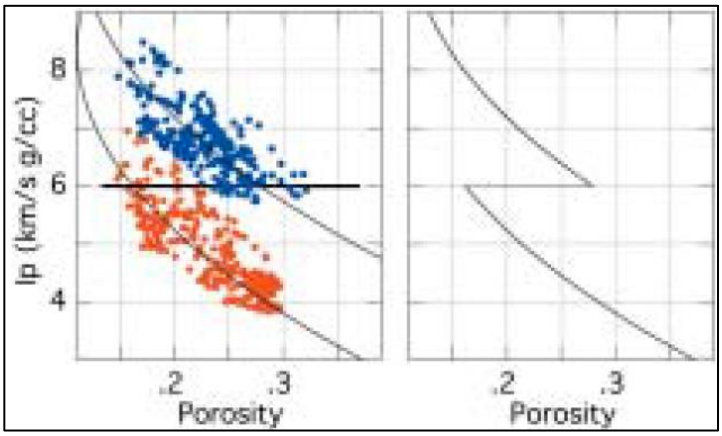

Figure 5-53. Distinct IP vs Porosity trends for gas and oil/water leg (Dvorkin & Alkhater, 2004).

PSA-I-21 Cross Plots

Crossplotting is a great way to visualise well log information. PSA-I-21 well log data was used to generate crossplots in Figure 5-54 to Figure 5-57.

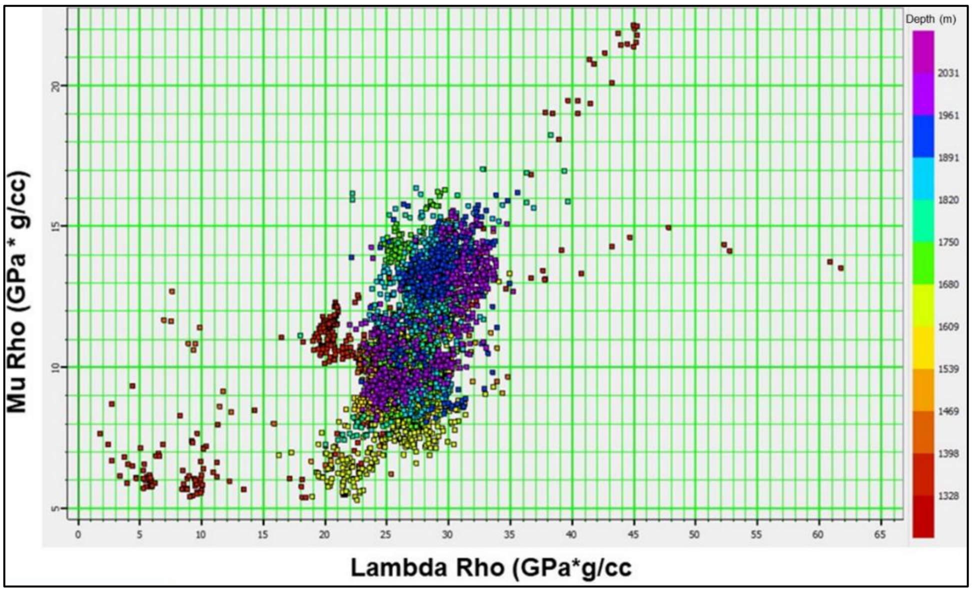

Figure 5-54. PSA-I-21 Lambda-Rho vs Mu-Rho. Gas-saturated sands plot within 20 GPa*g/cc in the Lambda-Rho domain. Lambda Rho is the incompressibility x density function. Mu-Rho is rigidity x density function.

`

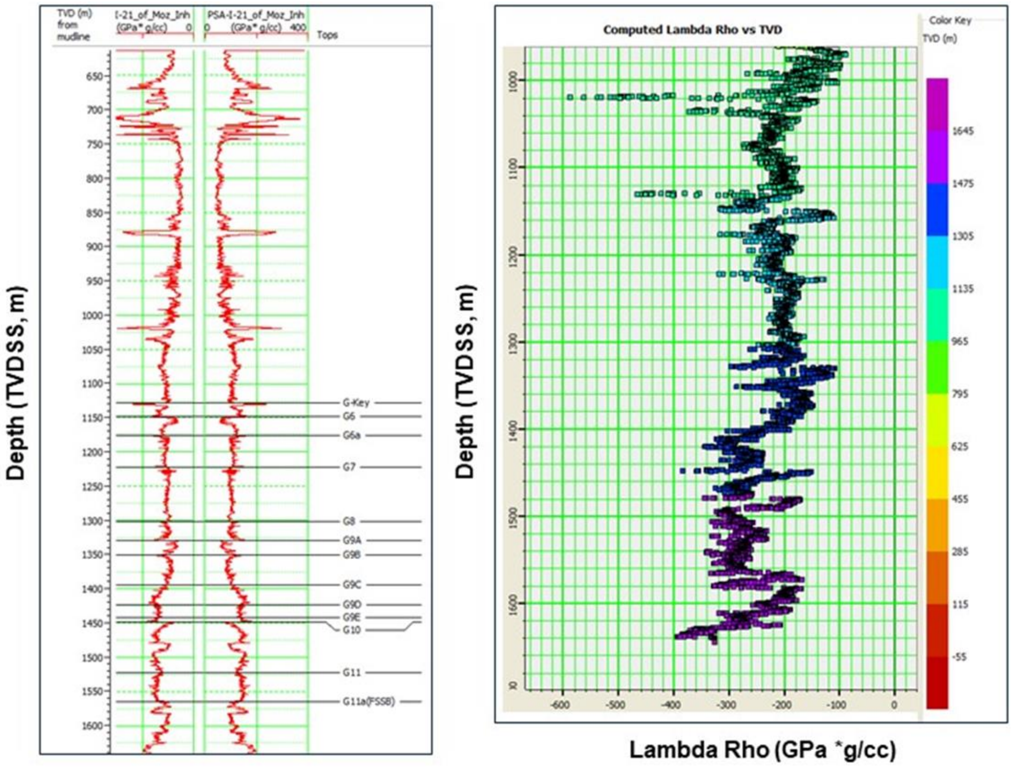

Figure 5-55. Cross Section of LMR from Figure 5-54, PSA-I-21.

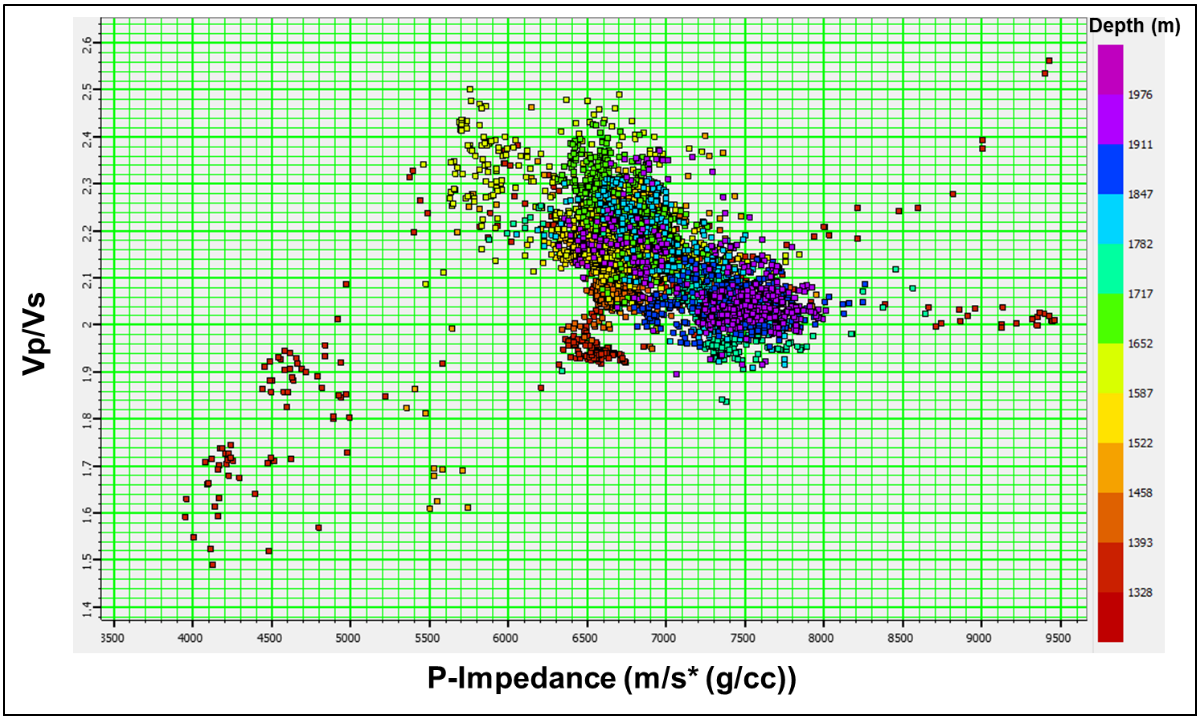

Figure 5-56. PSA-I-21 P-Impedance vs VpVs Ratio. Gas has a low VpVs ratio and relatively lower acoustic impedance. Gas in the reservoir decreases the density and bulk modulus resulting in low p-wave velocity values, and as a result, lower p-impedance.

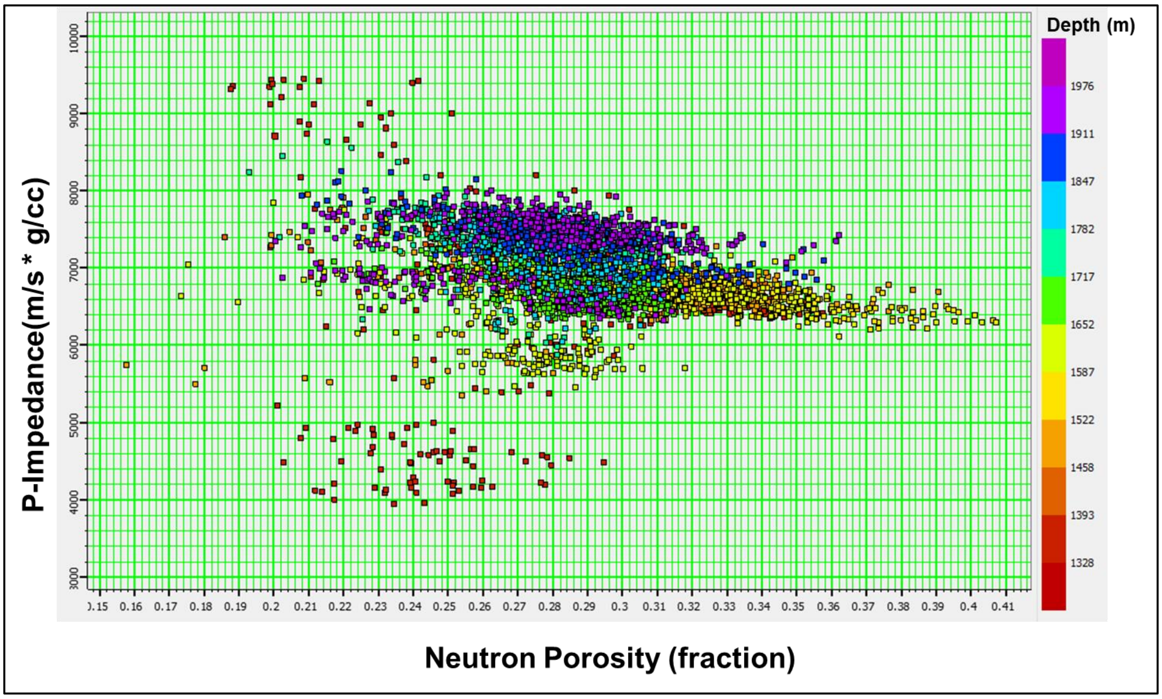

Figure 5-57. PSA-I-21 P-Impedance vs Porosity. Gas sands exhibit lower P-Impedance. This means gas could be identified using the P-impedance cut-off on the P-Impedance vs Porosity crossplot.

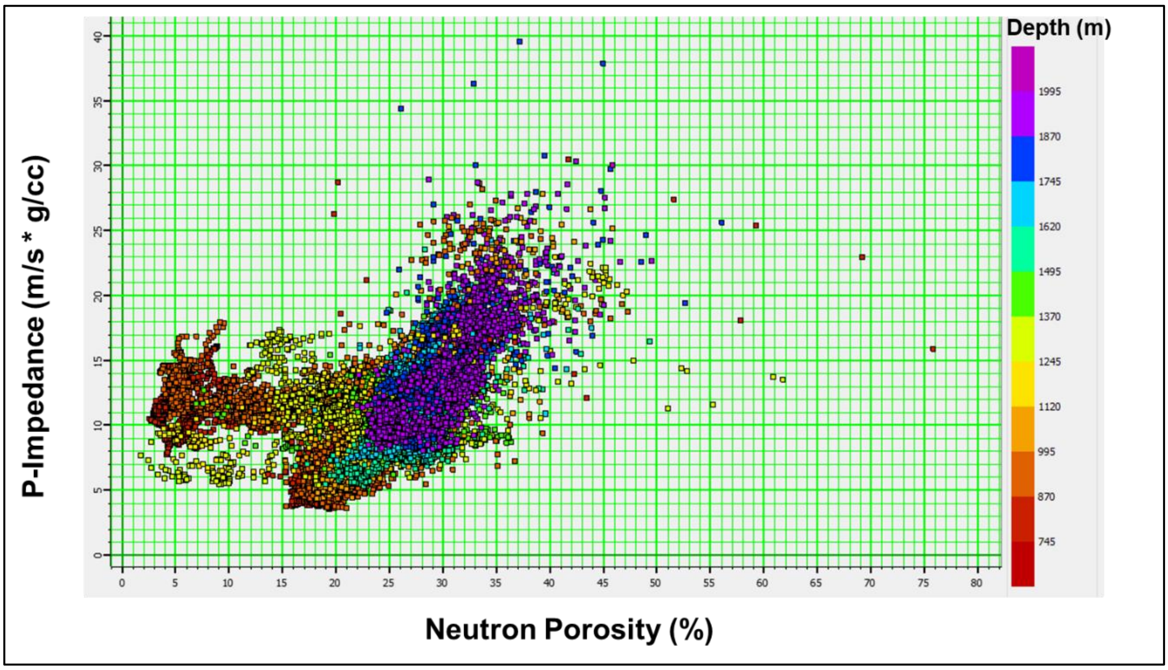

Figure 5-58. Lambda Mu Rho, Multiple wells.

`

5.7 Rock Physics Template (RPT) in Temane Lower Grudja reservoirs

Rock Physics Templates can be used throughout the Mozambique basin to identify rock physics trends, and in most cases to identify gas-bearing sands. The examples in Figure 5-59 to Figure 5-62 are from PSA-T-27 well. Unlike Inhassoro wells, PSA-T-27 intersected gas at G6, G6a, G8, G8A, G9, G10, G11, G11A, G12 and G12A. The lambda-Mu-Rho crossplot is colour-coded by depth showing the gas anomalies (low Mu-Rho, low Lambda-Rho) at various depth levels. Gas sands mainly fall below 20 GPa*g/cc in Temane in the Lambda-Rho domain.

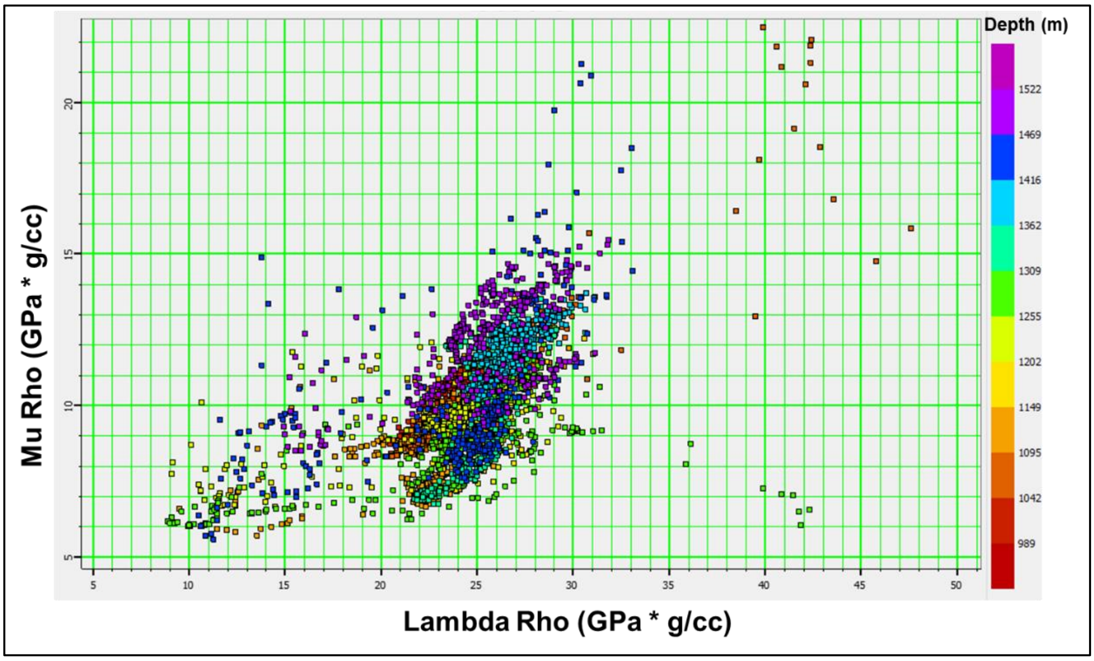

Figure 5-59. PSA-T-27 Lambda Mu Rho. The PSA-T-27 well found gas at multiple levels starting from G6 and can be seen plotting on the gas trend, at varying depths.

`

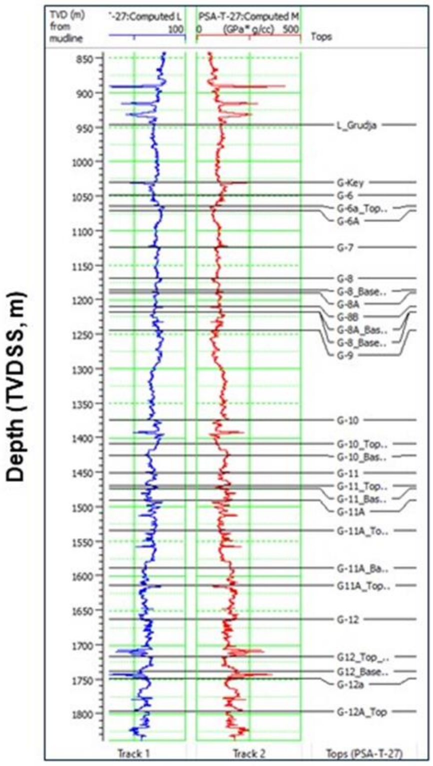

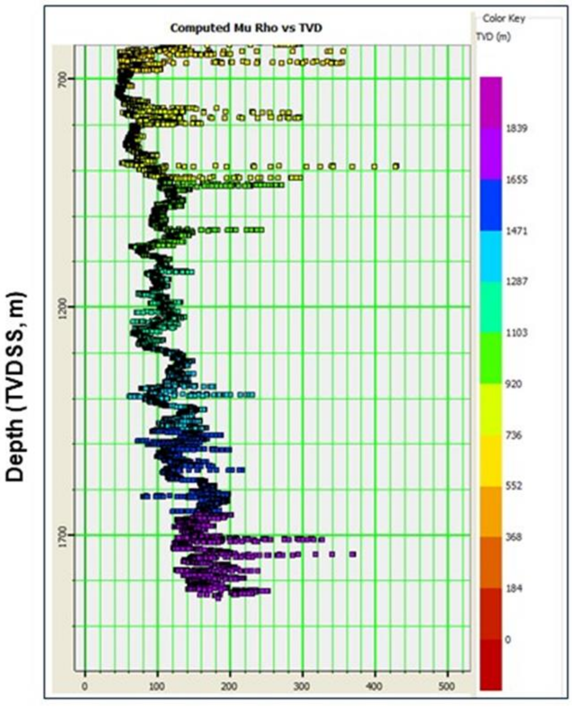

Figure 5-60. PSA-T-27 Well logs from Lambda Mu Rho (LMR) plot in Figure 5-59.

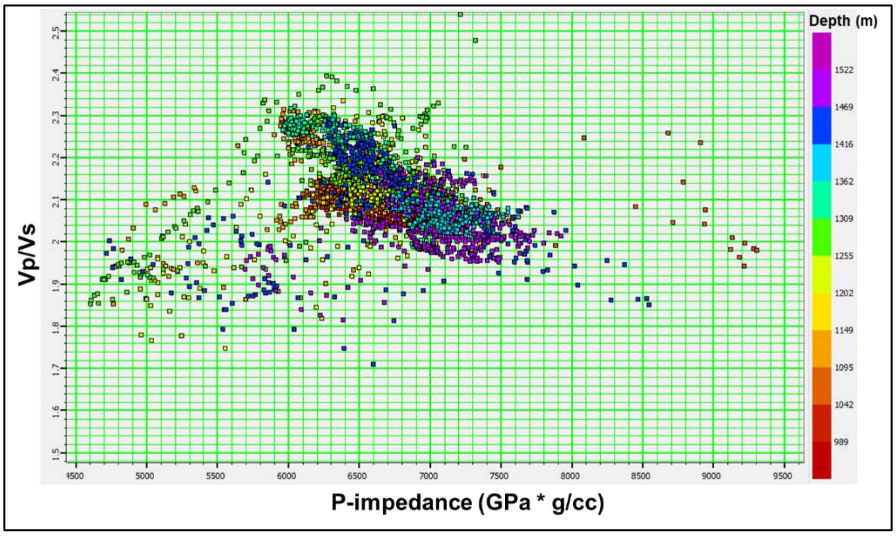

Figure 5-61. PSA-T-27 Rock Physics Template in the Vp/Vs vs Impedance domain.

`

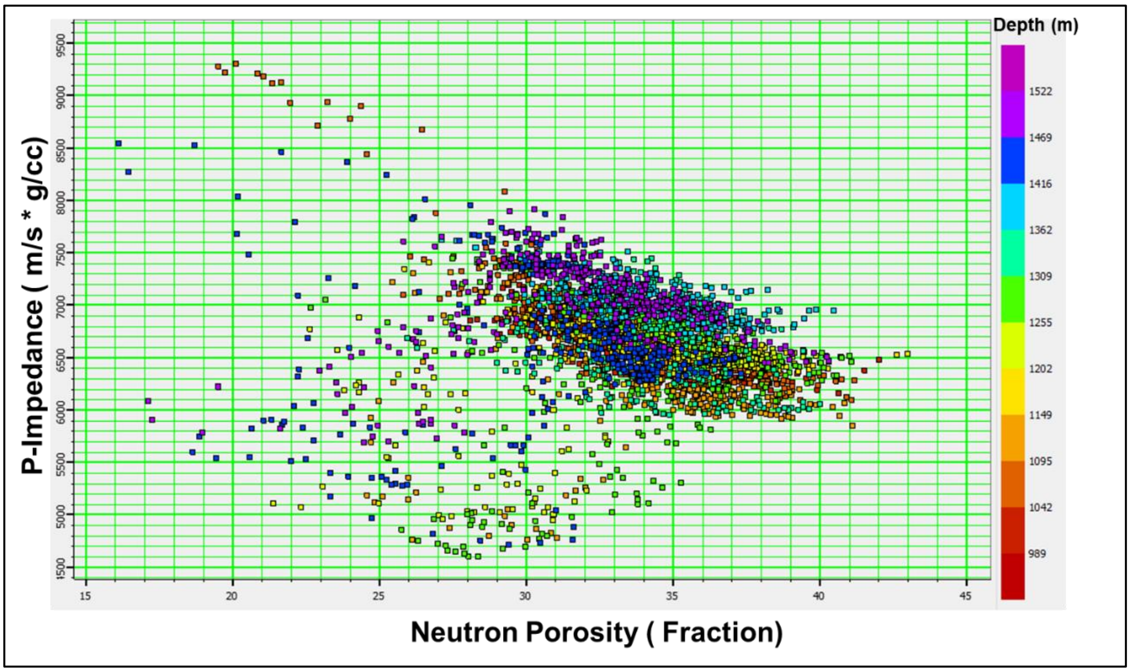

Figure 5-62. PSA-T-27 P-Impedance vs Neutron Porosity.

`

5.8 Rock Physics Template in Pande Lower Grudja reservoirs

The Pande field is a prolific producer at G6 and has many proven reservoirs deeper that require further delineation. Rock Physics Template can be created using well log information from wells drilled to deeper targets. As evident in Figure 5-63, the Pande field RPTs show Gas sand in the P-15 plot within 20 GPa*g/cc in the Lambda-Rho axis. There might be hydrocarbon-saturated sands beyond this point, but those are not unique. Crossplotting Vp/Vs versus P-Impedance (Figure 5-64) can also discriminate hydrocarbon-filled reservoir sands and brine-saturated reservoir facies.

PSA-P-26

The PSA-P-26 well was drilled to delineate deeper lower Grudja reservoirs, including the G10, G11, and G11A. Gas sands in Pande plot within 20 GPa*g/cc in the Lambda-Rho domain (Figure 5-65). No liquids were encountered on this well.

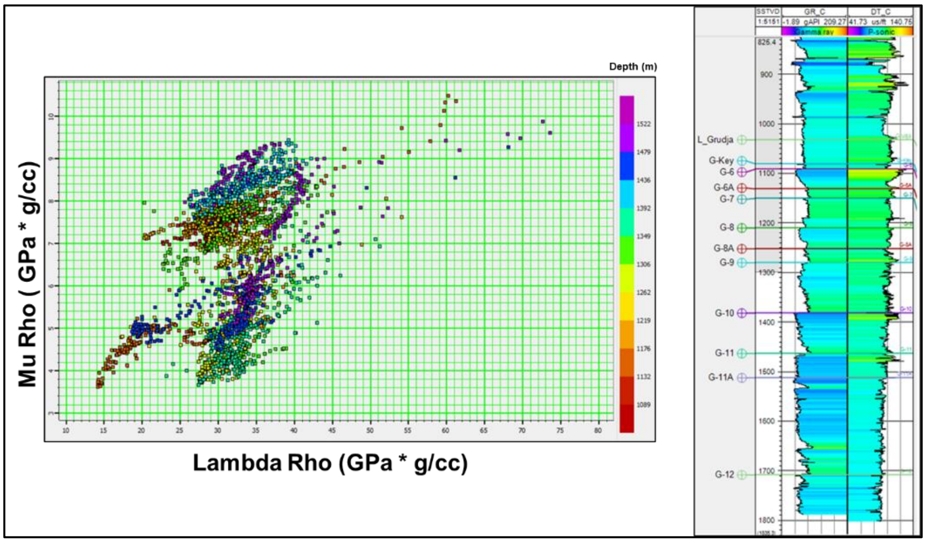

Figure 5-63. P-15, a crossplot of Mu Rho and Lambda Rho for P-15 well in the Pande field.

`

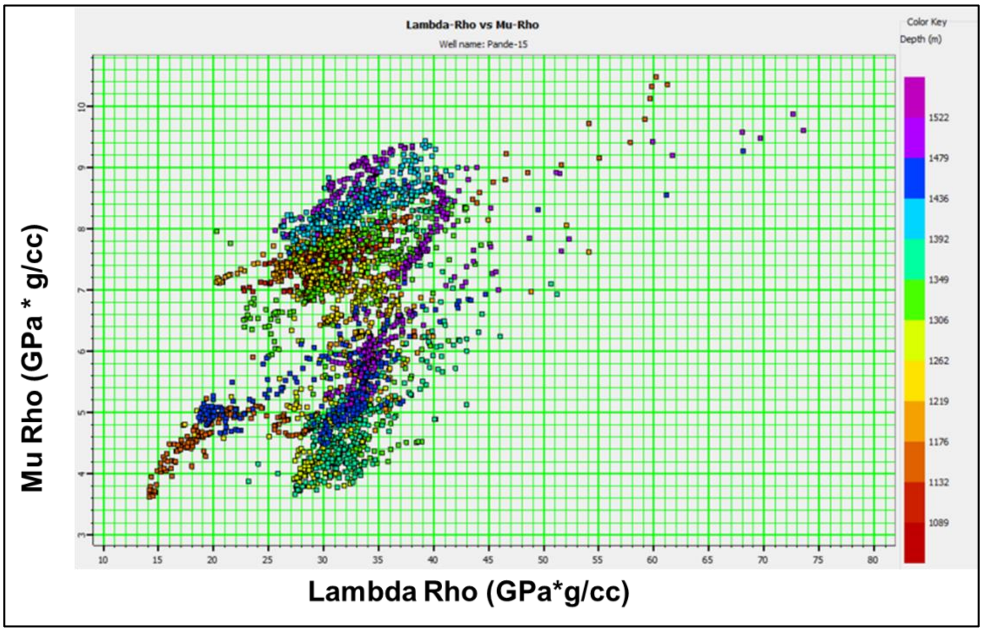

Figure 5-64. P-15, Vp/Vs vs P-Impedance. Three trends can be observed in the plot. A hydrocarbon-saturated reservoir trend, a brine-saturated reservoir, and a non-reservoir trend.

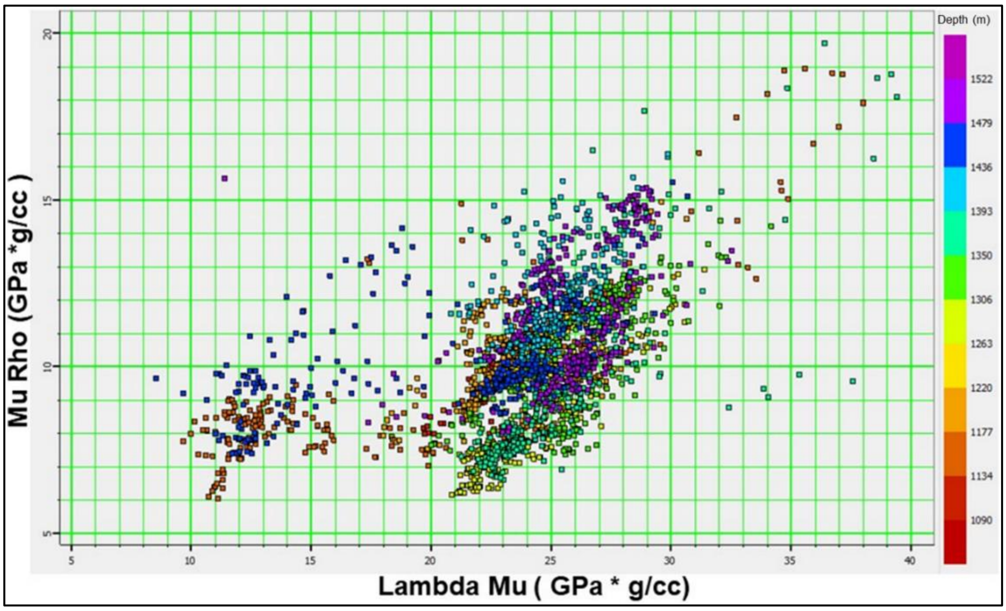

Figure 5-65. PSA-P-26 Lambda Mu Rho. Mu-Rho vs Lambda-Rho. Three trends can be observed in the plot. A hydrocarbon-saturated reservoir trend, a brine-saturated reservoir, and a non-reservoir trend.

`

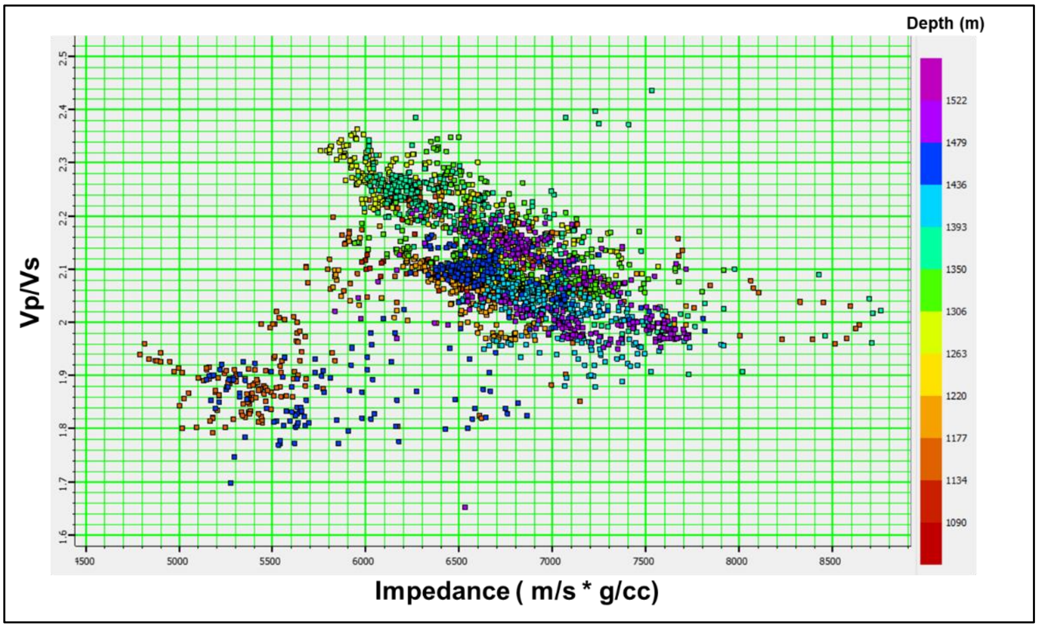

Figure 5-66. PSA-P-26 Vp/Vs vs P-Impedance. Gas-saturated reservoirs are plotted on the lower left corner, where there are lower impedance and lower Vp/Vs values.

`

6 Discussion

This study benefitted from the latest 3D seismic volume recently acquired in the Mozambique basin. This was the first 3D seismic acquisition onshore Mozambique and covered the Temane East area as well as Inhassoro Central (Figure 4-1). Recent wells were drilled to deeper lower Grudja levels (mainly G12A), and a full suite of well logs was acquired and, in some cases, the latest vertical seismic profile (VSP) data included. This enabled better calibration between well log data and seismic data. The availability of seismic gather data also facilitated seismic analysis of gathers to better understand the AVO behaviour which may be diminished in stacked data.

Rock physics understanding of the Mozambique Basin was built by crossplotting of elastic and petrophysical properties (for example Figure 5-5, and other figures in chapter 5). Hydrocarbon-bearing reservoirs of the Mozambican Basin typically show an anomalous amplitude on stacked seismic data. But this may not be unique, and thus always requires further analysis to confirm changes in fluid composition. Cross plotting was used to identify the highest correlation between petrophysical and elastic properties at the well (e.g., Figure 5-5). In the case of Figure 5-5, a drop in bulk modulus clearly shows that reservoir facies saturated with hydrocarbons exhibit lower bulk modulus than those from constant shale-volume trends. Figure 5-6 and Figure 5-7 show that elastic and geophysical properties when cross plotted with water saturation can give insights into expected seismic response, especially for cases where gas is introduced in a reservoir. However, not all elastic properties are sensitive to changes in fluid (for example the Shear velocity trend in Figure 5-6).

Other cross plots investigated include Vp/Vs vs Acoustic Impedance (Figure 5-45, Figure 5-56, Figure 5-64, and Figure 5-66), this builds from the conceptual trends for siliciclastic lithologies developed by (Odegaard & Avseth, 2004) (Figure 5-44). The Lambda Mu Rho (Mu Rho vs Lambda Mu) highlights the relationship between incompressibility vs rigidity and density - these are key attributes of a rock that determines the response of a wave as it traverses through the rock. All the Mu Rho vs Lambda Mu crossplots (Figure 5-47, Figure 5-54, Figure 5-59, Figure 5-63, Figure 5-65) show gas-bearing reservoir plots within the lower Lambda Rho and lower Mu Rho space.

`

These sensitivities to reservoir thickness, fluid composition, and saturation were tested through the use of wedge modelling and a fluid replacement model (more popularly referred to as fluid substitution model), for example, one done for PSA-T-27 well, as shown in Figure 5-8.

Quantitation interpretation methods are broad, and some are briefly discussed in chapter 4. This dissertation focused on seismic analysis and AVO analysis. Seismic analysis ensured that seismic gathers are conditioned, and compliant to AVO processes. Table 4 summarises the quantitative interpretation workflow followed in analysing Mozambique Basin seismic data. Conditioned gathers were used to produce primary AVO products (intercept, gradient, and curvature). Seismic inversion based on the coloured inversion method was applied to AVO products to produce inversion products which are proxies of reservoir properties. The proxies were based on correlations developed through cross-plotting of elastic and petrophysical properties. An example of inversion results is shown in Figure 5-4, which is a water saturation proxy, and an important reservoir characterisation item. Other typical inversion products are porosity and volume of shale. When these three reservoir facies are understood and delineated through inversion, the placement of new wells for exploration, appraisal, or production is improved and the risk of drilling dry holes is minimised.

Gradient analysis revealed that the onshore Mozambique Basin is mainly a class IV regime, which is characterised by a negative intercept and a positive gradient. Examples of Mozambique basin reservoirs exhibiting class IV behaviour include Pande G6 and G10 reservoirs, and Inhassoro G6 reservoirs. Class IV reservoirs are not popular and are often misinterpreted based on the interpreter’s bias or expectation of the typical behaviour of gas reservoirs.

`

7 Conclusion and Recommendations

7.1 Conclusion

This study focused on seismic and well log data interpretation of the Mozambique Basin reservoirs, with a detailed focus on the Inhassoro field. Seismic surveys of varying vintages were used for regional interpretation and for developing a basin-wide understanding of the geology, depositional systems, and structural regime formed as a result of tectonic events that took place before, during, and after the deposition of lower Grudja reservoirs. The seismic data vintages range from data as old as 1990 to more recent surveys of 2019. Most of the available 2D seismic data acquired before 2014 were reprocessed in 2014 to create a consistent seismic data processing vintage. This ensured that the data had the same temporal and amplitude information since they were processed using a consistent workflow despite some differences in data acquisition parameters.

Characterising Maastrichtian Age Reservoirs in Pande, Temane, and Inhassoro Fields

Modern Seismic Data Acquisition

To accurately characterize the Maastrichtian age reservoirs in the Mozambique basin, advanced seismic data was essential. A 125 square kilometre 3D seismic survey was conducted to aid in this characterization before delineation wells were placed. The parameters of the 3D seismic data were designed to image reservoir targets effectively and penetrate deeply enough to capture secondary deeper targets. This new 3D seismic data complemented the existing 2D seismic data and well information, enhancing the understanding of the lower Grudja reservoirs.

Quantitative Seismic Interpretation

- **Seismic data conditioning:** Quantitative interpretation showed that existing gathers, though processed, required further conditioning before use in AVO interpretation and seismic inversion.
- **AVO analysis:** Conditioned gathers revealed a different response compared to stacked data, exhibiting a class IV response instead of the previously considered class III response.
- **Seismic inversion:** This technique provided insights into reservoir properties and their distribution, such as porosity, shale volume, and water saturation.
- **Drilling target placement:** AVO analysis should be performed prior to placing drilling targets, as gradient analysis can predict the expected response at the reservoir level.

`

- **Utilisation of modern wells:** Modern wells with the latest data, even those outside the Inhassoro block, such as Pande-21 in the Pande field and PSA-T-27 in the Temane field, were used for quantitative interpretation.
- **Facies Understanding:** It is important to understand both reservoir and non-reservoir facies as they both affect the seismic amplitude response.
- **Proxies for reservoir properties:** Work on PSA-T-27 indicated that bulk density is a proxy for relative porosity and fluid saturation, while shear modulus serves as a proxy for relative shale volume.
- **AVO interpretation:** AVO interpretation, facilitated by cross-plotting gradient and intercept, helps determine if the reservoir exhibits behaviours consistent with hydrocarbon-bearing facies. Porosity significantly impacts the AVO response, with high porosity reservoirs typically showing class III and class IV responses.

Rock Physics Modelling

- **Importance:** Rock physics modelling and analysis are crucial for linking elastic rock properties with petrophysical properties to characterize reservoir and non-reservoir facies effectively.
- **Crossplotting:** Some rock physics models involve crossplotting velocity-porosity relationships. These relationships can be used to correlate with petrophysical properties. Incorporating core information into these relationships strengthens the rock physics diagnostics.
- **Rock Physics Templates (RPT):** Crossplots act as RPTs, enabling an understanding of the reservoir both vertically and laterally. For example, RPTs for Pande, Temane, and Inhassoro show that gas sands typically plot within 20 GPa*g/cc on the Lambda-Rho axis. Although hydrocarbon sands can plot beyond this point, they lack uniqueness.

7.2 Recommendation

The study contributed to the meaningful identification of commercial hydrocarbon accumulations from seismic to de-risk exploration targets, improved development well placement, and contributed to cost-effective business decisions based on a quantitative understanding of the behaviour of reservoir rocks and pore fluids in the basin away from existing well control. It is therefore recommended that a quantitative analysis of the basin be conducted before drilling new wells if data are available to enable such studies. Only one well was evaluated in Temane, PSA-T-27, using Rock Physics Templates (RPT). And only two

`

wells were evaluated in Pande, P-15, and PSA-P-26. It is therefore recommended that RPTs including more wells in Pande and Temane be conducted to validate if the trends observed in Inhassoro are valid through the basin. To further quantify and determine the accuracy of the inversion, it is recommended that a simultaneous AVO inversion for Vp, Vs, and Rho, or AI, SI, and Rho be run and seismic values at well location be extracted and used to calculate elastic properties and crossplot with well logs.

It is recommended that future work focus on incorporating information from new wells drilled after this study from the Mozambique basin to further calibrate the existing rock physics models, and to minimise drilling risk, which is finding no hydrocarbons at target reservoirs.

`

8 References

Aki, K. & Richards, P. G., 2002. *Quantitative Seismology.* 2nd ed. Sausalito: University Science Books.

Barkwith, D. & Wells, C., 2017. First onshore 3D seismic survey in Mozambique - Overcoming acquisition and processing challenges. *European Association of Geoscientists and Engineers,* pp. 1-3.

Batzle, M. L. & Wang, Z., 1992. Seismic properties of pore fluids. *Geophysics,* 57(11), pp. 1396-1408.

Becquey, M., Lavergne, M. & Willm, C., 1979. Acoustic impedance logs computed from seismic traces. *Geophysics,* 44(9), pp. 1485-1501.

Castagna, J. P., Swan, H. & Foster, D. J., 1998. Framework for AVO gradient and intercept interpretation. *Geophysics,* 63(3), pp. 948-956.

Castagna, J. P. & Swan, H. W., 1997. Principles of Cross Plotting. *The Leading Edge,* 16(4), pp. 337-344.

Chaouch, A. & Mari, J. L., 2006. 3D Land Seismic Surveys: Definition of Geophysical Parameters. *Oil and Gas Science and Technology,* 61(5), pp. 611-630.

Chopra, S. & Marfurt, K. J., 2005. Seismic Attributes: A Historical Perspective. *Geophysics,* 70(5), pp. 3-28.

Connolly, P., 1999. Elastic Impedance. *The Leading Edge,* 18(4), pp. 438-452.

Cordsen, A., Galbraith, M. & Peirce, J., 2000. *Planning Land 3-D Seismic Surveys.* Tulsa: Society of Exploration Geophysicists.

Coster, P. W., Lawrance, R. & Fortes, G., 1989. Mozambique: a new framework for hydrocarbon exploration. *Journal of Petroleum Geology,* 12(2), pp. 205-230.

Dvorkin, J., 2001. *Pore pressure and fluid detection from compressional and shear wave data.* s.l., European Association of Geoscientists and Engineers/ Society of Exploration Geophysicists research workshop on reservoir rocks, pp. 2214-4609.

Dvorkin, J. & Alkhater, S., 2004. Pore fluid and porosity mapping from seismic. *First Break,* 22(2).

Foster, D. J. & Keys, R. G., 1999. *Interpretating AVO responses.* Houston: Society of Exploration Geophysicists.

Gassmann, F., 1951. Elasticity of porous media (Uber die Elastizitat poroser Medien). *Veirteljahrsschrift der Naturforschenden Gesellschaft in Zürich,* 96(1951), pp. 1-23.

Goodway, B., Chen, T. & Downton, J., 1997. Improved AVO fluid detection and lithology discrimination using Lamé petrophysical parameters; “λρ”,“μρ”,&“λ/μ fluid stack”, from P and S inversions. *Society of Exploration Geophysics Technical Program Expanded Abstracts,* pp. 183-186.

Gwavava, O. & Swain, C. J., 1992. Evidence of crustal thinning beneath the Limpopo Belt and Lebombo monocline of southern Africa based on regional gravity studies and implications for the reconstruction of Gondwana. *Tectonophysics,* 212(1-2), pp. 1-20.

Hall, D., 1984. Dip-moveout by Fourier transform. *Geophysics,* 49(6), pp. 741-757.

`

Lächelt, S., 2004. The Geology and Mineral Resources of Mozambique. *Publications of the Direção Nacional de Geologia Moçambique (Geological Survey of Mozambique),* p. 515.

Mashaba, V. & Alterman, W., 2015. Calculation of water saturation in low resistivity gas reservoirs and pay-zones of the Cretaceous Grudja Formation, onshore Mozambique Basin. *Marine and Petroleum Geology,* 67(December 2015), pp. 249-261.

Matthews, A., Lawrence, S. R., Mamad, A. V. & Fortes, G., 2001. Mozambique basin may have a bright future under new geological Interpretation. *Oil and Gas Journal,* 99(27), pp. 70-75.

Mbatha, B. W., Makhubele, M. & Wells, C. H., 2017. *Mozambique Temane PSA-T-27 QI modelling,* Johannesburg: Sasol Internal Presentation.

Mbatha, B. W. & Wells, C. H., 2014. Pande PSA – Seismic Analysis and Inversion of lower Grudja facies. *Sasol Internal Report.*

Odegaard, E. & Avseth, P., 2004. Well log and seismic data analysis using rock physics templates. *first break,* 23(10), pp. 37-43.

Ostrander, W. J., 1984. Plane-Wave Reflection Coefficients for Gas Sands at Non-Normal Angles of Incidence. *Geophysics,* 49(10), pp. 1637-1648.

Otto, D. & Schueter, P., 2017. 3D CRS Processing Inhassoro Central 3D, Mozambique.

Rutherford, S. & Williams, R., 1989. Amplitude-versus-offset variations in gas sands. *Geophysics,* 54(6), pp. 680-688.

Salman, G. & Abdula, I., 1995. Development of the Mozambique and Ruvuma sedimentary basins, offshore Mozambique. *Sedimentary Geology,* 96(1-2), pp. 7-41.

Sasol, 2015. *Pande-Temane PSA Development Plan,* Johannesburg: s.n.

Schulte, B. W. & Manthei, D., 2014. Chasing Density – An Introduction to Seismic Acquisition, Processing, and Interpretation Methods Leading to Quantitative Interpretation. *Recorder,* 39(8).

Sheriff, R. E., 2002. *Encyclopaedic Dictionary of Applied Geophysics.* Fourth ed. Tulsa: Society of Exploration Geophysicists.

Sheriff, R. E., 2006. *Encyclopedic Dictionary of Applied Geophysics.* Fourth ed. Tulsa: Society of Exploration Geophysicists.

Shuey, R. T., 1985. A simplification of the Zoeppritz Equations. *Geophysics,* 50(4), pp. 609-614.

Simm, R. W. & Bacon, M., 2014. Seismic Amplitude: An Interpreter's Handbook. *Cambridge University Press.*

Smithson, T., 2015. *Oilfield Review.* [Online]
Available at: Smithson, T., 2015, The Defining Seriehttps://www.slb.com/resource-library/oilfield-review/defining-series/defining-porosity
[Accessed 12 02 2022].

Smith, T. M., Sondergeld, C. H. & Rai, C. S., 2003. Gassmann fluid substitutions: A tutorial. *Geophysics,* 68(2), pp. 430-440.

Stewart, R., 2001. VSP: An In-Depth Seismic Understanding. *Recorder,* 26(07).

`

Taner, M. T., Koehler, F. & Sheriff, R. E., 1979. Complex seismic trace analysis. *Geophysics,* 44(6), pp. 1041-1063.

TEEC, n.d. *TEEC.* [Online]
Available at: Common Reflection Surface theoryhttps://teec.de/wp-content/uploads/2018/11/CRS_4_Webseite.pdf
[Accessed 06 2020].

Walford, H. L., White, N. J. & Sydow, J. C., 2005. Solid sediment load history of the Zambezi.. *Earth and Planetary Science Letters,* 238(1-2), pp. 49-63.

Wellington, J. H., 1955. A Geographic Study. In: Physical Geography. *Physical Geography. Cambridge University Press,* p. 528.

Wells, C. H., 2016. Inhassoro Central 3D & Inhassoro South 2D - Seismic Survey Designs and Field Parameters. *Sasol.*

Wells, C. H., 2019. Sasol internal notes.

Whitcombe, D. C. P. R. P. a. R. T., 2002. Extended elastic impedance for fluid and lithology prediction. *Geophysics,* 67(1), pp. 63-69.

Wisconson Geological and Natural Survey , Univeristy of Wisconson-Madison, n.d. *Wisconsin Geological and Natural History Survey.* [Online]
Available at: Wisconsin Geological and Natural History Surhttps://wgnhs.wisc.edu/maps-data/data/rock-properties/understanding-porosity-density/
[Accessed 11 January 2022].

Yilmaz, O., 1987. *Seismic Data Analysis : Processing , Inversion , and Interpretation of Seismic Data.* Series: Investigations in Geophysics ed. Tulsa: Society of Exploration Geophysicists.

Zoeppritz, K., 1919. On the reflection and penetration of seismic waves through unstable layers. *Gottinger Nachrichten,* pp. 66-84.